DRAFT VERSION 18 MARCH 2026
Typeset using LaTeX **twocolumn** style in AASTeX631

GWTC-4.0: Tests of General Relativity. I. Overview and General Tests

THE LIGO SCIENTIFIC COLLABORATION, THE VIRGO COLLABORATION, AND THE KAGRA COLLABORATION

(Compiled: 18 March 2026)

ABSTRACT

The worldwide LIGO–Virgo–KAGRA network of gravitational-wave (GW) detectors continues to increase in sensitivity, thus increasing the quantity and quality of the detected GW signals from compact binary coalescences. These signals allow us to perform ever-more sensitive tests of general relativity (GR) in the dynamical and strong-field regime of gravity. This paper is the first of three, where we present the results of a suite of tests of GR using the binary signals included in the fourth GW Transient Catalog (GWTC-4.0), i.e., up to and including the first part of the fourth observing run of the detectors (O4a). We restrict our analysis to the 91 confident signals, henceforth called *events*, that were measured by at least two detectors, and have false alarm rates $\leq 10^{-3}\,\mathrm{yr}^{-1}$. These include 42 events from O4a. This first paper presents an overview of the methods, selection of events and GR tests, and serves as a guidemap for all three papers. Here we focus on the four general tests of consistency, where we find no evidence for deviations from our models. Specifically, for all the events considered, we find consistency of the residuals with noise. The final mass and final spin as inferred from the low- and high-frequency parts of the waveform are consistent with each other. We also find no evidence for deviations from the GR predictions for the amplitudes of subdominant GW multipole moments, or for non-GR modes of polarization. We thus find that GR, without new physics beyond it, is still consistent with these GW events. The results of the two additional papers in this trio also find overall consistency with vacuum GR, with more than 90% of the events being consistent with GR at the 90% credible level. While one of the ringdown analyses finds the GR value in the tails for its combined results, this may be due in part to catalog variance.

1. INTRODUCTION

The past decade has seen a surge of precision measurements of black holes (BHs) and neutron stars (NSs). For gravitational waves (GWs), this started with the direct observation of GWs from the merging of binary BHs (BBHs; Abbott et al. 2016a), binary NSs (BNSs; Abbott et al. 2017a), and NS–BH binaries (NSBHs; Abbott et al. 2021a). These observations have enabled a wide variety of new tests of Einstein's theory of general relativity (GR), starting with Abbott et al. (2016b) for BBHs, Abbott et al. (2019a) for BNSs, and Abbott et al. (2025) for NSBHs.

Precision electromagnetic observations of BHs and NSs include measurements of short-period stars around Sgr A*, which provide constraints on relativistic precession, redshift, and a putative fifth force (Do et al. 2019; Abuter et al. 2020; Abd El Dayem et al. 2025). Additionally, observations of BH shadows (Akiyama et al. 2019a, 2022a) have enabled tests of the Kerr metric (Akiyama et al. 2019b, 2022b), while measurements of isolated NS masses and radii (Bogdanov et al. 2019; Miller et al. 2019; Riley et al. 2019) provide constraints on parity violation in gravity (Silva et al. 2021). These tests complement standard laboratory and astrophysical tests of GR (Will 2014; Berti et al. 2015), including tests using the double pulsar (Kramer et al. 2021) and cosmological observations (reviewed in, e.g., Ferreira 2019; Ishak 2019).

Among these precision measurements, the first three observing runs of the GW observatories Advanced LIGO (Aasi et al. 2015) and Advanced Virgo (Acernese et al. 2015) have provided new tests of GR across regimes previously untestable, by analyzing GW signals from compact binary coalescences (CBCs) (Abbott et al. 2016b, 2017b,c, 2019a,b, 2020b, 2021b, 2025). The tests reported to date have found consistency with GR in all but a few cases where data quality was suspected to be problematic (Abbott et al. 2025). We now update these results by including the significant compact binary signals from the first part of the fourth observing run (O4a) of the advanced-detector network, as reported by the LIGO–Virgo–KAGRA Collaboration (LVK) in Abac et al. (2025b), and adding additional tests. Specifically, this paper (Paper I), along with its two subsequent parts, Abac et al. (2025c) and Abac et al. (2025d), henceforth Paper II and Paper III, report the results of 19 tests of GR as well as a test for an acceleration along the line of sight. We combine together the results of the tests on all significant signals to date whenever possible.

The full author list is given at the end.
For correspondence: LSC P&P Committee, for LVK Publications, via lvc.publications@ligo.org

The signals analyzed constitute the fourth Gravitational-Wave Transient Catalog (GWTC-4.0; Abac et al. 2025b,e), and include the new O4a observations (from 2023 May 24 to 2024 January 16) together with those from the previous runs, O1 (the first observing run, from 2015 September 12 to 2016 January 19; Abbott et al. 2016c), O2 (the second observing run, from 2016 November 30 to 2017 August 25; Abbott et al. 2019c), O3a (the first part of the third observing run, from 2019 April 1 to 2019 October 1; Abbott et al. 2021c, 2024), and O3b (the second part of the third observing run, from 2019 November 1 to 2020 March 27; Abbott et al. 2023). All the candidates in the catalog are consistent with being CBC signals, generated by either BBHs, BNSs, or NSBHs.

In these papers, we restrict ourselves to candidates that have passed the selection criteria of having a confident false-alarm rate (FAR) $\leq 10^{-3}\,\mathrm{yr}^{-1}$ (the same as in Abbott et al. 2021b, 2025), and having been seen by at least two detectors. We henceforth refer to these in the context of the test of GR papers as *events*. Thus, of the O4a candidates, this paper covers 42 new events, while specifically excluding the single-detector events GW230529_181500 (shortened to GW230529; Abac et al. 2024) and GW230814_230901 (shortened to GW230814_23 to avoid confusion with GW230814_061920; Abac et al. 2025f). The tests of GR on those two events are reported elsewhere (Sänger et al. 2024; Abac et al. 2025f). Many of the tests covered have additional, narrower selection criteria for choosing which events are relevant for them, based on the required and supported physical parameters, available data, etc.; these are described in the respective sections.

GW observations enable testing many different aspects of GR or its alternatives and extensions (Will 2014; Colleoni et al. 2024; Yunes et al. 2025; Gupta 2026), among them the linearized theory of the GWs themselves, and the dynamical and highly nonlinear theory of the two-body system generating them.

In this series of papers, we perform 19 distinct tests of GR. We give each test an abbreviated (or acronym) uppercase name, as used for them in Tables 1–5. When a single test uses or compares multiple models, we write the model names in the typewriter font (as in `KerrPostmerger`), and software packages are indicated with their own font (as in BILBY). We subdivide our tests into three papers:

1. This paper (Paper I) includes tests of consistency, either consistency of each signal's residual with the noise, or internal consistency of the signal with itself, according to GR expectations. We present the results of the residuals test (RT; Abbott et al. 2019b); the inspiral–merger–ringdown (IMR) consistency test (IMRCT; Hughes & Menou 2005; Ghosh et al. 2016, 2018); the subdominant multipole amplitudes (SMA) test (Puecher et al. 2022); and the test of the polarization content (POL; Wong et al. 2021).

2. Paper II features parameterized tests, using quantifiable parameters for various imaginable deviations from GR signals in possible alternatives of extensions of GR. These parameters can refer to any physics involved with either the generating system or the propagation of the waves. The parametrized tests of GW generation, grouped in the tables as PAR, constrain deviations in post-Newtonian (PN) coefficients (Blanchet & Sathyaprakash 1994, 1995; Arun et al. 2006a,b; Maggiore 2007; Will 2014; Blanchet 2024) in the inspiral and phenomenological coefficients in the post-inspiral. These include both the FTI (inspiral only; Mehta et al. 2023) and TIGER (Li et al. 2012; Agathos et al. 2014; Meidam et al. 2018; Roy et al. 2026) single-parameter tests, as well as the principal component analysis (PCA) applied to their multi-parameter inspiral versions (Mahapatra et al. 2025). The parameterized tests of GW generation also include the spin-induced moments (SIM) tests (Mehta et al. 2023; Divyajyoti et al. 2024), using either Phenom or EOB waveforms. Additionally, we test for the presence of a line-of-sight acceleration (LOSA; Vijaykumar et al. 2023; Tiwari et al. 2025), which is not a beyond-GR effect, but could be confused for a GR deviation. The tests for parameterized deviations in the propagation of the GWs, grouped under the abbreviation PRP, are the MDR test for a modified dispersion relation (Baka et al. 2025a), and the SSB test for spacetime symmetry breaking, specifically anisotropic birefringent propagation (Haegel et al. 2023).

3. Paper III presents tests of the final remnant object. These include tests comparing the object's immediate ringdown to that expected from the quasi-normal modes (QNMs) of a Kerr BH in vacuum (for the appropriate events), and searches for any post-ringdown (echo) content. The ringdown analyses, grouped as RD, are PYRING (Carullo et al. 2019), pSEOBNR (Brito et al. 2018; Ghosh et al. 2021; Pompili et al. 2025), and QNM rational filter (QNMRF; Ma et al. 2022, 2023a,b; Lu et al. 2025). The echo searches are subdivided into searches for echoes using proposed waveform models, grouped as E-WFM, namely the ADA templates (Abedi et al. 2017; Lo et al. 2019) and BHP templates (Nakano et al. 2017; Uchikata et al. 2019, 2023), and minimally modeled searches for echoes, grouped as E-MM, namely the BAYESWAVE (Tsang et al. 2018) and coherent WaveBurst (CWB; Miani et al. 2023) analyses.

Of these, almost half of the tests are new, namely SMA, PCA, SIM-EOB, LOSA, SSB, PYRING (`KerrPostmerger`), QNMRF, E-WFM-BHP, and E-MM-CWB; additionally TIGER is significantly updated (Roy et al. 2026) compared to the version last used in an LVK testing GR paper (Abbott et al. 2021b). The companion paper about constraints on cosmology (Abac et al. 2025g) also presents constraints on dissipative propagation effects (GW friction) obtained using that paper's methods.

All the tests and their specific paper and section, as well as highlights of the improvements with respect to GWTC-3.0 (see Abac et al. 2025e for catalog designations) and main re-

Table 1. Summary of TGR pipelines and new results across Papers I–III

Test	Paper	Section	Quantity	Parameter	Main Result	Improvement
RT	I	4.1	p-value for the presence of a residual signal	p-value	Consistent with uniform dist.	$\cdots$
IMRCT	I	4.2	Fractional deviation in remnant mass and spin	$\left\{\frac{\Delta M_{\rm f}}{\bar{M}_{\rm f}}, \frac{\Delta\chi_{\rm f}}{\bar{\chi}_{\rm f}}\right\}$	$\left\{0.00^{+0.07}_{-0.06}, -0.05^{+0.11}_{-0.11}\right\}$	$\{2.0, 2.5\}$
SMA	I	4.3	Frac. deviation in amplitude of higher multipole moments	δA_{33}	$-0.21^{+1.82}_{-3.39}$	New
POL	I	5	Bayes factors between different polarization hypotheses	$\log_{10}\mathcal{B}^{X}_{\rm T}$	$-14.72^{+0.59}_{-0.59} - 0.10^{+0.57}_{-0.57}$	$0.21 - 10.48$
PAR	II	2.1	FTI: PN deformation params	$\lvert\delta\hat{\varphi}_k\rvert$	$\leq 1.6\times10^{-3} - 1.5$	$1.2 - 5.5$
		2.1	TIGER: PN deformation params	$\lvert\delta\hat{\varphi}_k\rvert$	$\leq 5.3\times10^{-4} - 1.2$	$1.3 - 3.9$
		2.1	TIGER: Post-inspiral deformation params	$\left\lvert\delta\hat{b}_k\right\rvert, \lvert\delta\hat{c}_k\rvert$	$\leq 7.7\times10^{-3} - 0.28$	Maj. Update
		2.2	PCA: Best-constrained combination of PN deformation params	$\delta\hat{\varphi}^{(1)}_{\rm PCA,FTI}, \delta\hat{\varphi}^{(1)}_{\rm PCA,TIGER}$	$-0.01^{+0.04}_{-0.03}, 0.01^{+0.06}_{-0.06}$	New
SIM	II	2.3	Phenom: Deformation in spin-induced multipole parameter	$\delta\kappa_s$	-19^{+28}_{-34}	1.4
		2.3	EOB: Deformation in spin-induced multipole param	$\delta\kappa_s$	-49^{+95}_{-176}	New
LOSA	II	2.4	Line-of-sight acceleration	$a/c\,[{\rm s}^{-1}]$	$0.42^{+2.00}_{-1.87}\times10^{-6}$	New
MDR	II	3.1	Magnitude of dispersion	$\lvert A_\alpha\rvert\,[{\rm peV}^{2-\alpha}]$	$\leq (0.01 - 351)\times10^{-22}$	$1.48 - 2.88$
		3.1	Graviton mass bound	$m_g\,[{\rm eV}/c^2]$	$\leq 1.92\times10^{-23}$	1.16
SSB	II	3.2	Constraints on anisotropic birefringent propagation	$\left\lvert k^{(5)}_{00}\right\rvert\,[{\rm m}]$	$\leq 1.52\times10^{-14}$	New
RD	III	2.1	pyRing (`KerrPostmerger`): Frac. dev. in freq. & damp. time	$\left\{\delta\hat{f}_{220}, \delta\hat{\tau}_{220}\right\}$	$\left\{0.10^{+0.23}_{-0.18}, 0.18^{+0.27}_{-0.26}\right\}$	New
		2.2	pSEOBNR: Frac. deviations in frequency & damping time	$\left\{\delta\hat{f}_{220}, \delta\hat{\tau}_{220}\right\}$	$\left\{0.00^{+0.06}_{-0.06}, 0.16^{+0.18}_{-0.16}\right\}$	$\{1.09, 1.52\}$
		2.3	QNMRF: Detection statistic for subdominant ringdown modes	$\mathcal{D} - \mathcal{D}_{1\%}$	221: ≤ 3.1	New
E-WFM	III	3.1	ADA: Bayes factor for IMR plus echoes to IMR only	$\log_{10}\mathcal{B}^{\rm IMRE}_{\rm IMR}$	≤ 1.1	$\cdots$
		3.1	BHP: Bayes factor for IMR plus echoes to IMR only	$\log_{10}\mathcal{B}^{\rm IMRE}_{\rm IMR}$	≤ 0.2	New
E-MM	III	3.2	BayesWave: Signal-to-noise Bayes factor for echoes	$\log_{10}\mathcal{B}^{\rm signal}_{\rm noise}$	≤ -1.8	$\cdots$
		3.3	cWB: p-value for the presence of echoes	p-value	Consistent with uniform dist.	New

Note—Analysis abbreviations are defined in the text. The main results and improvements are calculated using the combined results unless otherwise specified, and use the hierarchically combined results if available. For analyses where we quote bounds on two parameters inferred simultaneously, we enclose the parameters in curly brackets. The improvements are computed relative to the previous analyses reported in the GWTC-3.0 test of GR paper (Abbott et al. 2021b), when applicable, or for updated analyses applied to GWTC-3.0; otherwise, "New" is given. For most tests, the improvement is defined as $X_{\text{GWTC-3.0}}/X_{\text{GWTC-4.0}}$, where X denotes the width of the 90% credible interval for the parameters for each test. For the tests where we give ranges for the main result and improvements, we quote the minimum and maximum over all different cases of that test independently. Thus, the endpoints of the improvement range do not necessarily correspond to the endpoints of the main result range. For two new tests, the main results were obtained with individual pre-O4 events: The SMA result is from GW190814, while the LOSA result is from GW170817. For IMRCT and pSEOBNR, the improvement is with respect to the two-dimensional hierarchical analysis (Zhong et al. 2024), not the one-dimensional hierarchical analysis performed in the GWTC-3.0 testing GR paper. For POL, the improvement is the difference of the $\log_{10}$ Bayes factors (GWTC-3.0 minus GWTC-4.0), to illustrate the increased support for GR. The upper bounds for FTI are only for O4a, and the improvement factors are obtained by comparing O4a with results reported in the GWTC-3.0 testing GR paper. As no TIGER results were reported in the latter, its improvement factors are obtained by comparing GWTC-4.0 with a recent analysis of GWTC-3.0 events (Roy et al. 2026). The pyRing results are also only for O4a, as are the upper bounds on Bayes factors for E-WFM and E-MM-BayesWave. The QNMRF parameter given is the detection statistic for the 221 mode minus the threshold corresponding to a 1% false alarm probability, computed over a period when including the 221 mode improves consistency with the IMR results, here for GW231028_153006. The $\cdots$ marker for improvements is used for RT, where the result of overall consistency is maintained; for ADA, a test absent from the GWTC-3.0 analysis, but previously run (in an older implementation) in the GWTC-2.0 testing GR paper; and for BayesWave, which quoted p-values rather than Bayes factors for GWTC-3.0.

sults, are summarized in Table 1. We find improvements in the constraints due to including the additional events, as expected, notably improvements in the PN coefficient constraints of up to 5.5 (FTI) and 3.9 (TIGER), though some of this improvement is due to changes to the portion of the signal where the PN coefficient deviations are implemented. The IMRCT analysis has improvements of up to 2.5, while the MDR analysis has improvements of up to almost a factor of three. Additionally, some O4a events give notable constraints on their own. For instance, the likely NSBH GW230518_125908 provides a constraint on the -1PN coefficient that is comparable to the combined GWTC-4.0 constraint, and provides constraints on many higher PN coefficients that are significantly better than those from all of GWTC-3.0 (see Section 2.1 of Paper II). For the pSEOBNR ringdown analysis, the loud event GW231226_101520 provides a constraint on deviations in the damping time of the dominant QNM that is slightly better than the GWTC-3.0 hierarchical constraint (see Section 2.2 of Paper III). However, the loud event GW250114 (Abac et al. 2025h) from the second part of the fourth observing run (O4b)

Table 2. Event selection table for the analyses in this paper, from the first part of the fourth observing run (O4a; Abac et al. 2025b)

O4a				Paper I				Paper II				Paper III		
Event Name	SNR	IFOs	$(1{+}z)\mathcal{M}/M_\odot$	RT	IMRCT	SMA	POL	PAR	SIM	LOSA	PRP	RD	E-WFM	E-MM
GW230518_125908	$14.2^{+0.2}_{-0.4}$	HL	$2.94^{+0.00}_{-0.00}$	✓	···	···	✓	✓	···	···	···	···	···	✓
GW230601_224134	$12.3^{+0.2}_{-0.3}$	HL	$73.0^{+8.3}_{-11.8}$	✓	···	···	✓	✓	···	···	✓	✓	✓	✓
GW230605_065343	$10.5^{+0.3}_{-0.4}$	HL	$14.44^{+0.28}_{-0.24}$	✓	···	···	✓	✓	···	···	✓	···	✓	✓
GW230606_004305	$10.3^{+0.3}_{-0.4}$	HL	$39.5^{+5.9}_{-5.8}$	✓	✓	···	✓	✓	···	···	✓	···	✓	✓
GW230609_064958	$9.8^{+0.3}_{-0.5}$	HL	$40.1^{+5.7}_{-5.9}$	✓	~~✓~~	···	✓	✓	···	···	✓	✓	✓	✓
GW230624_113103	$9.7^{+0.4}_{-0.5}$	HL	$24.5^{+3.1}_{-2.4}$	✓	···	···	✓	✓	···	···	✓	···	✓	✓
GW230627_015337	$28.5^{+0.1}_{-0.1}$	HL	$6.41^{+0.01}_{-0.01}$	✓	···	···	✓	✓	···	···	✓	···	✓	✓
GW230628_231200	$15.5^{+0.2}_{-0.3}$	HL	$35.8^{+2.8}_{-2.7}$	✓	✓	···	✓	✓	···	···	✓	✓	✓	✓
GW230630_234532	$9.4^{+0.3}_{-0.5}$	HL	$8.57^{+0.06}_{-0.09}$	✓	···	···	✓	✓	···	···	✓	···	✓	✓
GW230702_185453	$9.5^{+0.3}_{-0.5}$	HL	$33.0^{+4.8}_{-3.9}$	✓	···	···	✓	✓	···	···	✓	···	✓	✓
GW230731_215307	$11.9^{+0.2}_{-0.3}$	HL	$9.46^{+0.07}_{-0.06}$	✓	···	···	✓	✓	···	···	✓	···	✓	✓
GW230811_032116	$12.8^{+0.3}_{-0.4}$	HL	$33.3^{+3.0}_{-2.6}$	✓	✓	···	✓	✓	···	···	✓	✓	✓	✓
GW230814_061920	$9.4^{+0.3}_{-0.5}$	HL	77^{+12}_{-18}	✓	···	···	✓	✓	···	···	✓	✓	✓	✓
GW230824_033047	$10.0^{+0.2}_{-0.4}$	HL	$65.8^{+8.0}_{-12.7}$	✓	···	···	✓	✓	···	···	✓	✓	✓	✓
GW230904_051013	$10.2^{+0.3}_{-0.5}$	HL	$9.06^{+0.06}_{-0.06}$	✓	···	···	✓	✓	···	···	✓	···	✓	✓
GW230914_111401	$16.2^{+0.2}_{-0.3}$	HL	$59.4^{+7.8}_{-11.3}$	✓	···	···	✓	✓	···	···	✓	✓	✓	✓
GW230919_215712	$15.7^{+0.2}_{-0.3}$	HL	$26.4^{+1.2}_{-1.2}$	✓	✓	···	✓	✓	✓	···	✓	···	✓	✓
GW230920_071124	$10.1^{+0.3}_{-0.4}$	HL	$35.8^{+4.1}_{-3.4}$	✓	✓	···	✓	✓	···	···	✓	···	✓	✓
GW230922_020344	$11.8^{+0.3}_{-0.4}$	HL	$38.2^{+3.6}_{-3.2}$	✓	✓	···	✓	✓	···	···	✓	✓	✓	✓
GW230922_040658	$11.4^{+0.2}_{-0.4}$	HL	105^{+15}_{-29}	✓	···	···	✓	✓	···	···	✓	✓	✓	✓
GW230924_124453	$12.9^{+0.2}_{-0.3}$	HL	$31.7^{+2.4}_{-2.0}$	✓	✓	···	✓	✓	···	···	✓	✓	✓	✓
GW230927_043729	$10.5^{+0.2}_{-0.4}$	HL	$41.0^{+4.3}_{-3.8}$	✓	···	···	✓	✓	···	···	✓	✓	✓	✓
GW230927_153832	$19.7^{+0.2}_{-0.2}$	HL	$20.14^{+0.41}_{-0.41}$	✓	✓	···	✓	✓	···	···	✓	✓	✓	✓
GW230928_215827	$8.9^{+0.4}_{-0.6}$	HL	61^{+10}_{-14}	✓	···	···	✓	✓	···	···	✓	✓	✓	✓
GW231001_140220	$9.6^{+0.3}_{-0.5}$	HL	81^{+17}_{-20}	✓	···	···	✓	✓	···	···	✓	✓	✓	✓
GW231020_142947	$10.5^{+0.3}_{-0.4}$	HL	$9.99^{+0.10}_{-0.10}$	✓	···	···	✓	✓	✓	···	✓	···	✓	✓
GW231028_153006	$21.0^{+0.2}_{-0.2}$	HL	107^{+10}_{-27}	✓	···	···	✓	✓	···	···	✓	✓	✓	✓
GW231102_071736	$13.3^{+0.2}_{-0.3}$	HL	$71.7^{+7.8}_{-10.5}$	✓	···	···	✓	✓	···	···	✓	✓	✓	✓
GW231104_133418	$11.0^{+0.2}_{-0.4}$	HL	$11.31^{+0.10}_{-0.10}$	✓	···	···	✓	✓	✓	···	✓	···	✓	✓
GW231108_125142	$12.4^{+0.2}_{-0.3}$	HL	$23.79^{+0.96}_{-0.97}$	✓	✓	···	✓	✓	···	···	✓	✓	✓	✓
GW231110_040320	$11.0^{+0.3}_{-0.4}$	HL	$18.02^{+0.69}_{-0.48}$	✓	···	···	✓	✓	✓	···	✓	···	✓	✓
GW231113_200417	$10.1^{+0.3}_{-0.5}$	HL	$9.82^{+0.08}_{-0.08}$	✓	···	···	✓	✓	✓	···	✓	···	✓	✓
GW231114_043211	$9.8^{+0.3}_{-0.5}$	HL	$14.61^{+0.37}_{-0.31}$	✓	···	···	✓	✓	···	···	✓	···	✓	✓
GW231118_005626	$10.5^{+0.3}_{-0.5}$	HL	$17.62^{+0.40}_{-0.54}$	✓	···	···	✓	✓	✓	···	✓	···	✓	✓
GW231118_090602	$10.9^{+0.4}_{-0.4}$	HL	$10.53^{+0.12}_{-0.09}$	✓	···	···	✓	✓	✓	···	✓	···	✓	✓

Table 2 *continued*

Table 2 *(continued)*

O4a				Paper I				Paper II				Paper III		
Event Name	SNR	IFOs	$(1+z)\mathcal{M}/M_\odot$	RT	IMRCT	SMA	POL	PAR	SIM	LOSA	PRP	RD	E-WFM	E-MM
GW231123_135430	$20.7^{+0.2}_{-0.3}$	HL	137^{+21}_{-27}	✓	···	$\not\checkmark$	✓	···	···	···	$\not\checkmark$	++	✓	✓
GW231206_233134	$11.0^{+0.3}_{-0.4}$	HL	$41.9^{+4.7}_{-4.9}$	✓	✓	···	✓	✓	···	···	✓	✓	✓	✓
GW231206_233901	$21.0^{+0.1}_{-0.2}$	HL	$36.1^{+2.3}_{-2.3}$	✓	✓	···	✓	✓	···	···	✓	✓	✓	✓
GW231213_111417	$9.7^{+0.2}_{-0.4}$	HL	$44.4^{+7.2}_{-6.5}$	✓	···	···	✓	✓	···	···	✓	✓	✓	✓
GW231223_032836	$8.8^{+0.3}_{-0.5}$	HL	$55.0^{+9.3}_{-15.0}$	✓	···	···	✓	✓	···	···	✓	✓	✓	✓
GW231224_024321	$12.9^{+0.2}_{-0.3}$	HL	$8.48^{+0.06}_{-0.06}$	✓	···	···	✓	✓	···	···	✓	···	✓	✓
GW231226_101520	$33.7^{+0.1}_{-0.1}$	HL	$39.8^{+1.6}_{-1.6}$	✓	✓	···	✓	✓	···	···	✓	✓	✓	✓

NOTE— For each event we give the matched-filter network signal-to-noise ratio (SNR), the redshifted chirp mass, $(1+z)\mathcal{M}$ (e.g., Abac et al. 2025e), and the interferometers (IFOs) used for the analysis of the events, which are Hanford (H) and Livingston (L) for all O4a events, and may include Virgo (V) for previous runs, in Tables 3–5 below. More details about the events appear in the relevant GWTC papers (for O4a events, Abac et al. 2025b). A ✓ indicates an event meeting our selection criteria for an analysis, and thus included in our results. A $\not\checkmark$ indicates an event that originally met the selection criteria, but technical difficulties in its analysis prevented obtaining meaningful results. A ··· indicates that an event does not meet an analysis's selection criteria.

Table 3. Updated table of events from the second half of the third observing run (O3b; Abbott et al. 2023)

O3b				Paper I				Paper II				Paper III		
Event Name	SNR	IFOs	$(1+z)\mathcal{M}/M_\odot$	RT	IMRCT	SMA	POL	PAR	SIM	LOSA	PRP	RD	E-WFM	E-MM
GW191109_010717	$17.2^{+0.5}_{-0.5}$	HL	$60.1^{+9.8}_{-9.3}$	✓	···	···	✓	$\not\checkmark$	···	···	$\not\checkmark$	✓	+	++
GW191129_134029	$13.1^{+0.2}_{-0.3}$	HL	$8.49^{+0.06}_{-0.05}$	✓	···	···	✓	✓	···	···	✓	···	+	++
GW191204_171526	$17.5^{+0.2}_{-0.2}$	HL	$9.69^{+0.05}_{-0.05}$	✓	···	···	✓	✓	✓	···	✓	···	+	++
GW191215_223052	$11.2^{+0.3}_{-0.4}$	HLV	$24.9^{+1.5}_{-1.4}$	✓	···	···	✓	✓	···	···	✓	···	+	++
GW191216_213338	$18.6^{+0.2}_{-0.2}$	HV	$8.94^{+0.05}_{-0.05}$	✓	···	···	✓	✓	✓	···	✓	···	···	++
GW191222_033537	$12.5^{+0.2}_{-0.3}$	HL	$51.0^{+7.2}_{-6.5}$	✓	···	···	✓	✓	···	···	✓	++	+	++
GW200115_042309	$11.3^{+0.3}_{-0.5}$	HLV	$2.58^{+0.01}_{-0.01}$	✓	···	···	✓	✓	···	$\not\checkmark$	···	···	+	++
GW200129_065458	$26.8^{+0.2}_{-0.2}$	HLV	$32.1^{+1.8}_{-2.6}$	✓	✓	···	✓	✓	++	···	✓	✓	+	++
GW200202_154313	$10.8^{+0.2}_{-0.4}$	HLV	$8.15^{+0.05}_{-0.05}$	✓	···	···	✓	✓	···	···	✓	···	+	++
GW200208_130117	$10.8^{+0.3}_{-0.5}$	HLV	$38.8^{+5.2}_{-4.8}$	✓	✓	···	✓	✓	···	···	✓	✓	+	++
GW200219_094415	$10.7^{+0.3}_{-0.5}$	HLV	$43.7^{+6.3}_{-6.2}$	✓	···	···	✓	✓	···	···	✓	···	+	++
GW200224_222234	$20.0^{+0.2}_{-0.2}$	HLV	$41.1^{+3.6}_{-3.8}$	✓	✓	···	✓	✓	···	···	✓	✓	+	++
GW200225_060421	$12.5^{+0.3}_{-0.4}$	HL	$17.65^{+0.98}_{-1.97}$	✓	✓	···	✓	✓	···	···	✓	···	+	++
GW200311_115853	$17.8^{+0.2}_{-0.2}$	HLV	$32.7^{+2.7}_{-2.8}$	✓	✓	···	✓	✓	···	···	✓	✓	+	++
GW200316_215756	$10.3^{+0.4}_{-0.7}$	HLV	$10.68^{+0.12}_{-0.12}$	✓	···	···	✓	✓	✓	···	$\not\checkmark$	···	+	++

NOTE—In addition to the notation used in Table 2, + indicates existing results from previous runs by external works, while ++ indicates previous results by the LVK exist, but are not used for the combined bounds here.

Table 4. Updated table of events from the first half of the third observing run (O3a; Abbott et al. 2021c, 2024)

O3a				Paper I				Paper II				Paper III		
Event Name	SNR	IFOs	$(1+z)\mathcal{M}/M_\odot$	RT	IMRCT	SMA	POL	PAR	SIM	LOSA	PRP	RD	E-WFM	E-MM
GW190408_181802	$14.6^{+0.2}_{-0.3}$	HLV	$23.8^{+1.2}_{-1.5}$	✓	✓	···	✓	✓	···	···	✓	++	++	+
GW190412	$19.8^{+0.2}_{-0.3}$	HLV	$15.24^{+0.37}_{-0.23}$	✓	++	✓	✓	✓	✓	···	✓	···	++	+
GW190421_213856	$10.7^{+0.2}_{-0.4}$	HL	$45.9^{+5.7}_{-6.3}$	✓	++	···	✓	✓	···	···	✓	···	++	···
GW190425	$12.4^{+0.3}_{-0.4}$	LV	$1.4873^{+0.0008}_{-0.0006}$	···	···	···	✓	···	···	✓	···	···	···	···
GW190503_185404	$12.1^{+0.2}_{-0.4}$	HLV	$37.8^{+6.1}_{-6.7}$	✓	✓	···	✓	✓	···	···	✓	···	++	···
GW190512_180714	$12.7^{+0.3}_{-0.4}$	HLV	$18.58^{+0.69}_{-0.66}$	✓	···	···	✓	✓	···	···	✓	++	++	+
GW190513_205428	$12.5^{+0.3}_{-0.4}$	HLV	$30.7^{+6.1}_{-3.4}$	✓	✓	···	✓	✓	···	···	✓	++	++	+
GW190517_055101	$10.8^{+0.5}_{-0.6}$	HLV	$36.2^{+4.2}_{-4.9}$	✓	···	···	✓	✓	···	···	✓	···	++	+
GW190519_153544	$15.9^{+0.2}_{-0.3}$	HLV	$65.1^{+8.7}_{-10.9}$	✓	++	···	✓	✓	···	···	✓	✓	++	+
GW190521	$14.3^{+0.4}_{-0.3}$	HLV	101^{+29}_{-34}	✓	···	···	✓	✓	···	···	···	++	++	+
GW190521_074359	$25.9^{+0.1}_{-0.2}$	HL	$39.8^{+3.2}_{-2.7}$	✓	✓	···	✓	✓	···	···	✓	✓	++	+
GW190602_175927	$13.2^{+0.2}_{-0.3}$	HLV	73^{+12}_{-18}	✓	···	···	✓	✓	···	···	✓	++	++	+
GW190630_185205	$16.4^{+0.2}_{-0.3}$	LV	$29.5^{+2.1}_{-1.7}$	✓	✓	···	✓	✓	···	···	✓	✓	++	···
GW190706_222641	$13.4^{+0.2}_{-0.4}$	HLV	77^{+12}_{-18}	✓	++	···	✓	✓	···	···	✓	++	++	+
GW190707_093326	$13.1^{+0.2}_{-0.4}$	HL	$9.90^{+0.11}_{-0.10}$	✓	···	···	✓	✓	···	···	✓	···	++	···
GW190708_232457	$13.4^{+0.2}_{-0.3}$	LV	$15.48^{+0.25}_{-0.24}$	✓	···	···	✓	✓	···	···	✓	++	++	···
GW190720_000836	$10.9^{+0.3}_{-0.8}$	HLV	$10.37^{+0.11}_{-0.11}$	✓	···	···	✓	✓	✓	···	✓	···	++	···
GW190727_060333	$11.7^{+0.2}_{-0.5}$	HLV	$45.2^{+5.8}_{-5.5}$	✓	++	···	✓	✓	···	···	✓	++	++	···
GW190728_064510	$13.1^{+0.3}_{-0.4}$	HLV	$10.14^{+0.11}_{-0.08}$	✓	···	···	✓	✓	✓	···	✓	···	++	···
GW190814	$25.3^{+0.1}_{-0.2}$	HLV	$6.42^{+0.02}_{-0.02}$	✓	✓	✓	✓	✓	···	···	✓	···	+	+
GW190828_063405	$16.5^{+0.2}_{-0.3}$	HLV	$34.6^{+3.5}_{-2.9}$	✓	✓	···	✓	✓	✓	···	✓	✓	++	+
GW190828_065509	$10.2^{+0.4}_{-0.5}$	HLV	$17.33^{+0.61}_{-0.71}$	✓	···	···	✓	✓	···	···	✓	···	++	···
GW190910_112807	$14.5^{+0.2}_{-0.3}$	LV	$43.6^{+4.4}_{-4.0}$	✓	++	···	✓	✓	···	···	✓	✓	++	···
GW190915_235702	$13.1^{+0.2}_{-0.3}$	HLV	$32.5^{+3.1}_{-3.1}$	✓	···	···	✓	✓	···	···	✓	++	++	+
GW190924_021846	$12.0^{+0.3}_{-0.4}$	HLV	$6.44^{+0.03}_{-0.02}$	✓	···	···	✓	✓	···	···	✓	···	++	···

NOTE—Notation is as in Table 3. The IMR results for GW190412 appeared in Abbott et al. (2020b).

Table 5. Updated table of events from the first (O1; Abbott et al. 2016c) and second (O2; Abbott et al. 2019c) observing runs

O1+O2				Paper I				Paper II				Paper III		
Event Name	SNR	IFOs	$(1+z)\mathcal{M}/M_\odot$	RT	IMRCT	SMA	POL	PAR	SIM	LOSA	PRP	RD	E-WFM	E-MM
GW150914	$26.0^{+0.1}_{-0.2}$	HL	$30.7^{+1.8}_{-1.6}$	✓	✓	···	✓	✓	···	···	✓	✓	++	+

Table 5 *continued*

Table 5 *(continued)*

O1+O2				Paper I				Paper II				Paper III		
Event Name	SNR	IFOs	$(1+z)\mathcal{M}/M_\odot$	RT	IMRCT	SMA	POL	PAR	SIM	LOSA	PRP	RD	E-WFM	E-MM
GW151012*	$9.3^{+0.3}_{-0.5}$	HL	$18.8^{+3.4}_{-1.5}$	++	···	···	···	++	···	···	++	···	+	+
GW151226	$12.7^{+0.3}_{-0.3}$	HL	$9.71^{+0.08}_{-0.06}$	✓	···	···	✓	✓	✓	···	✓	···	++	+
GW170104	$13.8^{+0.2}_{-0.3}$	HL	$25.7^{+1.7}_{-1.7}$	✓	✓	···	✓	✓	···	···	✓	✓	++	+
GW170608	$15.3^{+0.2}_{-0.3}$	HL	$8.50^{+0.05}_{-0.05}$	✓	···	···	✓	✓	···	···	✓	···	++	+
GW170729*	$10.7^{+0.4}_{-0.5}$	HLV	$52.5^{+9.2}_{-12.0}$	++	++	···	···	++	···	···	++	···	+	+
GW170809	$12.8^{+0.2}_{-0.3}$	HLV	$29.9^{+2.4}_{-2.0}$	✓	✓	···	✓	✓	···	···	✓	···	++	+
GW170814	$17.7^{+0.2}_{-0.3}$	HLV	$27.0^{+1.5}_{-1.3}$	✓	✓	···	✓	✓	···	···	✓	++	++	+
GW170817	$32.7^{+0.1}_{-0.1}$	HLV	$1.1976^{+0.0004}_{-0.0002}$	···	···	···	✓	++	···	✓	++	···	···	+
GW170818	$12.0^{+0.3}_{-0.4}$	HLV	$32.7^{+2.8}_{-2.5}$	✓	✓	···	✓	✓	···	···	✓	···	++	+
GW170823	$12.2^{+0.2}_{-0.3}$	HL	$39.1^{+5.4}_{-4.7}$	✓	✓	···	✓	✓	···	···	✓	++	++	+

NOTE—Notation is as in Table 3. The starred events GW151012 and GW170729 had previously been used for the indicated tests of GR in Abbott et al. (2016c, 2019b), but do not meet the current selection criteria. GW170817's PAR and PRP results appeared in Abbott et al. (2019a).

has now provided even better constraints on both PN coefficients and QNM deviations (Abac et al. 2026). Similarly, the loud O4b event GW241011 (Abac et al. 2025i), whose source was an unequal-mass binary, provides the best constraints for the SMA and SIM analyses.

Most of the tests are null tests, placing bounds on deviations from GR (or more generally, deviations from the waveform models for isolated, quasi-circular binaries used in the analysis) instead of constraining a specific alternative theory as modeling CBCs (or even single objects) in modified theories is much more complicated than in GR (Will 1994; Berti et al. 2015; Abac et al. 2025a; Yunes et al. 2025). Illustrative translations of the bounds on deviations in PN coefficients to constraints on specific alternative theories (with many caveats) are given in Section 2.1 of Paper II.

Overall, the results of tests in all three of these papers show consistency with GR. There are a few events which indicate inconsistency for one or more of the analyses, and these cases are discussed for in the papers describing each respective analysis. The standard consistency measure we use is finding GR within the 90% credible interval. Thus, given enough events and analyses, some are expected to be inconsistent, statistically. We therefore find that our results for individual events are still fully explainable assuming GR and statistical noise. We additionally find that certain apparent deviations from GR are due to prior effects or systematic uncertainties in waveform modeling, as discussed in Paper II. There are also certain analyses for which we find that there are more significant deviations from GR when combining together events than for the individual events, specifically SIM, where the apparent deviation is driven by correlations with the effective inspiral spin, and both pyRing and pSEOBNR, where there are apparently quite significant deviations in the combined results: For pyRing, GR is only found at 94.7% credibility when including all the O4a events analyzed, though if one restricts to only the events with a significant ringdown signal, GR is found at 80% credibility, and a bootstrapping analysis finds that even this deviation may not be as significant, due to the finite number of events considered (cf. Pacilio et al. 2024). For pSEOBNR, GR is found at 98.6% or 99.3% credibility depending on how the events are combined, with similar reductions in significance from the bootstrapping analysis. Indeed, GR is found at a credibility of 92.2% or 96.2% when including the loud O4b event GW250114 (Abac et al. 2025h, 2026). Thus, these combined results do not provide significant evidence of a deviation from GR.

The rest of this paper is organized as follows: Section 2 discusses the events included, and details which tests were performed for each. Section 3 describes the general methods common between many of the tests. Section 4 describes our consistency tests, namely the residuals test (Section 4.1), the inspiral–merger–ringdown consistency (Section 4.2), and the subdominant multipole amplitude test (Section 4.3). Section 5 describes the test for possible non-GR polarizations. Section 6 provides overall concluding remarks.

2. THE GRAVITATIONAL-WAVE EVENTS

All the events passing the selection criteria, and an enumeration of which events contributed to which sort of test, and appear in which paper (I/II/III), are given in Tables 2–5, subdivided by observing run. We also give some basic information about the events, including their matched-filter network SNR and redshifted chirp mass, $(1+z)\mathcal{M}$, as a well-measured combination of the masses (e.g., Abac et al. 2025e). These are obtained from the parameter estimation analyses in the cited GWTC papers (for O4a events, the GWTC-4.0 results paper; Abac et al. 2025b). We further list the interferometers (IFOs) used for the analysis of the events (H = Hanford, L =

Livingston, V = Virgo). For the O4a run, all events use data from only the Hanford and Livingston detectors.

The events analyzed in this work are drawn from GWTC-4.0 (Abac et al. 2025b). This catalog includes all events detected by the LVK before 2024 January 31. Compared to previous versions of the catalog, this version additionally contains events from the first part of O4a. During O4a, the LIGO Hanford and Livingston observatories accumulated 126 d of coincident data across a period of 237 d in 2023 and early 2024; Virgo and KAGRA were mostly offline for upgrades. For inclusion in the general relativity tests described in this work, an event must have a false alarm rate $\leq 10^{-3}\,\mathrm{yr}^{-1}$ in at least one search and must have at least two observatories used for their analysis. Thus, for O4a, both LIGO observatories must be used in the analysis of the events. For GWTC-1.0, the tests of GR (Abbott et al. 2019b) were applied to all events in that initial catalog, due to the smaller number of total events. The events GW151012 and GW170729 were analyzed in that paper and appear in the event tables here, but they do not satisfy the significance criterion. Thus, they are not included in combined results.

The selection criteria used for applying tests of GR to subsequent editions of the catalog, GWTC-2.0 and GWTC-3.0 (Abbott et al. 2021b, 2025), are the same as the ones for the present paper, though the multiple-detector criterion was not applied explicitly in the GWTC-2.0 testing GR paper, because it was already satisfied for all events considered. Additionally, while we include the likely BNSs GW170817 and GW190425 in this paper, they were previously excluded from the testing GR catalog papers, though GW170817 had a paper dedicated to testing GR results (Abbott et al. 2019a). As in the GWTC-3.0 testing GR paper (Abbott et al. 2025), we also keep the three events (GW190421_213856, GW190521, and GW190910_112807) included in the GWTC-2.0 testing GR paper (Abbott et al. 2021b) whose significance dropped slightly below the threshold in the reanalysis in GWTC-2.1 (Abbott et al. 2024).

All events covered appear in the respective Tables 2–5. Further details about GW231123_135430 (shortened to GW231123) appear in its discovery paper (Abac et al. 2025j); there are also separate papers describing tests of GR on the exceptional single-detector events GW230529 (Sänger et al. 2024) and GW230814_23 (Abac et al. 2025f) that do not appear in this paper.

One might worry that the requirement that the events to which we apply the tests of GR are detected with a high significance means that we are a priori excluding events that have significant deviations from the waveform models used in the searches. However, the minimally modeled cWB search (Abac et al. 2025k) is able to detect signals that have the generic chirp structure expected for CBCs but differ from the exact predictions for BBHs in GR. This sensitivity of cWB is illustrated in Mishra et al. (2022) for the effects of precession or eccentricity that are not included in the template banks used in the modeled searches (Abac et al. 2025k), or the training set used for cWB. While cWB is mostly sensitive to signals from high-mass binaries, the inclusion of the cWB significance in the selection criteria means that we are at least not missing a significant population of non-GR signals in the set of events to which we apply tests of GR.

Previous catalog papers suffered from the incorrect implementation of the detector calibration uncertainty. As described in Abac et al. (2025k), this affected parameter estimation, but produced only a negligible effect on the posteriors, with changes typically within the error from statistical sampling (Baka et al. 2025b). For O4a events, we performed all the tests of GR with the correct calibration uncertainty, but how we handle pre-O4a results differs between analyses. SMA, PCA, SIM-EOB, LOSA, and E-WFM all have used the correct calibration uncertainty in analyzing pre-O4a events, while pyRing and QNMRF do not use the calibration uncertainties. Post-inspiral TIGER, SIM-Phenom, and pSEOBNR have rerun the analysis with the correct calibration priors, while the MDR analysis reweights the old results to the correct calibration. The FTI and SSB analyses currently only present results for O4a events. POL has used the correct calibration uncertainty except for using older maximum-likelihood parameter-estimation results obtained with the incorrect calibration uncertainty to determine the time–frequency cluster used in the analysis. However, the POL analysis has a fairly broad frequency resolution, so using the corrected parameter estimation results is not expected to make a significant difference in the POL results. E-MM-cWB uses simulated signals generated using posterior samples from parameter estimation to compute a background, but this procedure is insensitive to the fine details of the waveform and is thus unaffected by the error. RT, IMRCT, and inspiral TIGER currently use the previous results with the incorrect calibration, though these will be updated later. E-MM-BayesWave uses the incorrect calibration as well, but the calibration enters only through the parameter-estimation results used to determine the stretch of data for the analysis. As such, this analysis should be only minimally affected. Analyses corrected to the proper calibration showed only a negligible difference in the results, even for tests combining multiple observations.

Previous catalog papers also employed a likelihood function with a small error due to an incorrectly applied window correction, as discussed in more detail in Section 3.

Finally, all events were checked for data quality issues, as discussed in Section 4 of Abac et al. (2025k) and glitch mitigation has been performed for events when appropriate, as discussed in Appendix B of Abac et al. (2025b). We have no evidence for data quality affecting the tests presented here.

3. METHODS FOR TESTING GR

3.1. *Bayesian Inference*

The detection of the GW events is followed by Bayesian inference of parameters assuming one or several waveform models within GR. This is usually carried out using the Bilby package (Ashton et al. 2019; Romero-Shaw et al. 2020), which many of our tests also employ, often with the BilbyTGR plugin (Ashton et al. 2025b). The detailed description of the parameter estimation within GR is given in the companion paper Abac et al. (2025k). We consider a short data segment $d(t)$ around each detected signal and model it as a sum of Gaussian colored noise and the GW signal. This model defines the likelihood $p(d|\boldsymbol{\theta}, \mathbb{M})$, such that the residuals should have a Gaussian distribution after subtracting the correctly modeled GW signal (see Section 4.1 below). Here we assume that the observed data are described by a model $\mathbb{M}$ parameterized by $\boldsymbol{\theta}$. For example, in several tests we consider a model extended beyond GR parameterized by $\boldsymbol{\theta}_{\rm GR}, \boldsymbol{\theta}_{\rm nGR}$. The likelihood for a network of detectors is given as a product of likelihoods, assuming that the measurements are independent.

We use agnostic priors $p(\boldsymbol{\theta}|\mathbb{M})$. In general, we choose uniform priors over a range that is wide enough to cover the region of parameter space where the posterior has support, while not compromising the efficiency of the sampling. Specifically, we choose the prior ranges to be wide enough to avoid *railing*, where there is significant posterior probability density right up to at least one prior boundary. The priors for GR parameters are described in Section 5.5 of Abac et al. (2025k), while the priors for non-GR parameters are specified in the description of each analysis. The detector calibration uncertainties translate into a possible frequency-dependent shift in the GW amplitude and phase which is modeled as a spline with Gaussian prior over its coefficients and marginalized over, as discussed in Section 5.4 of Abac et al. (2025k). The posterior distribution

$$p(\boldsymbol{\theta}|d, \mathbb{M}) = \frac{p(d|\boldsymbol{\theta}, \mathbb{M})p(\boldsymbol{\theta}|\mathbb{M})}{\mathcal{Z}(d|\mathbb{M})} \tag{1}$$

is sampled using numerical techniques, where $\mathcal{Z}(d|\mathbb{M})$ is the evidence of the considered model. A central part of several analyses presented here and in the companion papers is to evaluate which model fits better the observed data on the basis of the Bayes factor. The Bayes factor is equal to the posterior odds with equal prior given to all models, which we always assume:

$$\mathcal{B}^{\mathbb{M}_1}_{\mathbb{M}_2} = \frac{\mathcal{Z}(d|\mathbb{M}_1)}{\mathcal{Z}(d|\mathbb{M}_2)} = \frac{\int p(d|\boldsymbol{\theta}_{\mathbb{M}_1}, \mathbb{M}_1)p(\boldsymbol{\theta}_{\mathbb{M}_1}|\mathbb{M}_1)\,\mathrm{d}\boldsymbol{\theta}_{\mathbb{M}_1}}{\int p(d|\boldsymbol{\theta}_{\mathbb{M}_2}, \mathbb{M}_2)p(\boldsymbol{\theta}_{\mathbb{M}_2}|\mathbb{M}_2)\,\mathrm{d}\boldsymbol{\theta}_{\mathbb{M}_2}}. \tag{2}$$

In particular, the Bayes factor between GR and extended beyond GR (nGR) models is given as

$$\mathcal{B}^{\rm nGR}_{\rm GR} = \frac{\int p(d|\boldsymbol{\theta}_{\rm GR}, \boldsymbol{\theta}_{\rm nGR})p(\boldsymbol{\theta}_{\rm GR}, \boldsymbol{\theta}_{\rm nGR})\,\mathrm{d}\boldsymbol{\theta}_{\rm GR}\,\mathrm{d}\boldsymbol{\theta}_{\rm nGR}}{\int p(d|\boldsymbol{\theta}_{\rm GR})p(\boldsymbol{\theta}_{\rm GR})\,\mathrm{d}\boldsymbol{\theta}_{\rm GR}} \tag{3}$$

We typically use nested sampling (Skilling 2006) to evaluate the evidence for the considered models. We use two implementations of the nested-sampling algorithm. Most of the tests used Dynesty (Speagle 2020) embedded in the Bilby package (Ashton et al. 2019; Romero-Shaw et al. 2020). Another implementation of nested sampling, cpnest (Veitch et al. 2025), was used only by pyRing. During sampling, SMA, TIGER, and SIM analytically marginalized out the distance and time of coalescence (Romero-Shaw et al. 2020); LOSA marginalized out the distance and coalescence phase (Veitch et al. 2015); while IMRCT, FTI, PCA, and pSEOBNR marginalized out only the distance (Abac et al. 2025k). Among all the tests working within the Bayesian framework, only the two analyses using BayesWave (RT and E-MM-BayesWave) performed the trans-dimensional sampling using a reversible-jump Markov Chain Monte Carlo algorithm (Cornish & Littenberg 2015).

The results of the parameter estimation are presented as a set of samples for each model $\{\theta_i(\mathbb{M})\}$ as well as a single number that quantifies the agreement with GR. For some analyses this number is a Bayes factor, while for others where GR is a nested model of a more general model (like in the example above), it is the quantile at which GR is found for the marginalized distributions, with smaller values indicating better consistency with GR. For some tests examining a two-dimensional deviation space, we also quote the two-dimensional GR quantile $\mathcal{Q}^{\rm 2D}_{\rm GR}$, denoting the fraction of the posterior enclosed by the isoprobability contour that passes through the GR value. Thus, smaller values of $\mathcal{Q}^{\rm 2D}_{\rm GR}$ indicate better consistency with GR. The same definition holds for higher-dimensional GR quantiles.

3.2. *Waveform Models and Automation*

The deviations from GR are implemented on top of the GR waveform models. RT, IMRCT, SMA, TIGER, PCA, SIM, MDR, SSB, and E-WFM have used the IMRPhenomXPHM model (Pratten et al. 2021) as the default, usually in its IMRPhenomXPHM_SpinTaylor version (Colleoni et al. 2025b). Thus, we will use IMRPhenomXPHM as a shorthand for IMRPhenomXPHM_SpinTaylor in these papers, and use IMRPhenomXPHM_MSA to specify the original model from Pratten et al. (2021) which is used by SIM. FTI, PCA, and SIM have used the SEOBNRv5HM_ROM model (Pompili et al. 2023) and pSEOBNR uses SEOBNRv5PHM (Ramos-Buades et al. 2023). MDR has also used NRSur7dq4 (Varma et al. 2019) for tests of waveform systematic errors. In addition, the FTI analysis also used SEOBNRv4_ROM_NRTidalv2_NSBH (Matas et al. 2020) for GW230518_125908. The analysis performed by LOSA is based on IMRPhenomXP (Pratten et al. 2021, in its original version, which we refer to as IMRPhenomXP_MSA, for clarity), IMRPhenomXP_NRTidalv2 (Colleoni et al. 2025a), and IMRPhenomNSBH (Thompson et al. 2020). A detailed description of these models and references is given in Abac et al. (2025k). The pre-O4 analysis used earlier versions of these waveform models, as described in Abbott et al. (2023).

Some tests of GR require multiple runs probing a discrete set of models. In order to avoid human error in preparing and conducting these runs, we have used automation through the Asimov software library (Williams et al. 2023) together with CBCFlow (Ashton et al. 2025a) for fetching the metadata for some analyses.

We also use *injections*, i.e., simulated signals (either with or without noise), to check the performance of these analyses, and in particular to assess potential deviations from GR.

3.3. *Windowing and the Likelihood*

Late in the paper preparation process, we discovered an error in the likelihood functions used in our analysis (see Section 5.10 in Abac et al. 2025k; Talbot et al. 2025). We incorrectly applied a correction factor intended to compensate for the power loss when applying the Tukey window to our data. Due to the late discovery of the likelihood issue, we were not able to correct all analyses. POL, PYRING, QNMRF, and E-MM-CWB are unaffected. We were able to correct SMA, FTI, TIGER, PCA, SIM, MDR, SSB, and pSEOBNR by reweighting the posteriors. IMRCT, LOSA, and E-WFM analyses were rerun with the correct likelihood, although pre-O4 IMRCT results are not yet corrected. The RES and E-MM-BAYESWAVE analyses are left with the incorrect likelihood and will be corrected later. However, using the correct likelihood leads only to a small difference in the posteriors, although they are systematically wider and the Bayes factor with respect to the noise systematically lower. As an example, for the MDR analysis, the Bayes factors are 21% lower, the posteriors have standard deviations larger by 7%, and their means move by 2% of standard deviation on average for O4a results. The error also applies to previous analyses from O1 to O3, but with lesser effects due to different window settings used. For MDR, the Bayes factors, standard deviations, and means for the GWTC-3.0 results move by 1%, 4%, and 1% respectively. These changes do not modify the overall conclusion of our tests, i.e., that we have no evidence that GR is violated.

3.4. *Hierarchical Inference*

With the ever-increasing number of GW observations, it is important to accurately combine information across the detections made to place the most stringent bounds on deviations from GR. With this in mind, we employ hierarchical inference techniques to construct a summary of the underlying distribution of possible deviations present in the data (Isi et al. 2019; Mandel et al. 2019; Zimmerman et al. 2019). For cases where the parameterized effect is identical across observations, such as in propagation tests, the combined constraint is summarized by single measure of the parameterized effect from all observations. However, in the case where individual observations may not share a common parameter, such as in null tests like those for deviations in PN coefficients, we instead infer the structure of a Gaussian distribution fit to the collection of measured deviation parameters from all events, parameterized with a mean μ and standard deviation σ (Isi et al. 2019). If multiple deviation parameters are measured and hierarchically combined, we infer the full multi-dimensional Gaussian structure and thus have correlation coefficients ρ along with the means and standard deviations (Zhong et al. 2024). This is the first application of the multi-dimensional hierarchical inference technique in an LVK testing GR analysis.

4. TESTS OF CONSISTENCY

4.1. *Residual test*

The residual test involves checking for excess coherent power remaining in the detector network after the best-fit GR template is subtracted from the data. If GR is the correct theory of gravitation, a GR-based template should capture all the features of the astrophysical signal and thus the residuals should be consistent with instrumental noise. We use the same method as in previous analyses (Abbott et al. 2019b, 2021b, 2025).

The noise in ground based GW detectors comes from various sources (Aasi et al. 2015; Abbott et al. 2016d). Detector noise is assumed to be stationary and Gaussian, so the data time series $\boldsymbol{d}(t)$ is composed of the Gaussian noise $\boldsymbol{n}(t)$ and the GW model waveform $\boldsymbol{h}(t)$, and can be modeled as:

$$\boldsymbol{d}(t) = \boldsymbol{h}(t) + \boldsymbol{n}(t), \tag{4}$$

where the boldface notation indicates a quantity with a component corresponding to each detector. Here we choose for the best-fit model of the signal the set of parameters that maximize the likelihood of observing the recorded data under the assumption that the signal is present in the data. These maximum-likelihood parameters minimize the difference between the data $\boldsymbol{d}(t)$ and the template $\boldsymbol{h}(t)$.

Once the best-fit (maximum-likelihood) waveform $\boldsymbol{h}_{\mathrm{maxL}}(t)$ is inferred using a GR template, where we use IMRPHENOMXPHM for the O4a events, the residual $\boldsymbol{r}(t) = \boldsymbol{d}(t) - \boldsymbol{h}_{\mathrm{maxL}}(t)$ can be obtained. If $\boldsymbol{h}_{\mathrm{maxL}}$ is an accurate estimate of the signal based on GR, the residual $\boldsymbol{r}(t)$ should be consistent with noise. This is tested by analyzing the residual using BAYESWAVE (Cornish & Littenberg 2015; Cornish et al. 2021, 2024). BAYESWAVE uses a template-independent model based on Morlet–Gabor wavelets to characterize any coherent feature in the detector network. BAYESWAVE produces a discretized probability distribution in the parameter space of the wavelets, with each point corresponding to a residual that has a well defined SNR. Any loud multi-detector coherent features in the data $\boldsymbol{d}(t)$ that were not captured by the GR based model $\boldsymbol{h}(t)$ are reconstructed. If the true underlying signal was reliably reconstructed by the maximum-likelihood waveform $\boldsymbol{h}_{\mathrm{maxL}}$, the BAYESWAVE reconstruction will have a median that is consistent with noise (Johnson-McDaniel et al. 2022).

To quantify the results, we describe the loudness of the residual by calculating the 90th percentile of the network SNR distribution produced by BAYESWAVE, SNR_{90}. That is, there is a 90% probability that after subtracting $\boldsymbol{h}_{\mathrm{maxL}}$, the residual signal has an optimal network SNR $\leq \mathrm{SNR}_{90}$. For the case of Gaussian noise in the LIGO Hanford, LIGO Livingston, and Virgo network, this tends to be $\lesssim 5$ (Johnson-McDaniel et al. 2022).

We perform a more systematic assessment by defining a p-value under the null hypothesis that the residual is consistent with noise. This is done by running identical BAYESWAVE analysis on 200 randomly selected data segments around the event that cover a time window of 4096 s symmetric

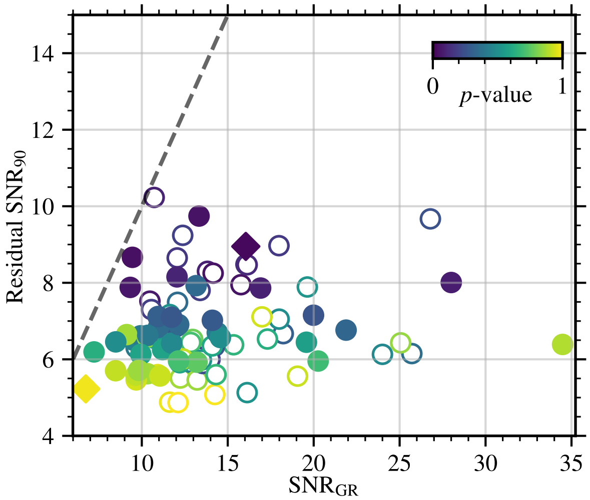

Figure 1. Results of the residuals analysis. Scatter plot of the SNR of the maximum-likelihood template ($\mathrm{SNR_{GR}}$) and the upper limit on the residual network SNR ($\mathrm{SNR_{90}}$) for each event. The color bar denotes the p-values of individual events. Solid (empty) circles represent the O4a (pre-O4a) events, where the pre-O4a events are from Abbott et al. (2019b, 2021b, 2025). The events with the highest and lowest p-values are shown by diamonds. The dashed line represents $\mathrm{SNR_{GR}} = \mathrm{SNR_{90}}$. We see that $\mathrm{SNR_{GR}} \geq \mathrm{SNR_{90}}$ for all events considered.

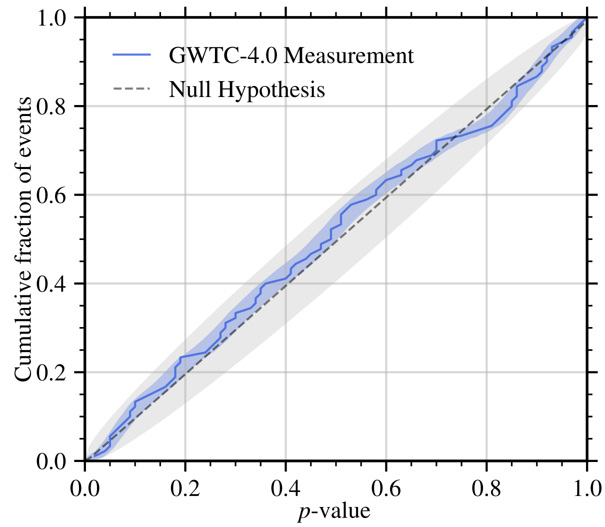

Figure 2. Results of the residuals analysis. The blue line shows the fraction of events with p-values of the residual SNR less than or equal to the value of the abscissa (PP plot). The 90% credible interval is represented by the shaded blue region due to the finite number of noise-only instantiations. The null hypothesis that the p-value is uniformly distributed over $[0, 1]$ is shown by the diagonal dashed line, with the shaded light grey area denoting the 90% credible interval around the null hypothesis due to the finite number of events.

about the event time and do not contain a known GW signal or any transient non-Gaussian features, and then calculating the probability that instrumental noise alone could produce an SNR^n_{90}, where $\mathrm{SNR}^n_{90} \geq \mathrm{SNR}_{90}$, giving the p-value $= P(\mathrm{SNR}^n_{90} \geq \mathrm{SNR}_{90})$. A higher chance for the residual power to originate from instrumental noise will be reflected in a higher p-value, whereas if the residual power is less likely to come from noise alone, the p-value would be smaller.

Finally, we can quantify how well the GR based template fits the signal in the data. Since our GR templates are not perfect, and we have a probabilistic measurement of the signal in the data, we can quantify this fit using the 90% lower bound on the fitting factor between the model and the signal:

$$\mathrm{FF}_{90} = \frac{\mathrm{SNR_{GR}}}{\sqrt{\mathrm{SNR}^2_{\mathrm{GR}} + \mathrm{SNR}^2_{90}}}, \tag{5}$$

where $\mathrm{SNR_{GR}}$ is the optimal network SNR for $\boldsymbol{h}_{\mathrm{maxL}}$. A value of $\mathrm{FF}_{90} = 1$ indicates perfect agreement between the GR template and the signal in the data.

All events that pass this paper's selection criteria and are analyzed with BBH waveforms are considered. We summarize the results for $\mathrm{SNR_{GR}}$, the residual SNR_{90}, FF_{90}, and p-values for each event in Table 6. Figure 1 shows SNR_{90} versus $\mathrm{SNR_{GR}}$ for both O4a events and pre-O4 events. We confirm that the residual SNR_{90} is always smaller than the original $\mathrm{SNR_{GR}}$. For O4a events, GW230919_215712 has the lowest p-value of 0.02 with a residual $\mathrm{SNR}_{90} = 8.95$, while GW231223_032836 has the highest p-value of 0.98 with a residual $\mathrm{SNR}_{90} = 5.23$. GW231001_140220 has the lowest FF_{90} of 0.75, and a low p-value of 0.04. The mean FF_{90} for O4a events is 0.87, which indicates agreement between the GR templates and the signals in the data.

If our best-fit template has successfully recovered the GW signals, then we expect that the contribution of the residual SNR_{90} comes from the detector noise. This means that the p-values should be distributed uniformly within $[0, 1]$. To confirm the distribution of p-values, we show the probability–probability (PP) plot in Figure 2. The measurement of p-values is subject to uncertainty due to finite number of background runs. If the p-value $\hat{p} = n/N$ is estimated by running on N background segments, of which n produce SNR_{90} greater than that of the event, the likelihood of the estimated p-values is given by a binomial function,

$$\mathcal{L}(\hat{p}) = \binom{N}{n} p^n (1-p)^{N-n}. \tag{6}$$

Assuming a uniform prior distribution for the p-value, the posterior is given by a beta distribution,

$$P(p|N, n) = \mathrm{Beta}(n+1, N-n+1). \tag{7}$$

In Figure 2, the shaded region around the PP curve represents the 90% credible interval of the p-value posterior.

Table 6. Results from the residuals analysis for O4a events.

Events	$\mathrm{SNR}_{\mathrm{GR}}$	Res. SNR_{90}	FF_{90}	p-value
GW230518_125908	12.01	6.86	0.87	0.28
GW230601_224134	13.33	9.74	0.81	0.05
GW230605_065343	10.65	6.56	0.85	0.53
GW230606_004305	10.92	5.60	0.89	0.95
GW230609_064958	9.51	6.50	0.83	0.44
GW230624_113103	9.93	6.61	0.83	0.41
GW230627_015337	28.00	8.01	0.96	0.08
GW230628_231200	14.39	6.70	0.91	0.42
GW230630_234532	10.33	5.62	0.88	0.86
GW230702_185453	8.47	5.70	0.83	0.91
GW230731_215307	10.97	6.84	0.85	0.35
GW230811_032116	14.57	6.57	0.91	0.49
GW230814_061920	9.12	6.65	0.81	0.86
GW230824_033047	10.32	6.57	0.84	0.82
GW230904_051013	10.35	6.63	0.84	0.40
GW230914_111401	16.91	7.86	0.91	0.09
GW230919_215712	16.05	8.95	0.87	0.02
GW230920_071124	11.21	6.25	0.87	0.58
GW230922_020344	11.74	6.42	0.88	0.47
GW230922_040658	9.94	6.13	0.85	0.58
GW230924_124453	12.14	6.91	0.87	0.34
GW230927_043729	9.33	7.88	0.77	0.06
GW230927_153832	19.99	7.15	0.94	0.26
GW230928_215827	7.22	6.19	0.77	0.63
GW231001_140220	9.45	8.67	0.75	0.04
GW231020_142947	10.95	7.12	0.84	0.30
GW231028_153006	20.26	5.95	0.96	0.69
GW231102_071736	13.16	7.93	0.86	0.34
GW231104_133418	9.67	5.46	0.87	0.93
GW231108_125142	13.21	5.92	0.91	0.75
GW231110_040320	9.66	5.59	0.87	0.90
GW231113_200417	11.06	5.56	0.89	0.92
GW231114_043211	8.49	6.46	0.80	0.49
GW231118_005626	11.73	7.10	0.86	0.27
GW231118_090602	12.05	8.15	0.83	0.10
GW231123_135430	19.58	6.45	0.95	0.56
GW231206_233134	12.14	5.96	0.90	0.70
GW231206_233901	21.88	6.76	0.96	0.33
GW231213_111417	9.82	5.71	0.86	0.85
GW231223_032836	6.74	5.23	0.80	0.98
GW231224_024321	14.11	7.02	0.90	0.28
GW231226_101520	34.48	6.39	0.98	0.88

NOTE—For each event we list the SNR of the best-fit waveform ($\mathrm{SNR}_{\mathrm{GR}}$), the 90% credible upper limit on the residual coherent network SNR (SNR_{90}), the 90% credible lower limit on the fitting factor FF_{90}, and the p-value calculated from the background analysis.

While the residuals analysis is in principle sensitive to any of the deviations from GR to which the other tests considered are sensitive, in practice it is less sensitive to a given GR deviation than a more specific test, particularly when the deviation is not well localized in time, as is the case for low-mass compact binary signals (Johnson-McDaniel et al. 2022).

4.2. *Inspiral–merger–ringdown consistency test*

The IMR consistency test checks for the consistency of the estimates of the final mass and final spin of the remnant BH inferred independently from the low- and high-frequency parts of the GW signal emitted by a BBH merger (Hughes & Menou 2005; Ghosh et al. 2016, 2018). For the current implementation of the IMR consistency test, we first estimate the component masses, dimensionless spins, and spin angles from both the low- and high-frequency portions of the signal. Next, we apply NR-calibrated fits on the masses and spins inferred for each frequency regime to compute the final mass and final spin of the remnant BH (Hofmann et al. 2016; Healy & Lousto 2017; Jiménez-Forteza et al. 2017), where the specifics of the calculation are described in Abac et al. (2025k). If the observed signal is correctly described by a quasi-circular BBH coalescence in GR, then the estimates of the mass and spin of the remnant BH from the two frequency regimes will be in agreement. However, any deviations from GR could lead to discrepancies between the two estimates. Some studies have shown that the IMR consistency test leads to false violations of GR for simulated GW signals with unequal masses along with either high spin or near-face-on inclinations (Narayan et al. 2023, 2026). The fraction of events affected by this bias is expected to be negligible in GWTC-4.0, and could be quantified by a performing a comprehensive set of simulations for future catalogs.

The separation between the low- and high-frequency parts of the signal is rather arbitrary as long as both parts have sufficient SNRs. In this analysis, we divide the signal in the frequency domain at the cutoff frequency $f_{\mathrm{c}}^{\mathrm{IMR}}$, the dominant multipole GW frequency of the innermost stable circular orbit of the remnant Kerr BH (Bardeen et al. 1972). To determine this, we compute the posterior distribution on the cutoff frequency from the posteriors on the masses and spins inferred using the full IMR signal. The median of the cutoff frequency is then used to split the GW signal. This is different than previous analyses where the cutoff frequency was calculated from the medians of the component masses and spins inferred from the full IMR signal (Abbott et al. 2019b, 2021b, 2025), though it only leads to a $\lesssim 1$ Hz difference in the results.

The low- and high-frequency regimes roughly correspond to the inspiral and post-inspiral, respectively, of the dominant mode of the waveform. To make sure that the two regimes of the signal have enough information, we calculate the SNR of the inspiral and the post-inspiral parts of the waveform for each event using their maximum a posteriori parameter values obtained from the full IMR signal.

We only perform the test on those events that have SNRs greater than 6 in both the inspiral and the post-inspiral parts (Abbott et al. 2019b, 2021b, 2025). We also impose an extra

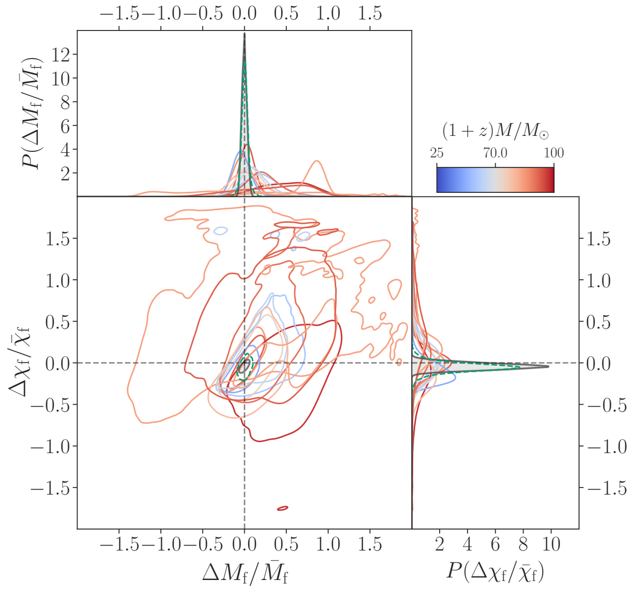

Figure 3. The main panel shows the 90% credible regions of the 2D posteriors on $(\Delta M_f/\bar{M}_f, \Delta\chi_f/\bar{\chi}_f)$ assuming a uniform prior, with $(0,0)$ being the expected value for GR. The side panels show the marginalized posterior on $\Delta M_f/\bar{M}_f$ and $\Delta\chi_f/\bar{\chi}_f$. The unfilled solid contours correspond to the individual O4a events, colored by their median redshifted total mass, while the filled contours are the results from the joint posterior. The dashed green contours correspond to hierarchically inferred bounds on the fractional deviation parameters.

constraint on the median value of the total redshifted mass $(1+z)M < 100\,M_\odot$ to ensure enough inspiral signal for heavier BBHs (Abbott et al. 2021b, 2025). We find that 13 events satisfy the selection criteria in O4a. The SNRs for the full IMR, inspiral, and post-inspiral regimes (for the maximum a posteriori waveform) along with the cutoff frequency $f_c^{\rm IMR}$ of the events analyzed are reported in Table 7.

We start by estimating the posterior distributions on the mass M_f and the dimensionless spin χ_f of the remnant BH from both the inspiral and the post-inspiral parts of the signal. To quantify the consistency between the two estimates, or a possible deviation from GR, we define two fractional deviation parameters $\Delta M_f/\bar{M}_f$ and $\Delta\chi_f/\bar{\chi}_f$:

$$\frac{\Delta M_f}{\bar{M}_f} = 2\frac{M_f^{\rm I} - M_f^{\rm PI}}{M_f^{\rm I} + M_f^{\rm PI}}, \quad \frac{\Delta\chi_f}{\bar{\chi}_f} = 2\frac{\chi_f^{\rm I} - \chi_f^{\rm PI}}{\chi_f^{\rm I} + \chi_f^{\rm PI}}, \tag{8}$$

where $\bar{M}_f$ and $\bar{\chi}_f$ denote the averages of the final mass and final spin obtained from analyzing the inspiral and post-inspiral parts of the signal, respectively. The superscripts here refer to the inspiral (I) and the post-inspiral (PI) portions of the signal. The two-dimensional posterior distribution of these fractional deviation parameters should peak around $(0,0)$ if the observed signal corresponds to a quasi-circular BBH merger described by GR.

Table 7. Results from the IMR consistency test for O4a events.

Event	$(1+z)M$ $[M_\odot]$	$f_c^{\rm IMR}$ [Hz]	$\rho_{\rm IMR}$	$\rho_{\rm I}$	$\rho_{\rm PI}$	$\mathcal{Q}_{\rm GR}^{\rm 2D}$ [%]
GW230606_004305	94^{+15}_{-12}	96	10.9	7.4	8.0	38.1
GW230609_064958*	95^{+13}_{-11}	94	9.5	6.0	7.4	···
GW230628_231200	$82.9^{+6.5}_{-5.7}$	118	14.4	10.9	9.5	90.1
GW230811_032116	$79.5^{+7.0}_{-5.4}$	121	14.6	12.4	7.7	14.7
GW230919_215712	$61.6^{+3.3}_{-2.9}$	174	16.1	14.2	7.6	7.6
GW230920_071124	$84.1^{+9.8}_{-7.0}$	115	11.1	8.5	7.2	59.9
GW230922_020344	$89.5^{+8.7}_{-7.2}$	111	11.7	8.6	8.0	38.3
GW230924_124453	$73.7^{+5.6}_{-4.6}$	133	12.1	9.9	7.1	9.9
GW230927_153832	$46.9^{+1.7}_{-1.1}$	207	20.0	17.7	9.4	37.0
GW231108_125142	$55.6^{+2.9}_{-2.5}$	166	13.2	11.3	6.9	32.0
GW231206_233134	$97.5^{+10.4}_{-9.9}$	96	11.7	8.4	8.2	88.6
GW231206_233901	$84.5^{+5.1}_{-4.5}$	113	21.9	16.5	14.4	24.5
GW231226_101520	$91.8^{+3.7}_{-3.5}$	102	34.5	26.7	21.8	14.8

NOTE—The median and 90% credible interval of the redshifted total mass come from the analysis in Abac et al. (2025b); $f_c^{\rm IMR}$ denotes the cutoff frequency between the inspiral and post-inspiral regimes; $\rho_{\rm IMR}$, $\rho_{\rm I}$, and $\rho_{\rm PI}$ are the SNR in the full signal, the inspiral part, and the post-inspiral part respectively; and the GR quantile $\mathcal{Q}_{\rm GR}^{\rm 2D}$ is defined in Section 3.1 (and here is obtained from the reweighted posterior). As discussed in the text, we were unable to obtain reliable results for GW230609_064958 due to its low $\rho_{\rm I}$.

We use a phenomenological quasi-circular, precessing frequency domain waveform model, IMRPHENOMXPHM, to perform parameter estimation on the inspiral and post-inspiral parts of the signals. We assume uniform priors on the detector-frame component masses and spins. These priors translate into nontrivial priors on $\Delta M_f/\bar{M}_f$ and $\Delta\chi_f/\bar{\chi}_f$. Thus, similar to previous analyses (Abbott et al. 2021b, 2025), we reweight the posteriors to obtain uniform priors on the deviation parameters. The results are plotted in Figure 3, where the contours correspond to 90% credible regions of the two-dimensional posteriors on the fractional deviation parameters for the O4a events which satisfy our selection criteria. We do not find any deviation from GR for any of the events. The two-dimensional GR quantile values $\mathcal{Q}_{\rm GR}^{\rm 2D}$ for the events are given in Table 7. $\mathcal{Q}_{\rm GR}^{\rm 2D}$ is defined as the fraction of the posterior enclosed by the isoprobability contour that passes through $(0,0)$, the GR value. Smaller values indicate better consistency with GR. All events in O4a have $\mathcal{Q}_{\rm GR}^{\rm 2D} \leq 90.1\%$.

We were unable to obtain reliable results for GW230609_064958 due to its low inspiral SNR, which led to significant railing in the chirp mass and luminosity distance posteriors even when extending the prior range to values well beyond those expected physically. We also

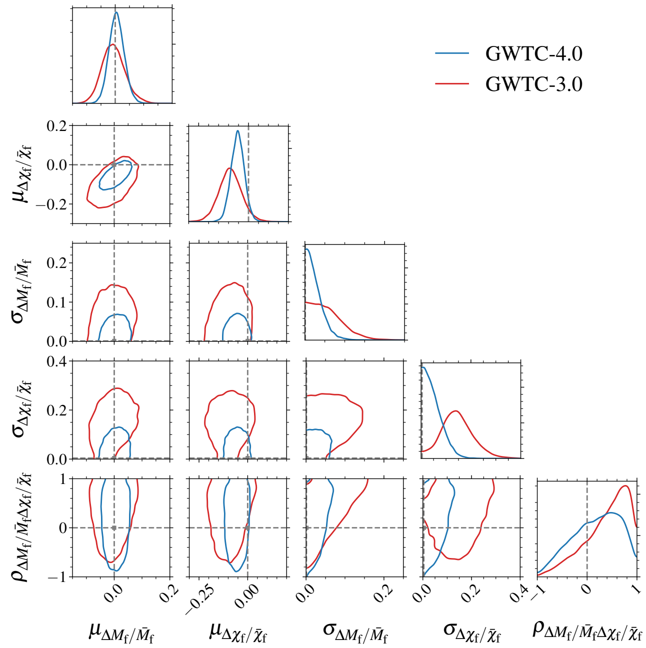

Figure 4. Result of the two-dimensional hierarchical analyses on $\Delta M_\mathrm{f}/\bar{M}_\mathrm{f}$ and $\Delta\chi_\mathrm{f}/\bar{\chi}_\mathrm{f}$ joint measurements from GWTC-4.0 events including GW190814. The five hyperparameters characterizing the population model are defined in the main text. The contours enclose 90% probability mass. The blue and red contours correspond to the estimates using GWTC-4.0 and GWTC-3.0 (Zhong et al. 2024; Abbott et al. 2025). GR corresponds to $\mu_{\Delta M_\mathrm{f}/\bar{M}_\mathrm{f}} = \sigma_{\Delta M_\mathrm{f}/\bar{M}_\mathrm{f}} = \mu_{\Delta\chi_\mathrm{f}/\bar{\chi}_\mathrm{f}} = \sigma_{\Delta\chi_\mathrm{f}/\bar{\chi}_\mathrm{f}} = 0$ (gray dashed line).

found significant railing in the mass-ratio posterior even when extending the prior range to the minimum value of 0.02 for which IMRPhenomXPHM is deemed to be able to be extrapolated without committing large errors (Abbott et al. 2023). Railing against the lower bound on the mass ratio also affects GW230920_071124 post-inspiral significantly, where there is also a long tail in the luminosity distance that has some slight railing against a prior boundary that is well above what is expected physically. However, the railing in the distance is slight enough that we quote results for this event even though the results are affected by our choice of prior boundaries. The railing in these cases with SNRs close to the cutoff suggests that we should increase the minimum SNR in the IMRCT selection criteria.

The deviations are only constrained modestly for most of the events with moderate SNRs. However, one can combine the likelihoods on the deviation parameters for multiple events to improve these constraints. We do this by first interpolating the reweighted posteriors on the fractional deviation parameters $\Delta M_\mathrm{f}/\bar{M}_\mathrm{f}$ and $\Delta\chi_\mathrm{f}/\bar{\chi}_\mathrm{f}$ of individual events on a grid with bounds $[-2, 2]$ for both the parameters, and then multiplying the interpolated posteriors to obtain the joint posterior. Here, we assume the deviation does not lie outside the above range for all events. As shown in gray in Figure 3, the joint posterior on the fractional deviation parameters of GWTC-4.0 events is consistent with the GR prediction with $(\Delta M_\mathrm{f}/\bar{M}_\mathrm{f})_\mathrm{joint} = -0.00^{+0.05}_{-0.05}$ and $(\Delta\chi_\mathrm{f}/\bar{\chi}_\mathrm{f})_\mathrm{joint} = -0.04^{+0.07}_{-0.06}$. The GR quantile of the joint posterior is 89.1%, an increase from the result of 79.6% obtained for GWTC-3.0 (Abbott et al. 2025).

Figure 4 shows the posterior distribution for the hyperparameters from the multi-dimensional hierarchical analysis, with contours indicating the 90% credible regions. The five hyperparameters are the mean and standard deviation of $\Delta M_\mathrm{f}/\bar{M}_\mathrm{f}$ ($\mu_{\Delta M_\mathrm{f}/\bar{M}_\mathrm{f}}$, $\sigma_{\Delta M_\mathrm{f}/\bar{M}_\mathrm{f}}$), the mean and standard deviation of $\Delta\chi_\mathrm{f}/\bar{\chi}_\mathrm{f}$ ($\mu_{\Delta\chi_\mathrm{f}/\bar{\chi}_\mathrm{f}}$, $\sigma_{\Delta\chi_\mathrm{f}/\bar{\chi}_\mathrm{f}}$), and the correlation between the two ($\rho_{\Delta M_\mathrm{f}/\bar{M}_\mathrm{f}\Delta\chi_\mathrm{f}/\bar{\chi}_\mathrm{f}}$). The GR prediction corresponds to $\mu_{\Delta M_\mathrm{f}/\bar{M}_\mathrm{f}} = \sigma_{\Delta M_\mathrm{f}/\bar{M}_\mathrm{f}} = \mu_{\Delta\chi_\mathrm{f}/\bar{\chi}_\mathrm{f}} = \sigma_{\Delta\chi_\mathrm{f}/\bar{\chi}_\mathrm{f}} = 0$, while $\rho_{\Delta M_\mathrm{f}/\bar{M}_\mathrm{f}\Delta\chi_\mathrm{f}/\bar{\chi}_\mathrm{f}}$ indicates the population-level correlation between $\Delta M_\mathrm{f}/\bar{M}_\mathrm{f}$ and $\Delta\chi_\mathrm{f}/\bar{\chi}_\mathrm{f}$. The addition of new events from the latest observation run yields a more stringent constraints on the hyperparameters. In the previous analysis using GWTC-3.0 events, the inclusion of the event GW190814 produced a non-zero peak in the $\sigma_{\Delta\chi_\mathrm{f}/\bar{\chi}_\mathrm{f}}$ posterior (Zhong et al. 2024), as illustrated in Figure 4. With the new events incorporated, however, the peak shifts back toward zero. We also show the population-marginalized constraint from the hierarchical analysis in Figure 3. The hierarchical inference finds that $(\Delta M_\mathrm{f}/\bar{M}_\mathrm{f})_\mathrm{hier} = 0.00^{+0.07}_{-0.06}$ and $(\Delta\chi_\mathrm{f}/\bar{\chi}_\mathrm{f})_\mathrm{hier} = -0.05^{+0.11}_{-0.11}$, and the GR quantile for the hierarchically combined distribution is 73.1%, considering both means and standard deviations. However, if one just considers the two means, which show a shift away from GR in Figure 4 similar to that seen in the joint posterior in Figure 3, then one obtains a GR quantile of 94.2%, larger than the one obtained from the joint posterior. We still find that this apparent deviation from GR is driven by GW190814, since if we exclude that event from the combined results, the GR quantile from the two means reduces to 78.7%, while the one from the combined posteriors reduces to 86.0%. The apparent GR deviation from GW190814 itself (GR quantile of 99.9%) is due to a prior effect, from its low post-inspiral SNR, as discussed in Abbott et al. (2021b). Specifically, the final spin inferred from the post-inspiral is around 0.7, while the final spin inferred from the many inspiral cycles is well constrained around 0.28. Thus, since this is purely due to the prior, there is no evidence for a GR deviation here.

4.3. *Subdominant multipole amplitudes*

GW radiation from compact binaries can be expressed using $s = -2$ spin-weighted spherical harmonics $Y^{\ell m}_{-2}(\theta, \phi)$ (Gelfand et al. 1958; Newman & Penrose 1966; Creighton & Anderson 2011) as

$$h(t, \theta_{JN}, \boldsymbol{\lambda}) = \sum_{\ell=2}^{\infty} \sum_{m=-\ell}^{\ell} Y^{\ell m}_{-2}(\theta_{JN}, 0)\, h_{\ell m}(t, \boldsymbol{\lambda}), \quad (9)$$

where $h(t)$ is the time-domain strain, (θ, ϕ) denotes the direction of radiation in the source-frame, and $\boldsymbol{\lambda}$ represents the source parameters, including component masses and spins.

Here we have used the convention in the IMRPHENOMXPHM waveform model, so $(\theta, \phi) = (\theta_{JN}, 0)$ (Pratten et al. 2021), where θ_{JN} is the angle between the total angular momentum of the binary and the line of sight. The quadrupolar $(\ell, m) = (2, \pm 2)$ multipole moments dominate the signal, but subdominant higher-order multipole moments (HOMs) become significant in asymmetric-mass systems, particularly for orientations that are not close to face-on or face-off ($\theta_{JN} = 0$ or π).

The SMA test evaluates the consistency of the HOM amplitudes with general relativity predictions (Islam et al. 2020; Puecher et al. 2022; Gupta et al. 2025). Using the IMRPHENOMXPHM waveform model, this test constrains amplitude deviations $\delta A_{\ell m}$ in the $(2, \pm 1)$ and $(3, \pm 3)$ multipole moments (currently just considered separately):

$$\begin{aligned} h(t, \theta_{JN}, \boldsymbol{\lambda}) = &\sum_{m=\pm 2} Y_{-2}^{2m}(\theta_{JN}, 0)\, h_{2m}(t, \boldsymbol{\lambda}) \\ &+ \sum_{m=\pm 1} \big(1 + \delta A_{21}\big) Y_{-2}^{2m}(\theta_{JN}, 0)\, h_{2m}(t, \boldsymbol{\lambda}) \\ &+ \sum_{m=\pm 3} \big(1 + \delta A_{33}\big) Y_{-2}^{3m}(\theta_{JN}, 0)\, h_{3m}(t, \boldsymbol{\lambda}) \\ &+ \sum_{\text{other HOM}} Y_{-2}^{\ell m}(\theta_{JN}, 0)\, h_{\ell m}(t, \boldsymbol{\lambda}). \end{aligned} \quad (10)$$

For a GW event, meaningful constraints on $\delta A_{\ell m}$ require sufficient SNR in the relevant (ℓ, m) multipole moment. The multipole moment-wise SNR, $\rho_{\ell m}$, is computed by using the component of $h_{\ell m}$ orthogonal to the $(2, 2)$ multipole moment, and calculating the corresponding optimal SNR (Mills & Fairhurst 2021). In the absence of a (ℓ, m) multipole moment in data, $\rho_{\ell m}$, in Gaussian noise, follows a χ distribution (i.e., the square root of a χ^2-distributed variable) with two degrees of freedom (Abbott et al. 2020b; Fairhurst et al. 2020; Mills & Fairhurst 2021). Deviations from this distribution indicate the presence of the multipole moment in the data. Events are selected for this test when the lower bound of the 68% credible interval of the $\rho_{\ell m}$ distribution exceeds 2.145 (the 90-th percentile of a χ distribution).

GW231123 (Abac et al. 2025j) is the only event from the O4a observing run that satisfies our selection criteria, exhibiting significant SNR in both the $(2, \pm 1)$ and $(3, \pm 3)$ multipoles. However, substantial waveform systematics were previously identified for this signal (Abac et al. 2025j). These waveform systematics are expected to impact tests of GR, and indeed, as discussed in Appendix A of Paper II, the MDR test finds significant apparent GR deviations when analyzing this event using the same IMRPHENOMXPHM model used for the SMA test. When the SMA test is applied to this event, the posterior distributions for both δA_{21} and δA_{33} accumulate near the edges of the prior range (we use uniform priors in the range $[-10, 10]$), indicating pronounced (spurious) deviations from GR (Gupta et al. 2025).

Additionally, events GW190412 (Abbott et al. 2020b) and GW190814 (Abbott et al. 2020c) from O3a exhibit sufficient SNR in the $(3, \pm 3)$ multipole moments to enable the application of this analysis. Figure 5 presents the resulting constraints on δA_{33} for these events. We find $\delta A_{33} = 0.53^{+3.43}_{-5.85}$ for GW190412, and $\delta A_{33} = -0.21^{+1.82}_{-3.39}$ for GW190814. GW190814 provides stronger constraints due to the higher SNR in the $(3, \pm 3)$ multipole moment, resulting from the significant asymmetry in the masses of the binary components. In both events the GR prediction ($\delta A_{33} = 0$) lies well within the 90% credible interval. However, in both cases, the posterior distributions for δA_{33} are characteristically bimodal, arising from degeneracies between δA_{33}, the binary inclination, and the reference orbital phase (Puecher et al. 2022). This bimodality reflects the limited ability of current data to disentangle multipole amplitude deviations from source geometry, rather than indicating a true departure from GR. Indeed, even for the loud O4b event GW241011 (Abac et al. 2025i), which allows this test to place the best constraints so far, due to the unequal masses of its source, the bimodality is reduced significantly, but not eliminated.

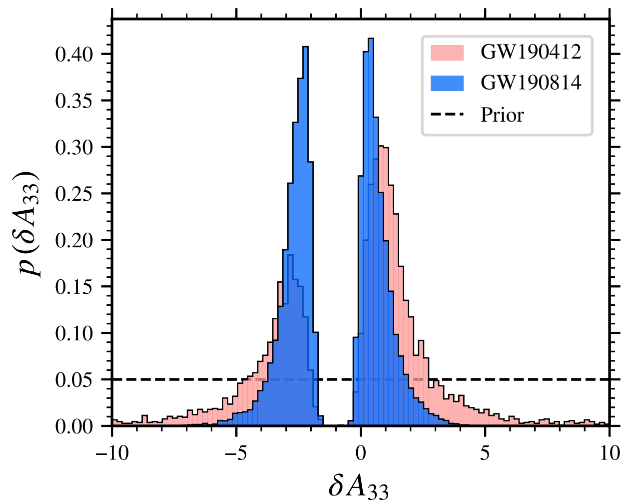

Figure 5. Constraints on amplitude deviation parameters $\delta A_{\ell m}$ for GW190412 and GW190814.

5. TESTS OF POLARIZATION

Polarization tests (Wong et al. 2021) involve constructing a linear combination of strain data, called the null stream, to eliminate excess power and compare the residual data to noise, allowing one to constrain possible non-tensorial polarizations of GWs. The null stream is determined geometrically, relying solely on the beam pattern function (Forward 1978; Gürsel & Tinto 1989; Nishizawa et al. 2009; Błaut 2012; Isi et al. 2015; Isi & Weinstein 2017), which describes detector responses to GWs, independent of the waveform morphology.

In the frequency domain, the observation model is expressed as

$$\tilde{\boldsymbol{d}}(f; \Delta \boldsymbol{t}) = \boldsymbol{F}(\alpha, \delta, \psi, t_{\text{event}}) \tilde{\boldsymbol{h}}(f) + \tilde{\boldsymbol{n}}(f; \Delta \boldsymbol{t}), \quad (11)$$

where $\tilde{\boldsymbol{d}}(f; \Delta \boldsymbol{t})$ is the time-shifted strain data at the geocenter, $\boldsymbol{F}(\alpha, \delta, \psi, t_{\text{event}})$ is the beam pattern matrix, $\tilde{\boldsymbol{h}}(f)$ represents

Table 8. Polarization modes and their corresponding basis choices for the polarization analysis.

Hypothesis	Polarization modes	Pol. basis modes
Scalar (S)	b	b
Vector (V)	x, y	x
Tensor (T)	$+, \times$	$+$
Tensor–scalar (TS)	$+, \times$, b	$+$
Tensor–vector (TV)	$+, \times$, x, y	$+$
Vector–scalar (VS)	x, y, b	x
Tensor–vector–scalar (TVS)	$+, \times$, x, y, b	$+$

NOTE—The tensor plus and cross modes are denoted as "$+$" and "$\times$," respectively, while the vector x and y modes are labeled "x" and "y." The scalar breathing mode is represented by "b." Only the breathing mode is considered for scalar polarizations, as the longitudinal mode is degenerate with it.

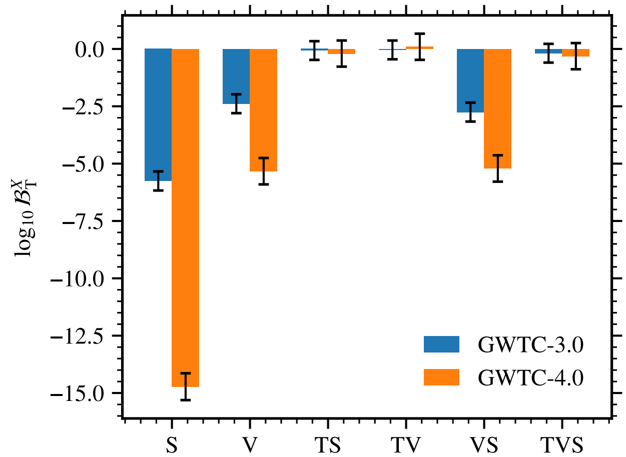

Figure 6. Comparison of $\log_{10}$ Bayes factors $\mathcal{B}_{\rm T}^X$ for various polarization hypotheses (S, V, TS, TV, VS, TVS) against the tensor hypothesis, for GWTC-3.0 and GWTC-4.0. Polarization states are projected onto one basis mode as detailed in Table 8. Positive (negative) values indicate that the hypothesis in the superscript is favored (disfavored) relative to the tensor hypothesis. Error bars represent 90% credible intervals.

polarization modes at the geocentric time, and $\tilde{\boldsymbol{n}}(f; \Delta \boldsymbol{t})$ is the detector noise, also time-shifted to the geocenter. α and δ denote the source's right ascension and declination, ψ is the polarization angle, and $\Delta \boldsymbol{t} = \Delta \boldsymbol{t}(\alpha, \delta, t_{\rm event})$ represents the time delays from the geocenter to the detectors. Since the beam pattern function varies negligibly over the duration of the GW transients considered, it is approximated as constant throughout.

The null stream construction can be formulated as a projection using the projector constructed from the beam pattern matrix $\boldsymbol{F}$ (Wong et al. 2021). The projector removes data within the hyperplane spanned by the column vectors of $\boldsymbol{F}$, irrespective of the waveform morphology of $\boldsymbol{h}(f)$. Here $\boldsymbol{F}$ defines the polarization model; for instance, in a scalar–tensor model:

$$\boldsymbol{F} = \left[\boldsymbol{f}_+ \;\; \boldsymbol{f}_\times \;\; \boldsymbol{f}_{\rm b} \right], \tag{12}$$

where the column vectors $\boldsymbol{f}_+$, $\boldsymbol{f}_\times$, and $\boldsymbol{f}_{\rm b}$ represent the plus, cross, and scalar breathing polarization modes, respectively. The ith entry of the column vectors, $\boldsymbol{f}_{+/\times/{\rm b}}$, corresponds to the beam pattern function of the ith detector for the $+/\times/$scalar breathing polarization mode. The scalar longitudinal mode, being degenerate with the scalar breathing mode, is excluded from the matrix.

The number of detectors must exceed the number of columns in the beam pattern matrix. However, for O1 and O4a, only two detectors were operational, constraining the analysis to a single effective polarization mode. We assume the polarization modes are similar to chosen basis modes indicated in Table 8, differing at most by a complex scaling factor (Wong et al. 2021), in a manner similar to the elliptical parameterization in Lee et al. (2025). This assumption defines the effective beam pattern matrix used in the analysis and imposes a simplifying structure on the polarization subspace (e.g., in the single basis mode case for tensorial signals, it is equivalent to testing consistency with $h_\times = \mathcal{C} h_+$ for a complex constant $\mathcal{C}$). However, the null-stream approach remains robust to such assumptions because it is a projection-based test that searches for excess power in the direction orthogonal to the assumed subspace, making it more tolerant to inaccuracies in the polarization model than fully modeled (template-based) searches, which require precise agreement in both polarization content and waveform evolution. A concrete illustration for non-tensorial signals is provided by scalar–tensor models, where one can choose the plus mode as the basis and assume similarity with the cross and scalar breathing modes, leading to the effective beam pattern matrix

$$\boldsymbol{F}_{\rm scalar-tensor,eff} = \left[\boldsymbol{f}_+ + \mathcal{C}_\times \boldsymbol{f}_\times + \mathcal{C}_{\rm b} \boldsymbol{f}_{\rm b} \right], \tag{13}$$

where $\mathcal{C}_\times$ and $\mathcal{C}_{\rm b}$ are complex scaling factors. This method, independent of the waveform of the basis mode $\tilde{h}_+$, is sensitive only to the geometric projection of the polarization modes in the detector responses. Assuming similarity between polarization modes addresses the limitation posed by the number of detectors. Any violation of this assumption would indicate a signal component orthogonal to the signal space of the GR waveform model, which should appear in the residual test described in Section 4.1. However, as discussed there, dedicated analyses are more sensitive to given GR deviations than the residuals test is.

We use a Bayesian framework to compute the evidence for each polarization hypothesis by sampling parameters $\boldsymbol{\theta} = \{\alpha, \delta, \psi, t_{\rm event}, \boldsymbol{\mathcal{C}}\}$ using the DYNESTY sampler. Here, $\boldsymbol{\mathcal{C}}$ are the complex scaling factors of the polarization modes relative to the basis mode(s). The number of scaling factors de-

Table 9. Results from the polarizations analysis.

Events	$\log_{10}\mathcal{B}_{\rm T}^{\rm S}$	$\log_{10}\mathcal{B}_{\rm T}^{\rm V}$	$\log_{10}\mathcal{B}_{\rm T}^{\rm TS}$	$\log_{10}\mathcal{B}_{\rm T}^{\rm TV}$	$\log_{10}\mathcal{B}_{\rm T}^{\rm VS}$	$\log_{10}\mathcal{B}_{\rm T}^{\rm TVS}$
GWTC-3.0	$-5.76^{+0.42}_{-0.42}$	$-2.39^{+0.41}_{-0.41}$	$-0.07^{+0.41}_{-0.41}$	$-0.04^{+0.41}_{-0.41}$	$-2.75^{+0.41}_{-0.41}$	$-0.19^{+0.41}_{-0.41}$
O4a	$-8.97^{+0.41}_{-0.41}$	$-2.94^{+0.40}_{-0.40}$	$-0.13^{+0.40}_{-0.40}$	$0.14^{+0.40}_{-0.40}$	$-2.46^{+0.40}_{-0.40}$	$-0.13^{+0.40}_{-0.40}$
GWTC-4.0	$-14.72^{+0.59}_{-0.59}$	$-5.33^{+0.58}_{-0.58}$	$-0.20^{+0.57}_{-0.57}$	$0.10^{+0.57}_{-0.57}$	$-5.21^{+0.58}_{-0.58}$	$-0.31^{+0.57}_{-0.57}$

NOTE—Combined $\log_{10}$ Bayes factors $\mathcal{B}$ for various polarization hypotheses against the tensor hypothesis, using both 2-detector and 3-detector events. Polarization states have been projected onto one basis mode as detailed in Table 8. The combined values are obtained by summing the individual $\log_{10}\mathcal{B}_{\rm T}^{X}$ under the assumption that the events are independent. Positive (negative) values indicate that the hypothesis indicated in the superscript is favored (disfavored) with respect to the tensor hypothesis. Error bars refer to 90% credible intervals.

pends on the assumed number of polarization and basis modes. For each polarization hypothesis, we choose a particular polarization mode as the basis, but its waveform morphology is not assumed or involved in the analysis. Instead, only the relative amplitudes $\mathcal{C}$ are used to construct the effective beam pattern matrix for null stream projection. After constructing the null stream time-shifted to the geocenter, we then perform the time–frequency transform (Necula et al. 2012) to obtain the time–frequency representation of the null stream.

The Bayes factor, defined in Equation (3), quantifies the relative plausibility of the hypotheses. We adopt the same uniform priors for sky position, polarization angle, and event time as in previous analyses. For GW170817, instead of adopting a uniform sky prior as for other events, we fix the sky position to the coordinates measured from electromagnetic counterparts (Abbott et al. 2017d). For the complex scaling factors $\mathcal{C}$, the amplitude prior is uniform from 0 to 1, and the phase prior is uniform from 0 to 2π. We report the base-10 logarithm of the Bayes factor $\log_{10}\mathcal{B}_{\rm T}^{X}$ comparing the non-tensor hypothesis X to the tensor hypothesis T.

The likelihood is calculated by summing the contributions of a predefined set of time–frequency pixels $\mathcal{I}$, known as the time–frequency cluster. The time–frequency cluster is constructed by performing the time–frequency transform on the maximum-likelihood GR waveform. The advantages of this approach include both improving the sensitivity of the tests and mitigating the impacts of instrumental noise. However, it reduces sensitivity to some non-tensorial polarizations, such as dominant dipolar scalar radiation at the orbital frequency during the inspiral in scalar–tensor theories (Bernard et al. 2022), when the non-tensorial radiation frequency significantly deviates from that of the tensorial radiation by more than the analysis's frequency resolution of $\Delta f = 16$ Hz in the time–frequency representation. This frequency resolution was selected as a practical choice that still sufficiently resolves the merger phase containing the dominant excess power in CBC signals, providing a corresponding time resolution of $\Delta t \simeq 1/(2\Delta f) \simeq 31$ ms, which is commensurate with the characteristic duration of the merger phase in stellar-mass BBH coalescences, thereby enabling the analysis to capture excess power during coalescence with minimal temporal smearing.

We analyze all the O4a events satisfying the selection criteria of this paper and reanalyze all events from GWTC-3.0 satisfying those criteria using the updated implementation. Figure 6 compares the results for events from GWTC-3.0 and GWTC-4.0. Table 9 lists the combined log Bayes factors for GWTC-3.0 events, O4a events, and GWTC-4.0 events. The scalar, vector, and vector–scalar hypotheses are strongly disfavored compared to the tensor hypothesis, indicating a clear preference for the tensorial polarization modes. After including O4a events, these hypotheses are even more disfavored, with improved constraints on their viability due to the additional data. In contrast, the tensor–scalar, tensor–vector, and tensor–vector–scalar hypotheses show only marginal improvements in their constraints with the inclusion of O4a events, but their results remain uninformative. Since the tensor hypothesis is a subset of these combined hypotheses, they are not expected to be strongly disfavored when the tensor hypothesis represents the ground truth.

6. CONCLUSIONS

The first part of the fourth observing run of the LVK has provided 42 confident events to which we have applied a set of tests of GR. We subjected each of these events, as well as the other confident events from previous observing runs in GWTC-4.0, as appropriate, to some or all of our 19 test pipelines, probing different regimes and potential deviations from GR.

Overall, we find that the data are consistent with GR for all of our gauntlet of tests. More specifically, regarding the four tests of consistency described in this paper, we find consistency of the residuals with noise for all the events. The final mass and final spin inferred using the low- and high-frequency parts of each signal are consistent with each other. We find no evidence for deviations from the GR predictions for the amplitudes of subdominant GW multipole moments, nor for non-GR modes of polarization. The quantitative bounds on deviations are summarized in Table 1, as well as their improvements over previous bounds, if appropriate.

The table also records the bounds and improvements for the tests described in Papers II and III, which are further discussed in those two papers. Example constraints on specific alternative theories from applying some of the PN coefficient bounds obtained in Paper II are given in that paper's Table 3, and that paper also discusses the caveats involved in such translations.

A subset of parameterized tests (from Paper II) and ringdown tests (from Paper III) have found that there are a few events which place the GR parameters outside the 90% posterior probability distribution. This is to be expected statistically with such a high number of tests and independent events, and these are analyzed further in the respective papers II & III. Additionally, there is an apparent GR deviation found in the combined results for the pSEOBNR ringdown test, whose significance is discussed in Paper III, along with studies that indicate a reduced significance. All this indicates the importance of controlling false GR deviations (Gupta et al. 2024) going forward. The effects of non-Gaussian noise (e.g., Kwok et al. 2022) and waveform modeling uncertainties (e.g., Dhani et al. 2025) are expected to be particularly important, with the expected growth in both event numbers and individual signal amplitudes relative to the noise arising from the increase in the detectors' sensitivities (Abbott et al. 2020a),[1] and thus their expanded reach out into the Universe. This is especially pertinent regarding the exceptional single detector events GW230529 (Abac et al. 2024) and GW230814_23 (Abac et al. 2025f), both excluded from these three papers for failing the multiple-detector criterion, but discussed in the separate dedicated papers (GW230529 is analyzed with tests of GR in Sänger et al. 2024), as well as for the two highest mass BBH events that do meet the selection criteria, GW231123 (Abac et al. 2025j) and GW231028_153006 (Abac et al. 2025b). These two high-mass events simultaneously offer the data most appropriate for ringdown analyses (see Section 2 in Paper III), and challenge the systematic accuracy of our waveform models and modeling of detector noise. The results obtained for GW231123 may be due to inaccuracies in waveform modeling, wave-optics lensing, or other features, as described in our dedicated paper on that event (Abac et al. 2025j). Future detector upgrades will provide even higher SNR events and a larger catalog of high-significance signals. These, combined with the more refined analyses required to exploit the data, will allow us to perform ever tighter tests of GR.

All strain data analyzed in this paper are available from the Gravitational Wave Open Science Center (Abac et al. 2025l). The data and scripts used to prepare the figures and tables are available at LIGO Scientific, Virgo, and KAGRA Collaboration (2026).

ACKNOWLEDGEMENTS

This material is based upon work supported by NSF's LIGO Laboratory, which is a major facility fully funded by the National Science Foundation. The authors also gratefully acknowledge the support of the Science and Technology Facilities Council (STFC) of the United Kingdom, the Max-Planck-Society (MPS), and the State of Niedersachsen/Germany for support of the construction of Advanced LIGO and construction and operation of the GEO 600 detector. Additional support for Advanced LIGO was provided by the Australian Research Council. The authors gratefully acknowledge the Italian Istituto Nazionale di Fisica Nucleare (INFN), the French Centre National de la Recherche Scientifique (CNRS) and the Netherlands Organization for Scientific Research (NWO) for the construction and operation of the Virgo detector and the creation and support of the EGO consortium. The authors also gratefully acknowledge research support from these agencies as well as by the Council of Scientific and Industrial Research of India, the Department of Science and Technology, India, the Science & Engineering Research Board (SERB), India, the Ministry of Human Resource Development, India, the Spanish Agencia Estatal de Investigación (AEI), the Spanish Ministerio de Ciencia, Innovación y Universidades, the European Union NextGenerationEU/PRTR (PRTR-C17.I1), the ICSC - CentroNazionale di Ricerca in High Performance Computing, Big Data and Quantum Computing, funded by the European Union NextGenerationEU, the Comunitat Autonòma de les Illes Balears through the Conselleria d'Educació i Universitats, the Conselleria d'Innovació, Universitats, Ciència i Societat Digital de la Generalitat Valenciana and the CERCA Programme Generalitat de Catalunya, Spain, the Polish National Agency for Academic Exchange, the National Science Centre of Poland and the European Union - European Regional Development Fund; the Foundation for Polish Science (FNP), the Polish Ministry of Science and Higher Education, the Swiss National Science Foundation (SNSF), the Russian Science Foundation, the European Commission, the European Social Funds (ESF), the European Regional Development Funds (ERDF), the Royal Society, the Scottish Funding Council, the Scottish Universities Physics Alliance, the Hungarian Scientific Research Fund (OTKA), the French Lyon Institute of Origins (LIO), the Belgian Fonds de la Recherche Scientifique (FRS-FNRS), Actions de Recherche Concertées (ARC) and Fonds Wetenschappelijk Onderzoek - Vlaanderen (FWO), Belgium, the Paris Île-de-France Region, the National Research, Development and Innovation Office of Hungary (NKFIH), the National Research Foundation of Korea, the Natural Sciences and Engineering Research Council of Canada (NSERC), the Canadian Foundation for Innovation (CFI), the Brazilian Ministry of Science, Technology, and Innovations, the International Center for Theoretical Physics South American Institute for Fundamental Research (ICTP-SAIFR), the Research Grants Council of Hong Kong, the National Natural Science Foundation of China (NSFC), the Israel Science Foundation (ISF), the US-Israel Binational Science Fund (BSF), the Leverhulme Trust, the Research Corporation, the National Science and Technology Council (NSTC), Taiwan, the United States Department of Energy, and the Kavli Foundation. The authors gratefully acknowledge the support of the NSF, STFC, INFN and CNRS for provision of computational resources.

This work was supported by MEXT, the JSPS Leading-edge Research Infrastructure Program, JSPS Grant-in-Aid for Specially Promoted Research 26000005, JSPS Grant-in-Aid for Scientific Research on Innovative Areas 2402: 24103006, 24103005, and 2905: JP17H06358, JP17H06361 and JP17H06364, JSPS Core-to-Core Program A. Advanced Research Networks, JSPS Grants-in-Aid for Scientific Re-

[1] LVK observing run plans https://observing.docs.ligo.org/plan

search (S) 17H06133 and 20H05639, JSPS Grant-in-Aid for Transformative Research Areas (A) 20A203: JP20H05854, the joint research program of the Institute for Cosmic Ray Research, University of Tokyo, the National Research Foundation (NRF), the Computing Infrastructure Project of the Global Science experimental Data hub Center (GSDC) at KISTI, the Korea Astronomy and Space Science Institute (KASI), the Ministry of Science and ICT (MSIT) in Korea, Academia Sinica (AS), the AS Grid Center (ASGC) and the National Science and Technology Council (NSTC) in Taiwan under grants including the Science Vanguard Research Program, the Advanced Technology Center (ATC) of NAOJ, and the Mechanical Engineering Center of KEK.

Additional acknowledgements for support of individual authors may be found in the following document: `https://dcc.ligo.org/LIGO-M2300033/public`.

For the purpose of open access, the authors have applied a Creative Commons Attribution (CC BY) license to any Author Accepted Manuscript version arising. We request that citations to this article use 'A. G. Abac *et al.* (LIGO-Virgo-KAGRA Collaboration), ...' or similar phrasing, depending on journal convention.

The following open-source software has been used:

Calibration of the Laser Interferometer Gravitational-Wave Observatory (LIGO) strain data was performed with a GstLAL-based calibration software pipeline (Viets et al. 2018). Calibration of the Virgo strain data is performed with C-based software (Acernese et al. 2022). Data-quality products and event-validation results were computed using the DMT (Zweizig, J. 2006), DQR (LIGO Scientific Collaboration and Virgo Collaboration 2018), DQSEGDB (Fisher et al. 2021), gwdetchar (Urban et al. 2021), hveto (Smith et al. 2011), iDQ (Essick et al. 2020), Omicron (Robinet et al. 2020) and PythonVirgoTools (Virgo Collaboration 2021) software packages and contributing software tools. Analyses in this catalog relied upon the LALSuite software library (LIGO Scientific, Virgo, and KAGRA Collaboration 2025; Wette 2020). The detection of the signals and subsequent significance evaluations in this catalog were performed with the GstLAL-based inspiral software pipeline (Messick et al. 2017; Sachdev et al. 2019; Hanna et al. 2020; Cannon et al. 2021), with the MBTA pipeline (Adams et al. 2016; Aubin et al. 2021), and with the PyCBC (Usman et al. 2016; Nitz et al. 2017; Davies et al. 2020) and the cWB (Klimenko et al. 2004, 2011, 2016) packages. Estimates of the noise spectra and glitch models were obtained using BayesWave (Cornish & Littenberg 2015; Littenberg et al. 2016; Cornish et al. 2021; Gupta & Cornish 2024). Noise subtraction for one candidate was also performed with gwsubtract (Davis et al. 2022). Source-parameter estimation was performed with the Bilby and Parallel-Bilby libraries (Ashton et al. 2019; Romero-Shaw et al. 2020; Smith et al. 2020) using the Dynesty nested sampling package (Speagle 2020). SEOBNRv5PHM waveforms used in parameter estimation were generated using pySEOBNR (Mihaylov et al. 2025). SMA, FTI, TIGER, SIM, LOSA, MDR, SSB, and pSEOBNR waveforms used for testing GR were generated using BilbyTGR (Ashton et al. 2025b). E-M waveforms used for constraining echoes were generated using echoes_waveform_models (Lo et al. 2025). Other analyses used cpnest (Veitch et al. 2025), IGWN Wave Compare (Sullivan et al. 2025), nullpol (Wong et al. 2025), and pyRing (Carullo et al. 2025). Quasinormal mode frequencies were computed using QNM (Stein 2019). The QNMRF analysis used Ma et al. (2025). The multi-dimensional hierarchical analysis results were produced using hierfit (Zhong et al. 2026). PESummary was used to postprocess and collate parameter-estimation results (Hoy & Raymond 2021). The various stages of the parameter-estimation analysis were managed with the Asimov library (Williams et al. 2023) together with CBCFlow (Ashton et al. 2025a). Plots were prepared with Matplotlib (Hunter 2007), seaborn (Waskom 2021), and GWpy (Macleod et al. 2021). NumPy (Harris et al. 2020), scikit-learn (Pedregosa et al. 2011), and SciPy (Virtanen et al. 2020) were used for analyses in the manuscript.

REFERENCES

Aasi, J., et al. 2015, Class. Quantum Grav., 32, 074001, doi: 10.1088/0264-9381/32/7/074001

Abac, A., et al. 2025a. https://arxiv.org/abs/2503.12263

Abac, A. G., et al. 2024, Astrophys. J. Lett., 970, L34, doi: 10.3847/2041-8213/ad5beb

—. 2025b. https://arxiv.org/abs/2508.18082

—. 2025c. https://dcc.ligo.org/LIGO-P2500066/public

—. 2025d. https://dcc.ligo.org/LIGO-P2500067/public

—. 2025e, Astrophys. J. Lett., 995, L18, doi: 10.3847/2041-8213/ae0c06

—. 2025f. https://arxiv.org/abs/2509.07348

—. 2025g. https://arxiv.org/abs/2509.04348

—. 2025h, Phys. Rev. Lett., 135, 111403, doi: 10.1103/kw5g-d732

—. 2025i, Astrophys. J. Lett., 993, L21, doi: 10.3847/2041-8213/ae0d54

—. 2025j, Astrophys. J. Lett., 993, L25, doi: 10.3847/2041-8213/ae0c9c

—. 2025k. https://arxiv.org/abs/2508.18081

—. 2025l. https://arxiv.org/abs/2508.18079

—. 2026, Phys. Rev. Lett., 136, 041403, doi: 10.1103/6c61-fm1n

Abbott, B. P., et al. 2016a, Phys. Rev. Lett., 116, 061102, doi: 10.1103/PhysRevLett.116.061102

—. 2016b, Phys. Rev. Lett., 116, 221101, doi: 10.1103/PhysRevLett.116.221101

—. 2016c, Phys. Rev. X, 6, 041015, doi: 10.1103/PhysRevX.6.041015

—. 2016d, Class. Quantum Grav., 33, 134001, doi: 10.1088/0264-9381/33/13/134001

—. 2017a, Phys. Rev. Lett., 119, 161101, doi: 10.1103/PhysRevLett.119.161101

—. 2017b, Phys. Rev. Lett., 119, 141101, doi: 10.1103/PhysRevLett.119.141101

—. 2017c, Phys. Rev. Lett., 118, 221101, doi: 10.1103/PhysRevLett.118.221101

—. 2017d, Astrophys. J. Lett., 848, L12, doi: 10.3847/2041-8213/aa91c9

—. 2019a, Phys. Rev. Lett., 123, 011102, doi: 10.1103/PhysRevLett.123.011102

—. 2019b, Phys. Rev. D, 100, 104036, doi: 10.1103/PhysRevD.100.104036

—. 2019c, Phys. Rev. X, 9, 031040, doi: 10.1103/PhysRevX.9.031040

—. 2020a, Living Rev. Relativity, 23, 3, doi: 10.1007/s41114-020-00026-9

Abbott, R., et al. 2020b, Phys. Rev. D, 102, 043015, doi: 10.1103/PhysRevD.102.043015

—. 2020c, Astrophys. J. Lett., 896, L44, doi: 10.3847/2041-8213/ab960f

—. 2021a, Astrophys. J. Lett., 915, L5, doi: 10.3847/2041-8213/ac082e

—. 2021b, Phys. Rev. D, 103, 122002, doi: 10.1103/PhysRevD.103.122002

—. 2021c, Phys. Rev. X, 11, 021053, doi: 10.1103/PhysRevX.11.021053

—. 2023, Phys. Rev. X, 13, 041039, doi: 10.1103/PhysRevX.13.041039

—. 2024, Phys. Rev. D, 109, 022001, doi: 10.1103/PhysRevD.109.022001

—. 2025, Phys. Rev. D, 112, 084080, doi: 10.1103/PhysRevD.112.084080

Abd El Dayem, K., et al. 2025, Astron. Astrophys., 698, L15, doi: 10.1051/0004-6361/202554676

Abedi, J., Dykaar, H., & Afshordi, N. 2017, Phys. Rev. D, 96, 082004, doi: 10.1103/PhysRevD.96.082004

Abuter, R., et al. 2020, Astron. Astrophys., 636, L5, doi: 10.1051/0004-6361/202037813

Acernese, F., et al. 2015, Class. Quantum Grav., 32, 024001, doi: 10.1088/0264-9381/32/2/024001

—. 2022, Class. Quantum Grav., 39, 045006, doi: 10.1088/1361-6382/ac3c8e

Adams, T., Buskulic, D., Germain, V., et al. 2016, Class. Quantum Grav., 33, 175012, doi: 10.1088/0264-9381/33/17/175012

Agathos, M., Del Pozzo, W., Li, T. G. F., et al. 2014, Phys. Rev. D, 89, 082001, doi: 10.1103/PhysRevD.89.082001

Akiyama, K., et al. 2019a, Astrophys. J. Lett., 875, L1, doi: 10.3847/2041-8213/ab0ec7

—. 2019b, Astrophys. J. Lett., 875, L6, doi: 10.3847/2041-8213/ab1141

—. 2022a, Astrophys. J. Lett., 930, L12, doi: 10.3847/2041-8213/ac6674

—. 2022b, Astrophys. J. Lett., 930, L17, doi: 10.3847/2041-8213/ac6756

Arun, K. G., Iyer, B. R., Qusailah, M. S. S., & Sathyaprakash, B. S. 2006a, Phys. Rev. D, 74, 024006, doi: 10.1103/PhysRevD.74.024006

—. 2006b, Class. Quantum Grav., 23, L37, doi: 10.1088/0264-9381/23/9/L01

Ashton, G., Udall, R., & Yarbrough, Z. 2025a, CBC Workflow. https://github.com/Rhiannon-Udall/cbcflow

Ashton, G., et al. 2019, Astrophys. J. Suppl. Ser., 241, 27, doi: 10.3847/1538-4365/ab06fc

Ashton, G., Talbot, C., Roy, S., et al. 2025b, Bilby TGR, v0.2, Zenodo, doi: 10.5281/zenodo.15676285

Aubin, F., et al. 2021, Class. Quantum Grav., 38, 095004, doi: 10.1088/1361-6382/abe913

Baka, T., Cirok, B., Haris, K., Noller, J., & Krishnendu, N. V. 2025a. https://arxiv.org/abs/2511.00497

Baka, T., Wright, M., Romero-Shaw, I., et al. 2025b, Correcting misspecification of calibration uncertainties in gravitational-wave data analysis with efficient reweighting, Tech. Rep. LIGO-T2500295, LIGO Project. https://dcc.ligo.org/LIGO-T2500295/public

Bardeen, J. M., Press, W. H., & Teukolsky, S. A. 1972, Astrophys. J., 178, 347, doi: 10.1086/151796

Bernard, L., Blanchet, L., & Trestini, D. 2022, JCAP, 08, 008, doi: 10.1088/1475-7516/2022/08/008

Berti, E., et al. 2015, Class. Quantum Grav., 32, 243001, doi: 10.1088/0264-9381/32/24/243001

Blanchet, L. 2024, Living Rev. Relativity, 27, 4, doi: 10.1007/s41114-024-00050-z

Blanchet, L., & Sathyaprakash, B. S. 1994, Class. Quantum Grav., 11, 2807, doi: 10.1088/0264-9381/11/11/020

—. 1995, Phys. Rev. Lett., 74, 1067, doi: 10.1103/PhysRevLett.74.1067

Błaut, A. 2012, Phys. Rev. D, 85, 043005, doi: 10.1103/PhysRevD.85.043005

Bogdanov, S., et al. 2019, Astrophys. J. Lett., 887, L25, doi: 10.3847/2041-8213/ab53eb

Brito, R., Buonanno, A., & Raymond, V. 2018, Phys. Rev. D, 98, 084038, doi: 10.1103/PhysRevD.98.084038

Cannon, K., Caudill, S., Chan, C., et al. 2021, SoftwareX, 14, 100680, doi: 10.1016/j.softx.2021.100680

Carullo, G., Del Pozzo, W., & Veitch, J. 2019, Phys. Rev. D, 99, 123029, doi: 10.1103/PhysRevD.99.123029

—. 2025, pyRing, 2.7.0, Zenodo, doi: 10.5281/zenodo.8165507

Colleoni, M., Krishnendu, N. V., Mourier, P., Bera, S., & Jiménez-Forteza, X. 2024, Testing Gravity with Binary Black Hole Gravitational Waves, ed. C. Bambi & A. Cárdenas-Avendaño (Singapore: Springer Nature Singapore), 239–274, doi: 10.1007/978-981-97-2871-8_7

Colleoni, M., Ramis Vidal, F. A., Johnson-McDaniel, N. K., et al. 2025a, Phys. Rev. D, 111, 064025, doi: 10.1103/PhysRevD.111.064025

Colleoni, M., Vidal, F. A. R., García-Quirós, C., Akçay, S., & Bera, S. 2025b, Phys. Rev. D, 111, 104019, doi: 10.1103/PhysRevD.111.104019

Cornish, N. J., & Littenberg, T. B. 2015, Class. Quantum Grav., 32, 135012, doi: 10.1088/0264-9381/32/13/135012

Cornish, N. J., Littenberg, T. B., Bécsy, B., et al. 2021, Phys. Rev. D, 103, 044006, doi: 10.1103/PhysRevD.103.044006

Cornish, N. J., et al. 2024, BayesWave software. https://git.ligo.org/lscsoft/bayeswave

Creighton, J. D. E., & Anderson, W. G. 2011, Gravitational-wave physics and astronomy: An introduction to theory, experiment and data analysis (Weinheim: John Wiley & Sons, Ltd), doi: 10.1002/9783527636037

Davies, G. S., Dent, T., Tápai, M., et al. 2020, Phys. Rev. D, 102, 022004, doi: 10.1103/PhysRevD.102.022004

Davis, D., Littenberg, T. B., Romero-Shaw, I. M., et al. 2022, Class. Quantum Grav., 39, 245013, doi: 10.1088/1361-6382/aca238

Dhani, A., Völkel, S. H., Buonanno, A., et al. 2025, Phys. Rev. X, 15, 031036, doi: 10.1103/5pks-qz6b

Divyajyoti, Krishnendu, N. V., Saleem, M., et al. 2024, Phys. Rev. D, 109, 023016, doi: 10.1103/PhysRevD.109.023016

Do, T., et al. 2019, Science, 365, 664, doi: 10.1126/science.aav8137

Essick, R., Godwin, P., Hanna, C., Blackburn, L., & Katsavounidis, E. 2020, Mach. Learn. Sci. Technol., 2, 015004, doi: 10.1088/2632-2153/abab5f

Fairhurst, S., Green, R., Hoy, C., Hannam, M., & Muir, A. 2020, Phys. Rev. D, 102, 024055, doi: 10.1103/PhysRevD.102.024055

Ferreira, P. G. 2019, Ann. Rev. Astron. Astrophys., 57, 335, doi: 10.1146/annurev-astro-091918-104423

Fisher, R. P., Hemming, G., Bizouard, M.-A., et al. 2021, SoftwareX, 14, 100677, doi: 10.1016/j.softx.2021.100677

Forward, R. L. 1978, Phys. Rev. D, 17, 379, doi: 10.1103/PhysRevD.17.379

Gelfand, I. M., Minlos, R. A., & Shapiro, Z. J. 1958, Predstavleniya gruppy vrashcheni i gruppy Lorentsa, ikh primeneniya [Representations of the rotation and Lorentz groups and their applications] (Gosudarstv. Izdat. Fiz.-Mat. Lit., Moscow, MR 0114876)

Ghosh, A., Brito, R., & Buonanno, A. 2021, Phys. Rev. D, 103, 124041, doi: 10.1103/PhysRevD.103.124041

Ghosh, A., Ghosh, A., Johnson-McDaniel, N. K., et al. 2016, Phys. Rev. D, 94, 021101(R), doi: 10.1103/PhysRevD.94.021101

Ghosh, A., Johnson-McDaniel, N. K., Ghosh, A., et al. 2018, Class. Quantum Grav., 35, 014002, doi: 10.1088/1361-6382/aa972e

Gupta, A. 2026, Class. Quantum Grav., 43, 053001, doi: 10.1088/1361-6382/ae470b

Gupta, A., et al. 2024, SciPost Phys. Comm. Rep., 5, doi: 10.21468/SciPostPhysCommRep.5

Gupta, I., Narayan, P., London, L., Tiwari, S., & Sathyaprakash, B. 2025. https://arxiv.org/abs/2511.11886

Gupta, T., & Cornish, N. J. 2024, Phys. Rev. D, 109, 064040, doi: 10.1103/PhysRevD.109.064040

Gürsel, Y., & Tinto, M. 1989, Phys. Rev. D, 40, 3884, doi: 10.1103/PhysRevD.40.3884

Haegel, L., O'Neal-Ault, K., Bailey, Q. G., et al. 2023, Phys. Rev. D, 107, 064031, doi: 10.1103/PhysRevD.107.064031

Hanna, C., et al. 2020, Phys. Rev. D, 101, 022003, doi: 10.1103/PhysRevD.101.022003

Harris, C. R., et al. 2020, Nature, 585, 357, doi: 10.1038/s41586-020-2649-2

Healy, J., & Lousto, C. O. 2017, Phys. Rev. D, 95, 024037, doi: 10.1103/PhysRevD.95.024037

Hofmann, F., Barausse, E., & Rezzolla, L. 2016, Astrophys. J. Lett., 825, L19, doi: 10.3847/2041-8205/825/2/L19

Hoy, C., & Raymond, V. 2021, SoftwareX, 15, 100765, doi: 10.1016/j.softx.2021.100765

Hughes, S. A., & Menou, K. 2005, Astrophys. J., 623, 689, doi: 10.1086/428826

Hunter, J. D. 2007, Comput. Sci. Eng., 9, 90, doi: 10.1109/MCSE.2007.55

Ishak, M. 2019, Living Rev. Relativity, 22, 1, doi: 10.1007/s41114-018-0017-4

Isi, M., Chatziioannou, K., & Farr, W. M. 2019, Phys. Rev. Lett., 123, 121101, doi: 10.1103/PhysRevLett.123.121101

Isi, M., & Weinstein, A. J. 2017, Tech. Note, LIGO-P1700276. https://arxiv.org/abs/1710.03794

Isi, M., Weinstein, A. J., Mead, C., & Pitkin, M. 2015, Phys. Rev. D, 91, 082002, doi: 10.1103/PhysRevD.91.082002

Islam, T., Mehta, A. K., Ghosh, A., et al. 2020, Phys. Rev. D, 101, 024032, doi: 10.1103/PhysRevD.101.024032

Jiménez-Forteza, X., Keitel, D., Husa, S., et al. 2017, Phys. Rev. D, 95, 064024, doi: 10.1103/PhysRevD.95.064024

Johnson-McDaniel, N. K., Ghosh, A., Ghonge, S., et al. 2022, Phys. Rev. D, 105, 044020, doi: 10.1103/PhysRevD.105.044020

Klimenko, S., Yakushin, I., Rakhmanov, M., & Mitselmakher, G. 2004, Class. Quantum Grav., 21, S1685, doi: 10.1088/0264-9381/21/20/011

Klimenko, S., Vedovato, G., Drago, M., et al. 2011, Phys. Rev. D, 83, 102001, doi: 10.1103/PhysRevD.83.102001

Klimenko, S., et al. 2016, Phys. Rev. D, 93, 042004, doi: 10.1103/PhysRevD.93.042004

Kramer, M., et al. 2021, Phys. Rev. X, 11, 041050, doi: 10.1103/PhysRevX.11.041050

Kwok, J. Y. L., Lo, R. K. L., Weinstein, A. J., & Li, T. G. F. 2022, Phys. Rev. D, 105, 024066, doi: 10.1103/PhysRevD.105.024066

Lee, Y. S. C., Doshi, S., Millhouse, M., & Melatos, A. 2025, Phys. Rev. D, 111, 082002, doi: 10.1103/PhysRevD.111.082002

Li, T. G. F., Del Pozzo, W., Vitale, S., et al. 2012, Phys. Rev. D, 85, 082003, doi: 10.1103/PhysRevD.85.082003

LIGO Scientific Collaboration and Virgo Collaboration. 2018, Data quality report user documentation, docs.ligo.org/detchar/data-quality-report/

LIGO Scientific, Virgo, and KAGRA Collaboration. 2025, LVK Algorithm Library - LALSuite, doi: 10.7935/GT1W-FZ16

—. 2026, Data release for GWTC-4.0: Tests of General Relativity. I. Overview and General Tests. https://dcc.ligo.org/P2600128/public

Littenberg, T. B., Kanner, J. B., Cornish, N. J., & Millhouse, M. 2016, Phys. Rev. D, 94, 044050, doi: 10.1103/PhysRevD.94.044050

Lo, R. K. L., Li, T. G. F., & Weinstein, A. J. 2019, Phys. Rev. D, 99, 084052, doi: 10.1103/PhysRevD.99.084052

Lo, R. K. L., Uchikata, N., Narikawa, T., Wang, Y., & Birnholtz, O. 2025, ECHOES_WAVEFORM_MODELS, v0.0.5. https://git.ligo.org/echoes_template_search/echoes_waveform_models

Lu, N., Ma, S., Piccinni, O. J., Sun, L., & Finch, E. 2025, Phys. Rev. D, 112, 064047, doi: 10.1103/h6jy-sd94

Ma, S., Sun, L., & Chen, Y. 2023a, Phys. Rev. D, 107, 084010, doi: 10.1103/PhysRevD.107.084010

—. 2023b, Phys. Rev. Lett., 130, 141401, doi: 10.1103/PhysRevLett.130.141401

Ma, S., Mitman, K., Sun, L., et al. 2022, Phys. Rev. D, 106, 084036, doi: 10.1103/PhysRevD.106.084036

Ma, S., et al. 2025, QNMRF software, https://github.com/Sizheng-Ma/qnm_filter, GitHub

Macleod, D., et al. 2021, gwpy/gwpy, Zenodo, doi: 10.5281/zenodo.597016

Maggiore, M. 2007, Gravitational Waves. Vol. 1: Theory and Experiments (Oxford University Press), doi: 10.1093/acprof:oso/9780198570745.001.0001

Mahapatra, P., et al. 2025, Phys. Rev. D, 112, 104007, doi: 10.1103/c1sj-jc4v

Mandel, I., Farr, W. M., & Gair, J. R. 2019, Mon. Not. R. Astron. Soc., 486, 1086, doi: 10.1093/mnras/stz896

Matas, A., et al. 2020, Phys. Rev. D, 102, 043023, doi: 10.1103/PhysRevD.102.043023

Mehta, A. K., Buonanno, A., Cotesta, R., et al. 2023, Phys. Rev. D, 107, 044020, doi: 10.1103/PhysRevD.107.044020

Meidam, J., et al. 2018, Phys. Rev. D, 97, 044033, doi: 10.1103/PhysRevD.97.044033

Messick, C., et al. 2017, Phys. Rev. D, 95, 042001, doi: 10.1103/PhysRevD.95.042001

Miani, A., Lazzaro, C., Prodi, G. A., et al. 2023, Phys. Rev. D, 108, 064018, doi: 10.1103/PhysRevD.108.064018

Mihaylov, D. P., Ossokine, S., Buonanno, A., et al. 2025, SoftwareX, 30, 102080, doi: 10.1016/j.softx.2025.102080

Miller, M. C., et al. 2019, Astrophys. J. Lett., 887, L24, doi: 10.3847/2041-8213/ab50c5

Mills, C., & Fairhurst, S. 2021, Phys. Rev. D, 103, 024042, doi: 10.1103/PhysRevD.103.024042

Mishra, T., et al. 2022, Phys. Rev. D, 105, 083018, doi: 10.1103/PhysRevD.105.083018

Nakano, H., Sago, N., Tagoshi, H., & Tanaka, T. 2017, PTEP, 2017, 071E01, doi: 10.1093/ptep/ptx093

Narayan, P., Johnson-McDaniel, N. K., & Gupta, A. 2023, Phys. Rev. D, 108, 064003, doi: 10.1103/PhysRevD.108.064003

—. 2026, Phys. Rev. D, 113, 044007, doi: 10.1103/5hbl-hr2x

Necula, V., Klimenko, S., & Mitselmakher, G. 2012, J. Phys. Conf. Ser., 363, 012032, doi: 10.1088/1742-6596/363/1/012032

Newman, E. T., & Penrose, R. 1966, J. Math. Phys., 7, 863, doi: 10.1063/1.1931221

Nishizawa, A., Taruya, A., Hayama, K., Kawamura, S., & Sakagami, M.-a. 2009, Phys. Rev. D, 79, 082002, doi: 10.1103/PhysRevD.79.082002

Nitz, A. H., Dent, T., Dal Canton, T., Fairhurst, S., & Brown, D. A. 2017, Astrophys. J., 849, 118, doi: 10.3847/1538-4357/aa8f50

Pacilio, C., Gerosa, D., & Bhagwat, S. 2024, Phys. Rev. D, 109, L081302, doi: 10.1103/PhysRevD.109.L081302

Pedregosa, F., et al. 2011, J. Machine Learning Res., 12, 2825

Pompili, L., Maggio, E., Silva, H. O., & Buonanno, A. 2025, Phys. Rev. D, 111, 124040, doi: 10.1103/ng8w-98sz

Pompili, L., et al. 2023, Phys. Rev. D, 108, 124035, doi: 10.1103/PhysRevD.108.124035

Pratten, G., et al. 2021, Phys. Rev. D, 103, 104056, doi: 10.1103/PhysRevD.103.104056

Puecher, A., Kalaghatgi, C., Roy, S., et al. 2022, Phys. Rev. D, 106, 082003, doi: 10.1103/PhysRevD.106.082003

Ramos-Buades, A., Buonanno, A., Estellés, H., et al. 2023, Phys. Rev. D, 108, 124037, doi: 10.1103/PhysRevD.108.124037

Riley, T. E., et al. 2019, Astrophys. J. Lett., 887, L21, doi: 10.3847/2041-8213/ab481c

Robinet, F., Arnaud, N., Leroy, N., et al. 2020, SoftwareX, 12, 100620, doi: 10.1016/j.softx.2020.100620

Romero-Shaw, I. M., et al. 2020, Mon. Not. R. Astron. Soc., 499, 3295, doi: 10.1093/mnras/staa2850

Roy, S., Haney, M., Pratten, G., Pang, P. T. H., & Van Den Broeck, C. 2026, Phys. Rev. D, 113, 024016, doi: 10.1103/855k-sys5

Sachdev, S., et al. 2019. https://arxiv.org/abs/1901.08580

Sänger, E. M., et al. 2024. https://arxiv.org/abs/2406.03568

Silva, H. O., Holgado, A. M., Cárdenas-Avendaño, A., & Yunes, N. 2021, Phys. Rev. Lett., 126, 181101, doi: 10.1103/PhysRevLett.126.181101

Skilling, J. 2006, Bayesian Analysis, 1, 833, doi: 10.1214/06-BA127

Smith, J. R., Abbott, T., Hirose, E., et al. 2011, Class. Quantum Grav., 28, 235005, doi: 10.1088/0264-9381/28/23/235005

Smith, R., Ashton, G., Vajpeyi, A., & Talbot, C. 2020, Mon. Not. R. Astron. Soc., 498, 4492, doi: 10.1093/mnras/staa2483

Speagle, J. S. 2020, Mon. Not. R. Astron. Soc., 493, 3132, doi: 10.1093/mnras/staa278

Stein, L. C. 2019, J. Open Source Softw., 4, 1683, doi: 10.21105/joss.01683

Sullivan, J., Ranjan, S., & Millhouse, M. 2025, IGWN Wave Compare. https://git.ligo.org/bayeswave/igwn-wave-compare

Talbot, C., et al. 2025, Class. Quantum Grav., 42, 235023, doi: 10.1088/1361-6382/ae1ac7

Thompson, J. E., Fauchon-Jones, E., Khan, S., et al. 2020, Phys. Rev. D, 101, 124059, doi: 10.1103/PhysRevD.101.124059

Tiwari, A., Vijaykumar, A., Kapadia, S. J., Ghosh, S., & Nielsen, A. B. 2025. https://arxiv.org/abs/2506.22272

Tsang, K. W., Rollier, M., Ghosh, A., et al. 2018, Phys. Rev. D, 98, 024023, doi: 10.1103/PhysRevD.98.024023

Uchikata, N., Nakano, H., Narikawa, T., et al. 2019, Phys. Rev. D, 100, 062006, doi: 10.1103/PhysRevD.100.062006

Uchikata, N., Narikawa, T., Nakano, H., et al. 2023, Phys. Rev. D, 108, 104040, doi: 10.1103/PhysRevD.108.104040

Urban, A. L., et al. 2021, gwdetchar/gwdetchar, Zenodo, doi: 10.5281/zenodo.597016

Usman, S. A., et al. 2016, Class. Quantum Grav., 33, 215004, doi: 10.1088/0264-9381/33/21/215004

Varma, V., Field, S. E., Scheel, M. A., et al. 2019, Phys. Rev. Research., 1, 033015, doi: 10.1103/PhysRevResearch.1.033015

Veitch, J., et al. 2015, Phys. Rev. D, 91, 042003, doi: 10.1103/PhysRevD.91.042003

Veitch, J., Pozzo, W. D., Lyttle, A., et al. 2025, johnveitch/cpnest: v0.11.8, v0.11.8, Zenodo, doi: 10.5281/zenodo.592884

Viets, A., et al. 2018, Class. Quantum Grav., 35, 095015, doi: 10.1088/1361-6382/aab658

Vijaykumar, A., Tiwari, A., Kapadia, S. J., Arun, K. G., & Ajith, P. 2023, Astrophys. J., 954, 105, doi: 10.3847/1538-4357/acd77d

Virgo Collaboration. 2021, PythonVirgoTools, v5.1.1, git.ligo.org/virgo/virgoapp/PythonVirgoTools

Virtanen, P., et al. 2020, Nat. Meth., 17, 261, doi: 10.1038/s41592-019-0686-2

Waskom, M. L. 2021, J. Open Source Softw., 6, 3021, doi: 10.21105/joss.03021

Wette, K. 2020, SoftwareX, 12, 100634, doi: 10.1016/j.softx.2020.100634

Will, C. M. 1994, Phys. Rev. D, 50, 6058, doi: 10.1103/PhysRevD.50.6058

—. 2014, Living Rev. Relativity, 17, 4, doi: 10.12942/lrr-2014-4

Williams, D., Veitch, J., Chiofalo, M. L., et al. 2023, J. Open Source Softw., 8, 4170, doi: 10.21105/joss.04170

Wong, I. C. F., Ng, T. C. K., & Cirok, B. 2025, nullpol software, GitHub. https://github.com/isaac-cf-wong/nullpol

Wong, I. C. F., Pang, P. T. H., Lo, R. K. L., Li, T. G. F., & Van Den Broeck, C. 2021. https://arxiv.org/abs/2105.09485

Yunes, N., Siemens, X., & Yagi, K. 2025, Living Rev. Relativity, 28, 3, doi: 10.1007/s41114-024-00054-9

Zhong, H., Isi, M., Chatziioannou, K., & Farr, W. M. 2024, Phys. Rev. D, 110, 044053, doi: 10.1103/PhysRevD.110.044053

Zhong, H., Isi, M., Farr, W. M., & Chatziioannou, K. 2026, HIERFIT, ND Hierarchical Analysis. https://git.ligo.org/haowen.zhong/2d-nd-hierarchical-analysis

Zimmerman, A., Haster, C.-J., & Chatziioannou, K. 2019, Phys. Rev. D, 99, 124044, doi: 10.1103/PhysRevD.99.124044

Zweizig, J. 2006, The Data Monitor Tool Project, labcit.ligo.caltech.edu/~jzweizig/DMT-Project.html

The LIGO Scientific Collaboration, the Virgo Collaboration, and the KAGRA Collaboration, A. G. Abac,[1] I. Abouelfettouh,[2] F. Acernese,[3,4] K. Ackley,[5] C. Adamcewicz,[6] S. Adhicary,[7] D. Adhikari,[8,9] N. Adhikari,[10] R. X. Adhikari,[11] V. K. Adkins,[12] S. Afroz,[13] A. Agapito,[14] D. Agarwal,[15] M. Agathos,[16] N. Aggarwal,[17] S. Aggarwal,[18] O. D. Aguiar,[19] I.-L. Ahrend,[20] L. Aiello,[21,22] A. Ain,[23] P. Ajith,[24] T. Akutsu,[25,26] S. Albanesi,[27,28] W. Ali,[29,30] S. Al-Kershi,[8,9] C. Alléné,[31] A. Allocca,[32,4] S. Al-Shammari,[33] P. A. Altin,[34] S. Alvarez-Lopez,[35] W. Amar,[31] O. Amarasinghe,[33] A. Amato,[36,37] F. Amicucci,[38,39] C. Amra,[40] A. Ananyeva,[11] S. B. Anderson,[11] W. G. Anderson,[11] M. Andia,[41] M. Ando,[42] M. Andrés-Carcasona,[43] T. Andrić,[44,45,8,9] J. Anglin,[46] S. Ansoldi,[47,48] J. M. Antelis,[49] S. Antier,[41] M. Aoumi,[50] E. Z. Appavuravther,[51,52] S. Appert,[11] S. K. Apple,[53] K. Arai,[11] A. Araya,[42] M. C. Araya,[11] M. Arca Sedda,[44,45] J. S. Areeda,[54] N. Aritomi,[2] F. Armato,[29,30] S. Armstrong,[55] N. Arnaud,[56] M. Arogeti,[57] S. M. Aronson,[12] K. G. Arun,[58] G. Ashton,[59] Y. Aso,[25,60] L. Asprea,[28] M. Assiduo,[61,62] S. Assis de Souza Melo,[63] S. M. Aston,[64] P. Astone,[38] F. Attadio,[39,38] F. Aubin,[65] K. AultONeal,[66] G. Avallone,[67] E. A. Avila,[49] S. Babak,[20] C. Badger,[68] S. Bae,[69] S. Bagnasco,[28] L. Baiotti,[70] R. Bajpai,[71] T. Baka,[72,37] A. M. Baker,[6] K. A. Baker,[73] T. Baker,[74] G. Baldi,[75,76] N. Baldicchi,[77,51] M. Ball,[78] G. Ballardin,[63] S. W. Ballmer,[79] S. Banagiri,[6] B. Banerjee,[44] D. Bankar,[80] T. M. Baptiste,[12] P. Baral,[10] M. Baratti,[81,82] J. C. Barayoga,[11] B. C. Barish,[11] D. Barker,[2] N. Barman,[80] P. Barneo,[83,84,85] F. Barone,[86,4] B. Barr,[87] L. Barsotti,[35] M. Barsuglia,[20] D. Barta,[88] A. M. Bartoletti,[89] M. A. Barton,[87] I. Bartos,[46] A. Basalaev,[8,9] R. Bassiri,[90] A. Basti,[82,81] M. Bawaj,[77,51] P. Baxi,[91] J. C. Bayley,[87] A. C. Baylor,[10] P. A. Baynard II,[57] M. Bazzan,[92,93] V. M. Bedakihale,[94] F. Beirnaert,[95] M. Bejger,[96] D. Belardinelli,[22] A. S. Bell,[87] D. S. Bellie,[97] L. Bellizzi,[81,82] W. Benoit,[18] I. Bentara,[56] J. D. Bentley,[98] M. Ben Yaala,[55] S. Bera,[99,100] F. Bergamin,[33] B. K. Berger,[90] S. Bernuzzi,[27] M. Beroiz,[11] C. P. L. Berry,[87] D. Bersanetti,[29] T. Bertheas,[101] A. Bertolini,[37,36] J. Betzwieser,[64] D. Beveridge,[73] G. Bevilacqua,[102] N. Bevins,[103] S. Bhagwat,[104] R. Bhandare,[105] S. A. Bhat,[80] R. Bhatt,[11] D. Bhattacharjee,[106,107] S. Bhattacharyya,[108] S. Bhaumik,[46] V. Biancalana,[102] A. Bianchi,[37,109] I. A. Bilenko,[110] G. Billingsley,[11] A. Binetti,[111] S. Bini,[11,75,76] C. Binu,[112] S. Biot,[113] O. Birnholtz,[114] S. Biscoveanu,[97] A. Bisht,[9] M. Bitossi,[63,81] M.-A. Bizouard,[115] S. Blaber,[116] J. K. Blackburn,[11] L. A. Blagg,[78] C. D. Blair,[73,64] D. G. Blair,[73] N. Bode,[8,9] N. Boettner,[98] G. Boileau,[115] M. Boldrini,[38] G. N. Bolingbroke,[117] A. Bolliand,[118,40] L. D. Bonavena,[46] R. Bondarescu,[83] F. Bondu,[119] E. Bonilla,[90] M. S. Bonilla,[54] A. Bonino,[104] R. Bonnand,[31,118] A. Borchers,[8,9] V. Boschi,[81] S. Bose,[120] V. Bossilkov,[64] Y. Bothra,[37,109] A. Boudon,[56] L. Bourg,[57] M. Boyle,[121] A. Bozzi,[63] C. Bradaschia,[81] P. R. Brady,[10] A. Branch,[64] M. Branchesi,[44,45] I. Braun,[106] T. Briant,[122] A. Brillet,[115] M. Brinkmann,[8,9] P. Brockill,[10] E. Brockmueller,[8,9] A. F. Brooks,[11] B. C. Brown,[46] D. D. Brown,[117] M. L. Brozzetti,[77,51] S. Brunett,[11] G. Bruno,[15] R. Bruntz,[123] J. Bryant,[104] Y. Bu,[124] F. Bucci,[62] J. Buchanan,[123] O. Bulashenko,[83,84] T. Bulik,[125] H. J. Bulten,[37] A. Buonanno,[126,1] K. Burtnyk,[2] R. Buscicchio,[127,128] D. Buskulic,[31] C. Buy,[101] R. L. Byer,[90] G. S. Cabourn Davies,[74] R. Cabrita,[15] V. Cáceres-Barbosa,[7] L. Cadonati,[57] G. Cagnoli,[129] C. Cahillane,[79] A. Calafat,[99] T. A. Callister,[130] E. Calloni,[32,4] S. R. Callos,[78] M. Canepa,[30,29] G. Caneva Santoro,[43] K. C. Cannon,[42] H. Cao,[35] L. A. Capistran,[131] E. Capocasa,[20] E. Capote,[2,11] G. Capurri,[82,81] G. Carapella,[67,132] F. Carbognani,[63] M. Carlassara,[8,9] J. B. Carlin,[124] T. K. Carlson,[133] M. F. Carney,[106] M. Carpinelli,[127,63] G. Carrillo,[78] J. J. Carter,[8,9] G. Carullo,[104,134] A. Casallas-Lagos,[135] J. Casanueva Diaz,[63] C. Casentini,[136,22] S. Y. Castro-Lucas,[137] S. Caudill,[133] M. Cavaglià,[107] R. Cavalieri,[63] A. Ceja,[54] G. Cella,[81] P. Cerdá-Durán,[138,139] E. Cesarini,[22] N. Chabbra,[34] W. Chaibi,[115] A. Chakraborty,[13] P. Chakraborty,[8,9] S. Chakraborty,[105] S. Chalathadka Subrahmanya,[98] J. C. L. Chan,[140] M. Chan,[116] K. Chang,[141] S. Chao,[142,141] P. Charlton,[143] E. Chassande-Mottin,[20] C. Chatterjee,[144] Debarati Chatterjee,[80] Deep Chatterjee,[35] M. Chaturvedi,[105] S. Chaty,[20] K. Chatziioannou,[11] A. Chen,[145] A. H.-Y. Chen,[146] D. Chen,[147] H. Chen,[142] H. Y. Chen,[148] S. Chen,[144] Yanbei Chen,[149] Yitian Chen,[121] H. P. Cheng,[150] P. Chessa,[77,51] H. T. Cheung,[91] S. Y. Cheung,[6] F. Chiadini,[151,132] G. Chiarini,[8,9,93] A. Chiba,[152] A. Chincarini,[29] M. L. Chiofalo,[82,81] A. Chiummo,[4,63] C. Chou,[146] S. Choudhary,[73] N. Christensen,[115,153] S. S. Y. Chua,[34] G. Ciani,[75,76] P. Ciecielag,[96] M. Cieślar,[125] M. Cifaldi,[22] B. Cirok,[154] F. Clara,[2] J. A. Clark,[11,57] T. A. Clarke,[6] P. Clearwater,[155] S. Clesse,[113] F. Cleva,[115,118] E. Coccia,[44,45,43] E. Codazzo,[156,157] P.-F. Cohadon,[122] S. Colace,[30] E. Colangeli,[74] M. Colleoni,[99] C. G. Collette,[158] J. Collins,[64] S. Colloms,[87] A. Colombo,[159,128] C. M. Compton,[2] G. Connolly,[78] L. Conti,[93] T. R. Corbitt,[12] I. Cordero-Carrión,[160] S. Corezzi,[77,51] M. Corman,[1] N. J. Cornish,[161] I. Coronado,[162] A. Corsi,[163] R. Cottingham,[64] M. W. Coughlin,[18] A. Couineaux,[38] P. Couvares,[11,57] D. M. Coward,[73] R. Coyne,[164] A. Cozzumbo,[44] J. D. E. Creighton,[10] T. D. Creighton,[165] P. Cremonese,[99] S. Crook,[64] R. Crouch,[2] J. Csizmazia,[2] J. R. Cudell,[166] T. J. Cullen,[11] A. Cumming,[87] E. Cuoco,[167,168] M. Cusinato,[138] L. V. Da Conceição,[169] T. Dal Canton,[41] S. Dal Pra,[170] G. Dálya,[101] O. Dan,[114] B. D'Angelo,[29] S. Danilishin,[36,37] S. D'Antonio,[38] K. Danzmann,[9,8,9] K. E. Darroch,[123] L. P. Dartez,[64] R. Das,[108] A. Dasgupta,[94] V. Dattilo,[63] A. Daumas,[20] N. Davari,[171,172] I. Dave,[105] A. Davenport,[137] M. Davier,[41] T. F. Davies,[73] D. Davis,[11] L. Davis,[73] M. C. Davis,[18] P. Davis,[173,174] E. J. Daw,[175] M. Dax,[1] J. De Bolle,[95] M. Deenadayalan,[80] J. Degallaix,[176] M. De Laurentis,[32,4] F. De Lillo,[23] S. Della Torre,[128] W. Del Pozzo,[82,81] A. Demagny,[31] F. De Marco,[39,38] G. Demasi,[177,62] F. De Matteis,[21,22] N. Demos,[35] T. Dent,[178] A. Depasse,[15] N. DePergola,[103] R. De Pietri,[179,180] R. De Rosa,[32,4] C. De Rossi,[63] M. Desai,[35] R. DeSalvo,[181] A. DeSimone,[182] R. De Simone,[151,132] A. Dhani,[1] R. Diab,[46] M. C. Díaz,[165] M. Di Cesare,[32,4] G. Dideron,[183] T. Dietrich,[1] L. Di Fiore,[4] C. Di Fronzo,[73] M. Di Giovanni,[39,38] T. Di Girolamo,[32,4] D. Diksha,[37,36] J. Ding,[20,184] S. Di Pace,[39,38] I. Di Palma,[39,38] D. Di Piero,[185,48] F. Di Renzo,[56] Divyajyoti,[33] A. Dmitriev,[104] J. P. Docherty,[87] Z. Doctor,[97] N. Doerksen,[169] E. Dohmen,[2] A. Doke,[133] A. Domiciano De Souza,[186] L. D'Onofrio,[38] F. Donovan,[35] K. L. Dooley,[33] T. Dooney,[72] S. Doravari,[80] O. Dorosh,[187] W. J. D. Doyle,[123] M. Drago,[39,38] J. C. Driggers,[2] L. Dunn,[124] U. Dupletsa,[44] P.-A. Duverne,[20] D. D'Urso,[171,156] P. Dutta Roy,[46] H. Duval,[188] S. E. Dwyer,[2] C. Eassa,[2] W. East,[183] M. Ebersold,[189,31] T. Eckhardt,[98] G. Eddolls,[79] A. Effler,[64] J. Eichholz,[34] H. Einsle,[115] M. Eisenmann,[25] M. Emma,[59] K. Endo,[152] R. Enficiaud,[1] L. Errico,[32,4] R. Espinosa,[165] M. Esposito,[4,32] R. C. Essick,[190] H. Estellés,[1] T. Etzel,[11] M. Evans,[35] T. Evstafyeva,[183] B. E. Ewing,[7] J. M. Ezquiaga,[140] F. Fabrizi,[61,62] V. Fafone,[21,22] S. Fairhurst,[33]

A. M. Farah,[130] B. Farr,[78] W. M. Farr,[191, 192] G. Favaro,[92] M. Favata,[193] M. Fays,[166] M. Fazio,[55] J. Feicht,[11] M. M. Fejer,[90] R. Felicetti,[185, 48] E. Fenyvesi,[88, 194] J. Fernandes,[195] T. Fernandes,[196, 138] D. Fernando,[112] S. Ferraiuolo,[197, 39, 38] T. A. Ferreira,[12] F. Fidecaro,[82, 81] P. Figura,[96] A. Fiori,[81, 82] I. Fiori,[63] M. Fishbach,[190] R. P. Fisher,[123] R. Fittipaldi,[198, 132] V. Fiumara,[199, 132] R. Flaminio,[31] S. M. Fleischer,[200] L. S. Fleming,[201] E. Floden,[18] H. Fong,[116] J. A. Font,[138, 139] F. Fontinele-Nunes,[18] C. Foo,[1] B. Fornal,[202] K. Franceschetti,[179] F. Frappez,[31] S. Frasca,[39, 38] F. Frasconi,[81] J. P. Freed,[66] Z. Frei,[203] A. Freise,[37, 109] O. Freitas,[196, 138] R. Frey,[78] W. Frischhertz,[64] P. Fritschel,[35] V. V. Frolov,[64] G. G. Fronzé,[28] M. Fuentes-Garcia,[11] S. Fujii,[204] T. Fujimori,[205] P. Fulda,[46] M. Fyffe,[64] B. Gadre,[72] J. R. Gair,[1] S. Galaudage,[186] V. Galdi,[206] R. Gamba,[7] A. Gamboa,[1] S. Gamoji,[181] D. Ganapathy,[207] A. Ganguly,[80] B. Garaventa,[29] J. García-Bellido,[208] C. García-Quirós,[189] J. W. Gardner,[34] K. A. Gardner,[116] S. Garg,[42] J. Gargiulo,[63] X. Garrido,[41] A. Garron,[99] F. Garufi,[32, 4] P. A. Garver,[90] C. Gasbarra,[21, 22] B. Gateley,[2] F. Gautier,[209] V. Gayathri,[10] T. Gayer,[79] G. Gemme,[29] A. Gennai,[81] V. Gennari,[101] J. George,[105] R. George,[148] O. Gerberding,[98] L. Gergely,[154] Archisman Ghosh,[95] Sayantan Ghosh,[195] Shaon Ghosh,[193] Shrobana Ghosh,[8, 9] Suprovo Ghosh,[210] Tathagata Ghosh,[80] J. A. Giaime,[12, 64] K. D. Giardina,[64] D. R. Gibson,[201] C. Gier,[55] S. Gkaitatzis,[82, 81] J. Glanzer,[11] F. Glotin,[41] J. Godfrey,[78] R. V. Godley,[8, 9] P. Godwin,[11] A. S. Goettel,[33] E. Goetz,[116] J. Golomb,[11] S. Gomez Lopez,[39, 38] B. Goncharov,[44] G. González,[12] P. Goodarzi,[211] S. Goode,[6] A. W. Goodwin-Jones,[15] M. Gosselin,[63] R. Gouaty,[31] D. W. Gould,[34] K. Govorkova,[35] A. Grado,[77, 51] V. Graham,[87] A. E. Granados,[18] M. Granata,[176] V. Granata,[212, 132] S. Gras,[35] P. Grassia,[11] J. Graves,[57] C. Gray,[2] R. Gray,[87] G. Greco,[51] A. C. Green,[37, 109] L. Green,[213] S. M. Green,[74] S. R. Green,[214] C. Greenberg,[133] A. M. Gretarsson,[66] H. K. Griffin,[18] D. Griffith,[11] H. L. Griggs,[57] G. Grignani,[77, 51] C. Grimaud,[31] H. Grote,[33] S. Grunewald,[1] D. Guerra,[138] D. Guetta,[215] G. M. Guidi,[61, 62] A. R. Guimaraes,[12] H. K. Gulati,[94] F. Gulminelli,[173, 174] H. Guo,[145] W. Guo,[73] Y. Guo,[37, 36] Anuradha Gupta,[216] I. Gupta,[7] N. C. Gupta,[94] S. K. Gupta,[46] V. Gupta,[18] N. Gupte,[1] J. Gurs,[98] N. Gutierrez,[176] N. Guttman,[6] F. Guzman,[131] D. Haba,[217] M. Haberland,[1] S. Haino,[218] E. D. Hall,[35] E. Z. Hamilton,[99] G. Hammond,[87] M. Haney,[37] J. Hanks,[2] C. Hanna,[7] M. D. Hannam,[33] O. A. Hannuksela,[219] A. G. Hanselman,[130] H. Hansen,[2] J. Hanson,[64] S. Hanumasagar,[57] R. Harada,[42] A. R. Hardison,[182] S. Harikumar,[187] K. Haris,[37, 72] I. Harley-Trochimczyk,[131] T. Harmark,[134] J. Harms,[44, 45] G. M. Harry,[220] I. W. Harry,[74] J. Hart,[106] B. Haskell,[96, 221, 222] C.-J. Haster,[213] K. Haughian,[87] H. Hayakawa,[50] K. Hayama,[223] M. C. Heintze,[64] J. Heinze,[104] J. Heinzel,[35] H. Heitmann,[115] F. Hellman,[207] A. F. Helmling-Cornell,[78] G. Hemming,[63] O. Henderson-Sapir,[117] M. Hendry,[87] I. S. Heng,[87] M. H. Hennig,[87] C. Henshaw,[57] M. Heurs,[8, 9] A. L. Hewitt,[224, 225] J. Heynen,[15] J. Heyns,[35] S. Higginbotham,[33] S. Hild,[36, 37] S. Hill,[87] Y. Himemoto,[226] N. Hirata,[25] C. Hirose,[227] D. Hofman,[176] B. E. Hogan,[66] N. A. Holland,[37, 109] K. Holley-Bockelmann,[144] I. J. Hollows,[175] D. E. Holz,[130] L. Honet,[113] D. J. Horton-Bailey,[207] J. Hough,[87] S. Hourihane,[11] N. T. Howard,[144] E. J. Howell,[73] C. G. Hoy,[74] C. A. Hrishikesh,[21] P. Hsi,[35] H.-F. Hsieh,[142] H.-Y. Hsieh,[142] C. Hsiung,[228] S.-H. Hsu,[146] W.-F. Hsu,[111] Q. Hu,[87] H. Y. Huang,[141] Y. Huang,[7] Y. T. Huang,[79] A. D. Huddart,[229] B. Hughey,[66] V. Hui,[31] S. Husa,[99] R. Huxford,[7] L. Iampieri,[39, 38] G. A. Iandolo,[36] M. Ianni,[22, 21] G. Iannone,[132] J. Iascau,[78] K. Ide,[230] R. Iden,[217] A. Ierardi,[44, 45] S. Ikeda,[147] H. Imafuku,[42] Y. Inoue,[141] G. Iorio,[92] P. Iosif,[185, 48] M. H. Iqbal,[34] J. Irwin,[87] R. Ishikawa,[230] M. Isi,[191, 192] K. S. Isleif,[231] Y. Itoh,[205, 232] M. Iwaya,[204] B. R. Iyer,[24] C. Jacquet,[101] P.-E. Jacquet,[122] T. Jacquot,[41] S. J. Jadhav,[233] S. P. Jadhav,[155] M. Jain,[133] T. Jain,[224] A. L. James,[11] K. Jani,[144] J. Janquart,[15] N. N. Janthalur,[233] S. Jaraba,[234] P. Jaranowski,[235] R. Jaume,[99] W. Javed,[33] A. Jennings,[2] M. Jensen,[2] W. Jia,[35] J. Jiang,[150] H.-B. Jin,[236, 237] G. R. Johns,[123] N. A. Johnson,[46] N. K. Johnson-McDaniel,[216] M. C. Johnston,[213] R. Johnston,[87] N. Johny,[8, 9] D. H. Jones,[34] D. I. Jones,[210] R. Jones,[87] H. E. Jose,[78] P. Joshi,[7] S. K. Joshi,[80] G. Joubert,[56] J. Ju,[238] L. Ju,[73] K. Jung,[239] J. Junker,[34] V. Juste,[113] H. B. Kabagoz,[64, 35] T. Kajita,[240] I. Kaku,[205] V. Kalogera,[97] M. Kalomenopoulos,[213] M. Kamiizumi,[50] N. Kanda,[232, 205] S. Kandhasamy,[80] G. Kang,[241] N. C. Kannachel,[6] J. B. Kanner,[11] S. A. KantiMahanty,[18] S. J. Kapadia,[80] D. P. Kapasi,[54] M. Karthikeyan,[133] M. Kasprzack,[11] H. Kato,[152] T. Kato,[204] E. Katsavounidis,[35] W. Katzman,[64] R. Kaushik,[105] K. Kawabe,[2] R. Kawamoto,[205] D. Keitel,[99] L. J. Kemperman,[117] J. Kennington,[7] F. A. Kerkow,[18] R. Kesharwani,[80] J. S. Key,[242] R. Khadela,[8, 9] S. Khadka,[90] S. S. Khadkikar,[7] F. Y. Khalili,[110] F. Khan,[8, 9] T. Khanam,[163] M. Khursheed,[105] N. M. Khusid,[191, 192] W. Kiendrebeogo,[115, 243] N. Kijbunchoo,[117] C. Kim,[244] J. C. Kim,[245] K. Kim,[246] M. H. Kim,[238] S. Kim,[247] Y.-M. Kim,[246] C. Kimball,[97] K. Kimes,[54] M. Kinnear,[33] J. S. Kissel,[2] S. Klimenko,[46] A. M. Knee,[116] E. J. Knox,[78] N. Knust,[8, 9] K. Kobayashi,[204] S. M. Koehlenbeck,[90] G. Koekoek,[37, 36] K. Kohri,[248, 249] K. Kokeyama,[33, 250] S. Koley,[44, 166] P. Kolitsidou,[104] A. E. Koloniari,[251] K. Komori,[42] A. K. H. Kong,[142] A. Kontos,[252] L. M. Koponen,[104] M. Korobko,[98] X. Kou,[18] A. Koushik,[23] N. Kouvatsos,[68] M. Kovalam,[73] T. Koyama,[152] D. B. Kozak,[11] S. L. Kranzhoff,[36, 37] V. Kringel,[8, 9] N. V. Krishnendu,[104] S. Kroker,[253] A. Królak,[254, 187] K. Kruska,[8, 9] J. Kubisz,[255] G. Kuehn,[8, 9] S. Kulkarni,[216] A. Kulur Ramamohan,[34] Achal Kumar,[46] Anil Kumar,[233] Praveen Kumar,[178] Prayush Kumar,[24] Rahul Kumar,[2] Rakesh Kumar,[94] J. Kume,[256, 257, 42] K. Kuns,[35] N. Kuntimaddi,[33] S. Kuroyanagi,[208, 258] S. Kuwahara,[42] K. Kwak,[239] K. Kwan,[34] S. Kwon,[42] G. Lacaille,[87] D. Laghi,[189, 101] A. H. Laity,[164] E. Lalande,[259] M. Lalleman,[23] P. C. Lalremruati,[260] M. Landry,[2] B. B. Lane,[35] R. N. Lang,[35] J. Lange,[148] R. Langgin,[213] B. Lantz,[90] I. La Rosa,[99] J. Larsen,[200] A. Lartaux-Vollard,[41] P. D. Lasky,[6] J. Lawrence,[165] M. Laxen,[64] C. Lazarte,[138] A. Lazzarini,[11] C. Lazzaro,[157, 156] P. Leaci,[39, 38] L. Leali,[18] Y. K. Lecoeuche,[116] H. M. Lee,[261] H. W. Lee,[262] J. Lee,[79] K. Lee,[238] R.-K. Lee,[142] R. Lee,[35] Sungho Lee,[246] Sunjae Lee,[238] Y. Lee,[141] I. N. Legred,[11] J. Lehmann,[8, 9] L. Lehner,[183] M. Le Jean,[176, 118] A. Lemaître,[263] M. Lenti,[62, 177] M. Leonardi,[75, 76, 264] M. Lequime,[40] N. Leroy,[41] M. Lesovsky,[11] N. Letendre,[31] M. Lethuillier,[56] Y. Levin,[6] K. Leyde,[74] A. K. Y. Li,[11] K. L. Li,[265] T. G. F. Li,[111] X. Li,[149] Y. Li,[97] Z. Li,[87] A. Lihos,[123] E. T. Lin,[142] F. Lin,[141] L. C.-C. Lin,[265] Y.-C. Lin,[142] C. Lindsay,[201] S. D. Linker,[181] A. Liu,[219] G. C. Liu,[228] Jian Liu,[73] F. Llamas Villarreal,[165] J. Llobera-Querol,[99] R. K. L. Lo,[140] J.-P. Locquet,[111] S. C. G. Loggins,[266] M. R. Loizou,[133] L. T. London,[68] A. Longo,[61, 62] D. Lopez,[166] M. Lopez Portilla,[72] M. Lorenzini,[21, 22] A. Lorenzo-Medina,[178] V. Loriette,[41] M. Lormand,[64] G. Losurdo,[267, 81] E. Lotti,[133] T. P. Lott IV,[57] J. D. Lough,[8, 9] H. A. Loughlin,[35] C. O. Lousto,[112] N. Low,[124] N. Lu,[34] L. Lucchesi,[81] H. Lück,[9, 8, 9] D. Lumaca,[22] A. P. Lundgren,[268, 269] A. W. Lussier,[259] R. Macas,[74] M. MacInnis,[35]

D. M. Macleod,[33] I. A. O. MacMillan,[11] A. Macquet,[41] K. Maeda,[152] S. Maenaut,[111] S. S. Magare,[80] R. M. Magee,[11] E. Maggio,[1] R. Maggiore,[37,109] M. Magnozzi,[29,30] M. Mahesh,[98] M. Maini,[164] S. Majhi,[80] E. Majorana,[39,38] C. N. Makarem,[11] D. Malakar,[107] J. A. Malaquias-Reis,[19] U. Mali,[190] S. Maliakal,[11] A. Malik,[105] L. Mallick,[169,190] A.-K. Malz,[59] N. Man,[115] M. Mancarella,[100] V. Mandic,[18] V. Mangano,[171,156] B. Mannix,[78] G. L. Mansell,[79] M. Manske,[10] M. Mantovani,[63] M. Mapelli,[92,93,270] C. Marinelli,[102] F. Marion,[31] A. S. Markosyan,[90] A. Markowitz,[11] E. Maros,[11] S. Marsat,[101] F. Martelli,[61,62] I. W. Martin,[87] R. M. Martin,[193] B. B. Martinez,[131] D. A. Martinez,[54] M. Martinez,[43,271] V. Martinez,[129] A. Martini,[75,76] J. C. Martins,[19] D. V. Martynov,[104] E. J. Marx,[35] L. Massaro,[36,37] A. Masserot,[31] M. Masso-Reid,[87] S. Mastrogiovanni,[38] T. Matcovich,[51] M. Matiushechkina,[8,9] L. Maurin,[209] N. Mavalvala,[35] N. Maxwell,[2] G. McCarrol,[64] R. McCarthy,[2] D. E. McClelland,[34] S. McCormick,[64] L. McCuller,[11] S. McEachin,[123] C. McElhenny,[123] G. I. McGhee,[87] K. B. M. McGowan,[144] J. McIver,[116] A. McLeod,[73] I. McMahon,[189] T. McRae,[34] R. McTeague,[87] D. Meacher,[10] B. N. Meagher,[79] R. Mechum,[112] Q. Meijer,[72] A. Melatos,[124] C. S. Menoni,[137] F. Mera,[2] R. A. Mercer,[10] L. Mereni,[176] K. Merfeld,[163] E. L. Merilh,[64] J. R. Mérou,[99] J. D. Merritt,[78] M. Merzougui,[115] C. Messick,[10] B. Mestichelli,[44] M. Meyer-Conde,[272] F. Meylahn,[8,9] A. Mhaske,[80] A. Miani,[75,76] H. Miao,[273] C. Michel,[176] Y. Michimura,[42] H. Middleton,[104] D. P. Mihaylov,[106] S. J. Miller,[11] M. Millhouse,[57] E. Milotti,[185,48] V. Milotti,[92] Y. Minenkov,[22] E. M. Minihan,[66] Ll. M. Mir,[43] L. Mirasola,[156,157] M. Miravet-Tenés,[138] C.-A. Miritescu,[43] A. Mishra,[24] C. Mishra,[108] T. Mishra,[46] A. L. Mitchell,[37,109] J. G. Mitchell,[66] S. Mitra,[80] V. P. Mitrofanov,[110] K. Mitsuhashi,[25] R. Mittleman,[35] O. Miyakawa,[50] S. Miyoki,[50] A. Miyoko,[66] G. Mo,[35] L. Mobilia,[61,62] S. R. P. Mohapatra,[11] S. R. Mohite,[7] M. Molina-Ruiz,[207] M. Mondin,[181] M. Montani,[61,62] C. J. Moore,[224] D. Moraru,[2] A. More,[80] S. More,[80] C. Moreno,[135] E. A. Moreno,[35] G. Moreno,[2] A. Moreso Serra,[83] S. Morisaki,[42,204] Y. Moriwaki,[152] G. Morras,[208] A. Moscatello,[92] M. Mould,[35] B. Mours,[65] C. M. Mow-Lowry,[37,109] L. Muccillo,[177,62] F. Muciaccia,[39,38] D. Mukherjee,[104] Samanwaya Mukherjee,[24] Soma Mukherjee,[165] Subroto Mukherjee,[94] Suvodip Mukherjee,[13] N. Mukund,[35] A. Mullavey,[64] H. Mullock,[116] J. Mundi,[220] C. L. Mungioli,[73] M. Murakoshi,[230] P. G. Murray,[87] D. Nabari,[75,76] S. L. Nadji,[8,9] A. Nagar,[28,274] N. Nagarajan,[87] K. Nakagaki,[50] K. Nakamura,[25] H. Nakano,[275] M. Nakano,[11] D. Nanadoumgar-Lacroze,[43] D. Nandi,[12] V. Napolano,[63] P. Narayan,[216] I. Nardecchia,[22] T. Narikawa,[204] H. Narola,[72] L. Naticchioni,[38] R. K. Nayak,[260] L. Negri,[72] A. Nela,[87] C. Nelle,[78] A. Nelson,[131] T. J. N. Nelson,[64] M. Nery,[8,9] A. Neunzert,[2] S. Ng,[54] T. C. K. Ng,[37,72,219] L. Nguyen Quynh,[276] S. A. Nichols,[12] A. B. Nielsen,[277] Y. Nishino,[25,42] A. Nishizawa,[278] S. Nissanke,[279,37] W. Niu,[7] F. Nocera,[63] J. Noller,[280] M. Norman,[33] C. North,[33] J. Novak,[118,234,281] R. Nowicki,[144] J. F. Nuño Siles,[208] L. K. Nuttall,[74] K. Obayashi,[230] J. Oberling,[2] J. O'Dell,[229] E. Oelker,[35] M. Oertel,[234,118,282,281] G. Oganesyan,[44,45] T. O'Hanlon,[64] M. Ohashi,[50] F. Ohme,[8,9] R. Oliveri,[118,282,281] R. Omer,[18] B. O'Neal,[123] M. Onishi,[152] K. Oohara,[283] B. O'Reilly,[64] M. Orselli,[51,77] R. O'Shaughnessy,[112] S. O'Shea,[87] S. Oshino,[50] C. Osthelder,[11] I. Ota,[12] D. J. Ottaway,[117] A. Ouzriat,[56] H. Overmier,[64] B. J. Owen,[284] R. Ozaki,[230] A. E. Pace,[7] R. Pagano,[12] M. A. Page,[25] A. Pai,[195] L. Paiella,[44] A. Pal,[285] S. Pal,[260] M. A. Palaia,[81,82] M. Pálfi,[203] P. P. Palma,[39,21,22] C. Palomba,[38] P. Palud,[20] H. Pan,[142] J. Pan,[73] K. C. Pan,[142] P. K. Panda,[233] Shiksha Pandey,[7] Swadha Pandey,[35] P. T. H. Pang,[37,72] F. Pannarale,[39,38] K. A. Pannone,[54] B. C. Pant,[105] F. H. Panther,[73] M. Panzeri,[61,62] F. Paoletti,[81] A. Paolone,[38,286] A. Papadopoulos,[87] E. E. Papalexakis,[211] L. Papalini,[81,82] G. Papigkiotis,[251] A. Paquis,[41] A. Parisi,[77,51] B.-J. Park,[246] J. Park,[287] W. Parker,[64] G. Pascale,[8,9] D. Pascucci,[95] A. Pasqualetti,[63] R. Passaquieti,[82,81] L. Passenger,[6] D. Passuello,[81] O. Patane,[2] A. V. Patel,[141] D. Pathak,[80] A. Patra,[33] B. Patricelli,[82,81] B. G. Patterson,[33] K. Paul,[108] S. Paul,[78] E. Payne,[11] T. Pearce,[33] M. Pedraza,[11] A. Pele,[11] F. E. Peña Arellano,[288] X. Peng,[104] Y. Peng,[57] S. Penn,[289] M. D. Penuliar,[54] A. Perego,[75,76] Z. Pereira,[133] C. Périgois,[290,93,92] G. Perna,[92] A. Perreca,[75,76,44] J. Perret,[20] S. Perriès,[56] J. W. Perry,[37,109] D. Pesios,[251] S. Peters,[166] S. Petracca,[206] C. Petrillo,[77] H. P. Pfeiffer,[1] H. Pham,[64] K. A. Pham,[18] K. S. Phukon,[104] H. Phurailatpam,[219] M. Piarulli,[101] L. Piccari,[39,38] O. J. Piccinni,[34] M. Pichot,[115] M. Piendibene,[82,81] F. Piergiovanni,[61,62] L. Pierini,[38] G. Pierra,[38] V. Pierro,[291,132] M. Pietrzak,[96] M. Pillas,[166] F. Pilo,[81] L. Pinard,[176] I. M. Pinto,[291,132,292,32] M. Pinto,[63] B. J. Piotrzkowski,[10] M. Pirello,[2] M. D. Pitkin,[224,87] A. Placidi,[51] E. Placidi,[39,38] M. L. Planas,[99] W. Plastino,[212,22] C. Plunkett,[35] R. Poggiani,[82,81] E. Polini,[35] J. Pomper,[81,82] L. Pompili,[1] J. Poon,[219] E. Porcelli,[37] E. K. Porter,[20] C. Posnansky,[7] R. Poulton,[63] J. Powell,[155] G. S. Prabhu,[80] M. Pracchia,[166] B. K. Pradhan,[80] T. Pradier,[65] A. K. Prajapati,[94] K. Prasai,[293] R. Prasanna,[233] P. Prasia,[80] G. Pratten,[104] G. Principe,[185,48] G. A. Prodi,[75,76] P. Prosperi,[81] P. Prosposito,[21,22] A. C. Providence,[66] A. Puecher,[1] J. Pullin,[12] P. Puppo,[38] M. Pürrer,[164] H. Qi,[16] J. Qin,[34] G. Quéméner,[174,118] V. Quetschke,[165] P. J. Quinonez,[66] N. Qutob,[57] R. Rading,[231] I. Rainho,[138] S. Raja,[105] C. Rajan,[105] B. Rajbhandari,[112] K. E. Ramirez,[64] F. A. Ramis Vidal,[99] M. Ramos Arevalo,[165] A. Ramos-Buades,[99,37] S. Ranjan,[57] K. Ransom,[64] P. Rapagnani,[39,38] B. Ratto,[66] A. Ravichandran,[133] A. Ray,[97] V. Raymond,[33] M. Razzano,[82,81] J. Read,[54] T. Regimbau,[31] S. Reid,[55] C. Reissel,[35] D. H. Reitze,[11] A. I. Renzini,[127,11] B. Revenu,[294,41] A. Revilla Peña,[83] R. Reyes,[181] L. Ricca,[15] F. Ricci,[39,38] M. Ricci,[38,39] A. Ricciardone,[82,81] J. Rice,[79] J. W. Richardson,[211] M. L. Richardson,[117] A. Rijal,[66] K. Riles,[91] H. K. Riley,[33] S. Rinaldi,[270] J. Rittmeyer,[98] C. Robertson,[229] F. Robinet,[41] M. Robinson,[2] A. Rocchi,[22] L. Rolland,[31] J. G. Rollins,[11] A. E. Romano,[295] R. Romano,[3,4] A. Romero,[31] I. M. Romero-Shaw,[224] J. H. Romie,[64] S. Ronchini,[7] T. J. Roocke,[117] L. Rosa,[4,32] T. J. Rosauer,[211] C. A. Rose,[57] D. Rosińska,[125] M. P. Ross,[53] M. Rossello-Sastre,[99] S. Rowan,[87] S. K. Roy,[191,192] S. Roy,[15] D. Rozza,[127,128] P. Ruggi,[63] N. Ruhama,[239] E. Ruiz Morales,[296,208] K. Ruiz-Rocha,[144] S. Sachdev,[57] T. Sadecki,[2] P. Saffarieh,[37,109] S. Safi-Harb,[169] M. R. Sah,[13] S. Saha,[142] T. Sainrat,[65] S. Sajith Menon,[215,39,38] K. Sakai,[297] Y. Sakai,[272] M. Sakellariadou,[68] S. Sakon,[7] O. S. Salafia,[159,128,127] F. Salces-Carcoba,[11] L. Salconi,[63] M. Saleem,[148] F. Salemi,[39,38] M. Sallé,[37] S. U. Salunkhe,[80] S. Salvador,[174,173] A. Salvarese,[148] A. Samajdar,[72,37] A. Sanchez,[2] E. J. Sanchez,[11] L. E. Sanchez,[11] N. Sanchis-Gual,[138] J. R. Sanders,[182] E. M. Sänger,[1] F. Santoliquido,[44,45] F. Sarandrea,[28] T. R. Saravanan,[80] N. Sarin,[6] P. Sarkar,[8,9] A. Sasli,[251] P. Sassi,[51,77] B. Sassolas,[176] B. S. Sathyaprakash,[7,33] R. Sato,[227] S. Sato,[152] Yukino Sato,[152] Yu Sato,[152] O. Sauter,[46] R. L. Savage,[2] T. Sawada,[50] H. L. Sawant,[80] S. Sayah,[176] V. Scacco,[21,22] D. Schaetzl,[11] M. Scheel,[149] A. Schiebelbein,[190]

M. G. Schiworski,[79] P. Schmidt,[104] S. Schmidt,[72] R. Schnabel,[98] M. Schneewind,[8,9] R. M. S. Schofield,[78] K. Schouteden,[111] B. W. Schulte,[8,9] B. F. Schutz,[33,8,9] E. Schwartz,[298] M. Scialpi,[299] J. Scott,[87] S. M. Scott,[34] R. M. Sedas,[64] T. C. Seetharamu,[87] M. Seglar-Arroyo,[43] Y. Sekiguchi,[300] D. Sellers,[64] N. Sembo,[205] A. S. Sengupta,[301] E. G. Seo,[87] J. W. Seo,[111] V. Sequino,[32,4] M. Serra,[38] A. Sevrin,[188] T. Shaffer,[2] U. S. Shah,[57] M. A. Shaikh,[261] L. Shao,[302] A. K. Sharma,[99] Preeti Sharma,[12] Prianka Sharma,[105] Ritwik Sharma,[18] S. Sharma Chaudhary,[107] P. Shawhan,[126] N. S. Shcheblanov,[303,263] E. Sheridan,[144] Z.-H. Shi,[142] M. Shikauchi,[42] R. Shimomura,[304] H. Shinkai,[304] S. Shirke,[80] D. H. Shoemaker,[35] D. M. Shoemaker,[148] R. W. Short,[2] S. ShyamSundar,[105] A. Sider,[158] H. Siegel,[191,192] D. Sigg,[2] L. Silenzi,[36,37] L. Silvestri,[39,170] M. Simmonds,[117] L. P. Singer,[305] Amitesh Singh,[216] Anika Singh,[11] D. Singh,[207] M. K. Singh,[33] N. Singh,[99] S. Singh,[217,60] A. M. Sintes,[99] V. Sipala,[171,156] V. Skliris,[33] B. J. J. Slagmolen,[34] D. A. Slater,[200] T. J. Slaven-Blair,[73] J. Smetana,[104] J. R. Smith,[54] L. Smith,[87,185,48] R. J. E. Smith,[6] W. J. Smith,[144] S. Soares de Albuquerque Filho,[61] M. Soares-Santos,[189] K. Somiya,[217] I. Song,[142] S. Soni,[35] V. Sordini,[56] F. Sorrentino,[29] H. Sotani,[306] F. Spada,[81] V. Spagnuolo,[37] A. P. Spencer,[87] P. Spinicelli,[63] A. K. Srivastava,[94] F. Stachurski,[87] C. J. Stark,[123] D. A. Steer,[307] J. Steinhoff,[1] N. Steinle,[169] J. Steinlechner,[36,37] S. Steinlechner,[36,37] N. Stergioulas,[251] P. Stevens,[41] M. StPierre,[164] M. D. Strong,[12] A. Strunk,[2] A. L. Stuver,[103,*] M. Suchenek,[96] S. Sudhagar,[96] Y. Sudo,[230] N. Sueltmann,[98] L. Suleiman,[54] K. D. Sullivan,[12] J. Sun,[241] L. Sun,[34] S. Sunil,[94] J. Suresh,[115] B. J. Sutton,[68] P. J. Sutton,[33] K. Suzuki,[217] M. Suzuki,[204] S. Swain,[104] B. L. Swinkels,[37] A. Syx,[118] M. J. Szczepańczyk,[308] P. Szewczyk,[125] M. Tacca,[37] H. Tagoshi,[204] S. C. Tait,[11] K. Takada,[204] H. Takahashi,[272] R. Takahashi,[25] A. Takamori,[42] S. Takano,[309] H. Takeda,[310,311] K. Takeshita,[217] I. Takimoto Schmiegelow,[44,45] M. Takou-Ayaoh,[79] C. Talbot,[130] M. Tamaki,[204] N. Tamanini,[101] D. Tanabe,[141] K. Tanaka,[50] S. J. Tanaka,[230] S. Tanioka,[33] D. B. Tanner,[46] W. Tanner,[8,9] L. Tao,[211] R. D. Tapia,[7] E. N. Tapia San Martín,[37] C. Taranto,[21,22] A. Taruya,[312] J. D. Tasson,[153] J. G. Tau,[112] D. Tellez,[54] R. Tenorio,[99] H. Themann,[181] A. Theodoropoulos,[138] M. P. Thirugnanasambandam,[80] L. M. Thomas,[11] M. Thomas,[64] P. Thomas,[2] J. E. Thompson,[210] S. R. Thondapu,[105] K. A. Thorne,[64] E. Thrane,[6] J. Tissino,[44,45] A. Tiwari,[80] Pawan Tiwari,[44] Praveer Tiwari,[195] S. Tiwari,[189] V. Tiwari,[104] M. R. Todd,[79] M. Toffano,[92] A. M. Toivonen,[18] K. Toland,[87] A. E. Tolley,[74] T. Tomaru,[25] V. Tommasini,[11] T. Tomura,[50] H. Tong,[6] C. Tong-Yu,[141] A. Torres-Forné,[138,139] C. I. Torrie,[11] I. Tosta e Melo,[313] E. Tournefier,[31] M. Trad Nery,[115] K. Tran,[123] A. Trapananti,[52,51] R. Travaglini,[168] F. Travasso,[52,51] G. Traylor,[64] M. Trevor,[126] M. C. Tringali,[63] A. Tripathee,[91] G. Troian,[185,48] A. Trovato,[185,48] L. Trozzo,[4] R. J. Trudeau,[11] T. Tsang,[33] S. Tsuchida,[314] L. Tsukada,[213] K. Turbang,[188,23] M. Turconi,[115] C. Turski,[95] H. Ubach,[83,84] N. Uchikata,[204] T. Uchiyama,[50] R. P. Udall,[11] T. Uehara,[315] K. Ueno,[42] V. Undheim,[277] L. E. Uronen,[219] T. Ushiba,[50] M. Vacatello,[81,82] H. Vahlbruch,[8,9] N. Vaidya,[11] G. Vajente,[11] A. Vajpeyi,[6] J. Valencia,[99] M. Valentini,[109,37] S. A. Vallejo-Peña,[295] S. Vallero,[28] V. Valsan,[10] M. van Dael,[37,316] E. Van den Bossche,[188] J. F. J. van den Brand,[36,109,37] C. Van Den Broeck,[72,37] M. van der Sluys,[37,72] A. Van de Walle,[41] J. van Dongen,[37,109] K. Vandra,[103] M. VanDyke,[120] H. van Haevermaet,[23] J. V. van Heijningen,[37,109] P. Van Hove,[65] J. Vanier,[259] M. VanKeuren,[106] J. Vanosky,[2] N. van Remortel,[23] M. Vardaro,[36,37] A. F. Vargas,[124] V. Varma,[133] A. N. Vazquez,[90] A. Vecchio,[104] G. Vedovato,[93] J. Veitch,[87] P. J. Veitch,[117] S. Venikoudis,[15] R. C. Venterea,[18] P. Verdier,[56] M. Vereecken,[15] D. Verkindt,[31] B. Verma,[133] Y. Verma,[105] S. M. Vermeulen,[11] F. Vetrano,[61] A. Veutro,[38,39] A. Viceré,[61,62] S. Vidyant,[79] A. D. Viets,[89] A. Vijaykumar,[190] A. Vilkha,[112] N. Villanueva Espinosa,[138] V. Villa-Ortega,[178] E. T. Vincent,[57] J.-Y. Vinet,[115] S. Viret,[56] S. Vitale,[35] H. Vocca,[77,51] D. Voigt,[98] E. R. G. von Reis,[2] J. S. A. von Wrangel,[8,9] W. E. Vossius,[231] L. Vujeva,[140] S. P. Vyatchanin,[110] J. Wack,[11] L. E. Wade,[106] M. Wade,[106] K. J. Wagner,[112] R. M. Wald,[130] L. Wallace,[11] E. J. Wang,[90] H. Wang,[217] J. Z. Wang,[91] W. H. Wang,[165] Y. F. Wang,[1] G. Waratkar,[195] J. Warner,[2] M. Was,[31] T. Washimi,[25] N. Y. Washington,[11] D. Watarai,[42] B. Weaver,[2] S. A. Webster,[87] N. L. Weickhardt,[98] M. Weinert,[8,9] A. J. Weinstein,[11] R. Weiss,[35,†] L. Wen,[73] K. Wette,[34] J. T. Whelan,[112] B. F. Whiting,[46] C. Whittle,[11] E. G. Wickens,[74] D. Wilken,[8,9,9] A. T. Wilkin,[211] B. M. Williams,[120] D. Williams,[87] M. J. Williams,[74] N. S. Williams,[1] J. L. Willis,[11] B. Willke,[9,8,9] M. Wils,[111] L. Wilson,[106] C. W. Winborn,[107] J. Winterflood,[73] C. C. Wipf,[11] G. Woan,[87] J. Woehler,[36,37] N. E. Wolfe,[35] H. T. Wong,[141] I. C. F. Wong,[219,111] K. Wong,[190] T. Wouters,[72,37] J. L. Wright,[2] M. Wright,[87,72] B. Wu,[79] C. Wu,[142] D. S. Wu,[8,9] H. Wu,[142] K. Wu,[120] Q. Wu,[53] Y. Wu,[97] Z. Wu,[101] E. Wuchner,[54] D. M. Wysocki,[10] V. A. Xu,[207] Y. Xu,[99] N. Yadav,[28] H. Yamamoto,[11] K. Yamamoto,[152] T. S. Yamamoto,[42] T. Yamamoto,[50] R. Yamazaki,[230] T. Yan,[104] K. Z. Yang,[18] Y. Yang,[146] Z. Yarbrough,[12] J. Yebana,[99] S.-W. Yeh,[142] A. B. Yelikar,[144] X. Yin,[35] J. Yokoyama,[317,42] T. Yokozawa,[50] S. Yuan,[73] H. Yuzurihara,[50] M. Zanolin,[66] M. Zeeshan,[112] T. Zelenova,[63] J.-P. Zendri,[93] M. Zeoli,[15] M. Zerrad,[40] M. Zevin,[97] L. Zhang,[11] N. Zhang,[57] R. Zhang,[150] T. Zhang,[104] C. Zhao,[73] J. Zhao,[318] Yue Zhao,[162] Yuhang Zhao,[20] Z.-C. Zhao,[318] Y. Zheng,[107] H. Zhong,[18] H. Zhou,[79] H. O. Zhu,[73] Z.-H. Zhu,[318,319] A. B. Zimmerman,[148] L. Zimmermann,[56] M. E. Zucker,[35,11] and J. Zweizig[11]

[1]*Max Planck Institute for Gravitational Physics (Albert Einstein Institute), D-14476 Potsdam, Germany*

[2]*LIGO Hanford Observatory, Richland, WA 99352, USA*

[3]*Dipartimento di Farmacia, Università di Salerno, I-84084 Fisciano, Salerno, Italy*

[4]*INFN, Sezione di Napoli, I-80126 Napoli, Italy*

[5]*University of Warwick, Coventry CV4 7AL, United Kingdom*

[6]*OzGrav, School of Physics & Astronomy, Monash University, Clayton 3800, Victoria, Australia*

[7]*The Pennsylvania State University, University Park, PA 16802, USA*

[8]*Max Planck Institute for Gravitational Physics (Albert Einstein Institute), D-30167 Hannover, Germany*

[9]*Leibniz Universität Hannover, D-30167 Hannover, Germany*

[10]*University of Wisconsin-Milwaukee, Milwaukee, WI 53201, USA*

[11]*LIGO Laboratory, California Institute of Technology, Pasadena, CA 91125, USA*

[12]*Louisiana State University, Baton Rouge, LA 70803, USA*
[13]*Tata Institute of Fundamental Research, Mumbai 400005, India*
[14]*Centre de Physique Théorique, Aix-Marseille Université, Campus de Luminy, 163 Av. de Luminy, 13009 Marseille, France*
[15]*Université catholique de Louvain, B-1348 Louvain-la-Neuve, Belgium*
[16]*Queen Mary University of London, London E1 4NS, United Kingdom*
[17]*University of California, Davis, Davis, CA 95616, USA*
[18]*University of Minnesota, Minneapolis, MN 55455, USA*
[19]*Instituto Nacional de Pesquisas Espaciais, 12227-010 São José dos Campos, São Paulo, Brazil*
[20]*Université Paris Cité, CNRS, Astroparticule et Cosmologie, F-75013 Paris, France*
[21]*Università di Roma Tor Vergata, I-00133 Roma, Italy*
[22]*INFN, Sezione di Roma Tor Vergata, I-00133 Roma, Italy*
[23]*Universiteit Antwerpen, 2000 Antwerpen, Belgium*
[24]*International Centre for Theoretical Sciences, Tata Institute of Fundamental Research, Bengaluru 560089, India*
[25]*Gravitational Wave Science Project, National Astronomical Observatory of Japan, 2-21-1 Osawa, Mitaka City, Tokyo 181-8588, Japan*
[26]*Advanced Technology Center, National Astronomical Observatory of Japan, 2-21-1 Osawa, Mitaka City, Tokyo 181-8588, Japan*
[27]*Theoretisch-Physikalisches Institut, Friedrich-Schiller-Universität Jena, D-07743 Jena, Germany*
[28]*INFN Sezione di Torino, I-10125 Torino, Italy*
[29]*INFN, Sezione di Genova, I-16146 Genova, Italy*
[30]*Dipartimento di Fisica, Università degli Studi di Genova, I-16146 Genova, Italy*
[31]*Univ. Savoie Mont Blanc, CNRS, Laboratoire d'Annecy de Physique des Particules - IN2P3, F-74000 Annecy, France*
[32]*Università di Napoli "Federico II", I-80126 Napoli, Italy*
[33]*Cardiff University, Cardiff CF24 3AA, United Kingdom*
[34]*OzGrav, Australian National University, Canberra, Australian Capital Territory 0200, Australia*
[35]*LIGO Laboratory, Massachusetts Institute of Technology, Cambridge, MA 02139, USA*
[36]*Maastricht University, 6200 MD Maastricht, Netherlands*
[37]*Nikhef, 1098 XG Amsterdam, Netherlands*
[38]*INFN, Sezione di Roma, I-00185 Roma, Italy*
[39]*Università di Roma "La Sapienza", I-00185 Roma, Italy*
[40]*Aix Marseille Univ, CNRS, Centrale Med, Institut Fresnel, F-13013 Marseille, France*
[41]*Université Paris-Saclay, CNRS/IN2P3, IJCLab, 91405 Orsay, France*
[42]*University of Tokyo, Tokyo, 113-0033, Japan*
[43]*Institut de Física d'Altes Energies (IFAE), The Barcelona Institute of Science and Technology, Campus UAB, E-08193 Bellaterra (Barcelona), Spain*
[44]*Gran Sasso Science Institute (GSSI), I-67100 L'Aquila, Italy*
[45]*INFN, Laboratori Nazionali del Gran Sasso, I-67100 Assergi, Italy*
[46]*University of Florida, Gainesville, FL 32611, USA*
[47]*Dipartimento di Scienze Matematiche, Informatiche e Fisiche, Università di Udine, I-33100 Udine, Italy*
[48]*INFN, Sezione di Trieste, I-34127 Trieste, Italy*
[49]*Tecnologico de Monterrey, Escuela de Ingeniería y Ciencias, 64849 Monterrey, Nuevo León, Mexico*
[50]*Institute for Cosmic Ray Research, KAGRA Observatory, The University of Tokyo, 238 Higashi-Mozumi, Kamioka-cho, Hida City, Gifu 506-1205, Japan*
[51]*INFN, Sezione di Perugia, I-06123 Perugia, Italy*
[52]*Università di Camerino, I-62032 Camerino, Italy*
[53]*University of Washington, Seattle, WA 98195, USA*
[54]*California State University Fullerton, Fullerton, CA 92831, USA*
[55]*SUPA, University of Strathclyde, Glasgow G1 1XQ, United Kingdom*
[56]*Université Claude Bernard Lyon 1, CNRS, IP2I Lyon / IN2P3, UMR 5822, F-69622 Villeurbanne, France*
[57]*Georgia Institute of Technology, Atlanta, GA 30332, USA*
[58]*Chennai Mathematical Institute, Chennai 603103, India*
[59]*Royal Holloway, University of London, London TW20 0EX, United Kingdom*
[60]*Astronomical course, The Graduate University for Advanced Studies (SOKENDAI), 2-21-1 Osawa, Mitaka City, Tokyo 181-8588, Japan*
[61]*Università degli Studi di Urbino "Carlo Bo", I-61029 Urbino, Italy*
[62]*INFN, Sezione di Firenze, I-50019 Sesto Fiorentino, Firenze, Italy*
[63]*European Gravitational Observatory (EGO), I-56021 Cascina, Pisa, Italy*
[64]*LIGO Livingston Observatory, Livingston, LA 70754, USA*
[65]*Université de Strasbourg, CNRS, IPHC UMR 7178, F-67000 Strasbourg, France*
[66]*Embry-Riddle Aeronautical University, Prescott, AZ 86301, USA*
[67]*Dipartimento di Fisica "E.R. Caianiello", Università di Salerno, I-84084 Fisciano, Salerno, Italy*
[68]*King's College London, University of London, London WC2R 2LS, United Kingdom*

[69]*Korea Institute of Science and Technology Information, Daejeon 34141, Republic of Korea*
[70]*International College, Osaka University, 1-1 Machikaneyama-cho, Toyonaka City, Osaka 560-0043, Japan*
[71]*Accelerator Laboratory, High Energy Accelerator Research Organization (KEK), 1-1 Oho, Tsukuba City, Ibaraki 305-0801, Japan*
[72]*Institute for Gravitational and Subatomic Physics (GRASP), Utrecht University, 3584 CC Utrecht, Netherlands*
[73]*OzGrav, University of Western Australia, Crawley, Western Australia 6009, Australia*
[74]*University of Portsmouth, Portsmouth, PO1 3FX, United Kingdom*
[75]*Università di Trento, Dipartimento di Fisica, I-38123 Povo, Trento, Italy*
[76]*INFN, Trento Institute for Fundamental Physics and Applications, I-38123 Povo, Trento, Italy*
[77]*Università di Perugia, I-06123 Perugia, Italy*
[78]*University of Oregon, Eugene, OR 97403, USA*
[79]*Syracuse University, Syracuse, NY 13244, USA*
[80]*Inter-University Centre for Astronomy and Astrophysics, Pune 411007, India*
[81]*INFN, Sezione di Pisa, I-56127 Pisa, Italy*
[82]*Università di Pisa, I-56127 Pisa, Italy*
[83]*Institut de Ciències del Cosmos (ICCUB), Universitat de Barcelona (UB), c. Martí i Franquès, 1, 08028 Barcelona, Spain*
[84]*Departament de Física Quàntica i Astrofísica (FQA), Universitat de Barcelona (UB), c. Martí i Franqués, 1, 08028 Barcelona, Spain*
[85]*Institut d'Estudis Espacials de Catalunya, c. Gran Capità, 2-4, 08034 Barcelona, Spain*
[86]*Dipartimento di Medicina, Chirurgia e Odontoiatria "Scuola Medica Salernitana", Università di Salerno, I-84081 Baronissi, Salerno, Italy*
[87]*IGR, University of Glasgow, Glasgow G12 8QQ, United Kingdom*
[88]*HUN-REN Wigner Research Centre for Physics, H-1121 Budapest, Hungary*
[89]*Concordia University Wisconsin, Mequon, WI 53097, USA*
[90]*Stanford University, Stanford, CA 94305, USA*
[91]*University of Michigan, Ann Arbor, MI 48109, USA*
[92]*Università di Padova, Dipartimento di Fisica e Astronomia, I-35131 Padova, Italy*
[93]*INFN, Sezione di Padova, I-35131 Padova, Italy*
[94]*Institute for Plasma Research, Bhat, Gandhinagar 382428, India*
[95]*Universiteit Gent, B-9000 Gent, Belgium*
[96]*Nicolaus Copernicus Astronomical Center, Polish Academy of Sciences, 00-716, Warsaw, Poland*
[97]*Northwestern University, Evanston, IL 60208, USA*
[98]*Universität Hamburg, D-22761 Hamburg, Germany*
[99]*IAC3–IEEC, Universitat de les Illes Balears, E-07122 Palma de Mallorca, Spain*
[100]*Aix-Marseille Université, Université de Toulon, CNRS, CPT, Marseille, France*
[101]*Laboratoire des 2 Infinis - Toulouse (L2IT-IN2P3), F-31062 Toulouse Cedex 9, France*
[102]*Università di Siena, Dipartimento di Scienze Fisiche, della Terra e dell'Ambiente, I-53100 Siena, Italy*
[103]*Villanova University, Villanova, PA 19085, USA*
[104]*University of Birmingham, Birmingham B15 2TT, United Kingdom*
[105]*RRCAT, Indore, Madhya Pradesh 452013, India*
[106]*Kenyon College, Gambier, OH 43022, USA*
[107]*Missouri University of Science and Technology, Rolla, MO 65409, USA*
[108]*Indian Institute of Technology Madras, Chennai 600036, India*
[109]*Department of Physics and Astronomy, Vrije Universiteit Amsterdam, 1081 HV Amsterdam, Netherlands*
[110]*Lomonosov Moscow State University, Moscow 119991, Russia*
[111]*Katholieke Universiteit Leuven, Oude Markt 13, 3000 Leuven, Belgium*
[112]*Rochester Institute of Technology, Rochester, NY 14623, USA*
[113]*Université libre de Bruxelles, 1050 Bruxelles, Belgium*
[114]*Bar-Ilan University, Ramat Gan, 5290002, Israel*
[115]*Université Côte d'Azur, Observatoire de la Côte d'Azur, CNRS, Artemis, F-06304 Nice, France*
[116]*University of British Columbia, Vancouver, BC V6T 1Z4, Canada*
[117]*OzGrav, University of Adelaide, Adelaide, South Australia 5005, Australia*
[118]*Centre national de la recherche scientifique, 75016 Paris, France*
[119]*Univ Rennes, CNRS, Institut FOTON - UMR 6082, F-35000 Rennes, France*
[120]*Washington State University, Pullman, WA 99164, USA*
[121]*Cornell University, Ithaca, NY 14850, USA*
[122]*Laboratoire Kastler Brossel, Sorbonne Université, CNRS, ENS-Université PSL, Collège de France, F-75005 Paris, France*
[123]*Christopher Newport University, Newport News, VA 23606, USA*
[124]*OzGrav, University of Melbourne, Parkville, Victoria 3010, Australia*
[125]*Astronomical Observatory Warsaw University, 00-478 Warsaw, Poland*

[126]*University of Maryland, College Park, MD 20742, USA*
[127]*Università degli Studi di Milano-Bicocca, I-20126 Milano, Italy*
[128]*INFN, Sezione di Milano-Bicocca, I-20126 Milano, Italy*
[129]*Université de Lyon, Université Claude Bernard Lyon 1, CNRS, Institut Lumière Matière, F-69622 Villeurbanne, France*
[130]*University of Chicago, Chicago, IL 60637, USA*
[131]*University of Arizona, Tucson, AZ 85721, USA*
[132]*INFN, Sezione di Napoli, Gruppo Collegato di Salerno, I-80126 Napoli, Italy*
[133]*University of Massachusetts Dartmouth, North Dartmouth, MA 02747, USA*
[134]*Niels Bohr Institute, Copenhagen University, 2100 København, Denmark*
[135]*Universidad de Guadalajara, 44430 Guadalajara, Jalisco, Mexico*
[136]*Istituto di Astrofisica e Planetologia Spaziali di Roma, 00133 Roma, Italy*
[137]*Colorado State University, Fort Collins, CO 80523, USA*
[138]*Departamento de Astronomía y Astrofísica, Universitat de València, E-46100 Burjassot, València, Spain*
[139]*Observatori Astronòmic, Universitat de València, E-46980 Paterna, València, Spain*
[140]*Niels Bohr Institute, University of Copenhagen, 2100 Kóbenhavn, Denmark*
[141]*National Central University, Taoyuan City 320317, Taiwan*
[142]*National Tsing Hua University, Hsinchu City 30013, Taiwan*
[143]*OzGrav, Charles Sturt University, Wagga Wagga, New South Wales 2678, Australia*
[144]*Vanderbilt University, Nashville, TN 37235, USA*
[145]*University of the Chinese Academy of Sciences / International Centre for Theoretical Physics Asia-Pacific, Bejing 100049, China*
[146]*Department of Electrophysics, National Yang Ming Chiao Tung University, 101 Univ. Street, Hsinchu, Taiwan*
[147]*Kamioka Branch, National Astronomical Observatory of Japan, 238 Higashi-Mozumi, Kamioka-cho, Hida City, Gifu 506-1205, Japan*
[148]*University of Texas, Austin, TX 78712, USA*
[149]*CaRT, California Institute of Technology, Pasadena, CA 91125, USA*
[150]*Northeastern University, Boston, MA 02115, USA*
[151]*Dipartimento di Ingegneria Industriale (DIIN), Università di Salerno, I-84084 Fisciano, Salerno, Italy*
[152]*Faculty of Science, University of Toyama, 3190 Gofuku, Toyama City, Toyama 930-8555, Japan*
[153]*Carleton College, Northfield, MN 55057, USA*
[154]*University of Szeged, Dóm tér 9, Szeged 6720, Hungary*
[155]*OzGrav, Swinburne University of Technology, Hawthorn VIC 3122, Australia*
[156]*INFN Cagliari, Physics Department, Università degli Studi di Cagliari, Cagliari 09042, Italy*
[157]*Università degli Studi di Cagliari, Via Università 40, 09124 Cagliari, Italy*
[158]*Université Libre de Bruxelles, Brussels 1050, Belgium*
[159]*INAF, Osservatorio Astronomico di Brera sede di Merate, I-23807 Merate, Lecco, Italy*
[160]*Departamento de Matemáticas, Universitat de València, E-46100 Burjassot, València, Spain*
[161]*Montana State University, Bozeman, MT 59717, USA*
[162]*The University of Utah, Salt Lake City, UT 84112, USA*
[163]*Johns Hopkins University, Baltimore, MD 21218, USA*
[164]*University of Rhode Island, Kingston, RI 02881, USA*
[165]*The University of Texas Rio Grande Valley, Brownsville, TX 78520, USA*
[166]*Université de Liège, B-4000 Liège, Belgium*
[167]*DIFA- Alma Mater Studiorum Università di Bologna, Via Zamboni, 33 - 40126 Bologna, Italy*
[168]*Istituto Nazionale Di Fisica Nucleare - Sezione di Bologna, viale Carlo Berti Pichat 6/2 - 40127 Bologna, Italy*
[169]*University of Manitoba, Winnipeg, MB R3T 2N2, Canada*
[170]*INFN-CNAF - Bologna, Viale Carlo Berti Pichat, 6/2, 40127 Bologna BO, Italy*
[171]*Università degli Studi di Sassari, I-07100 Sassari, Italy*
[172]*INFN, Laboratori Nazionali del Sud, I-95125 Catania, Italy*
[173]*Université de Normandie, ENSICAEN, UNICAEN, CNRS/IN2P3, LPC Caen, F-14000 Caen, France*
[174]*Laboratoire de Physique Corpusculaire Caen, 6 boulevard du maréchal Juin, F-14050 Caen, France*
[175]*The University of Sheffield, Sheffield S10 2TN, United Kingdom*
[176]*Université Claude Bernard Lyon 1, CNRS, Laboratoire des Matériaux Avancés (LMA), IP2I Lyon / IN2P3, UMR 5822, F-69622 Villeurbanne, France*
[177]*Università di Firenze, Sesto Fiorentino I-50019, Italy*
[178]*IGFAE, Universidade de Santiago de Compostela, E-15782 Santiago de Compostela, Spain*
[179]*Dipartimento di Scienze Matematiche, Fisiche e Informatiche, Università di Parma, I-43124 Parma, Italy*
[180]*INFN, Sezione di Milano Bicocca, Gruppo Collegato di Parma, I-43124 Parma, Italy*
[181]*California State University, Los Angeles, Los Angeles, CA 90032, USA*
[182]*Marquette University, Milwaukee, WI 53233, USA*

[183]Perimeter Institute, Waterloo, ON N2L 2Y5, Canada
[184]Corps des Mines, Mines Paris, Université PSL, 60 Bd Saint-Michel, 75272 Paris, France
[185]Dipartimento di Fisica, Università di Trieste, I-34127 Trieste, Italy
[186]Université Côte d'Azur, Observatoire de la Côte d'Azur, CNRS, Lagrange, F-06304 Nice, France
[187]National Center for Nuclear Research, 05-400 Świerk-Otwock, Poland
[188]Vrije Universiteit Brussel, 1050 Brussel, Belgium
[189]University of Zurich, Winterthurerstrasse 190, 8057 Zurich, Switzerland
[190]Canadian Institute for Theoretical Astrophysics, University of Toronto, Toronto, ON M5S 3H8, Canada
[191]Stony Brook University, Stony Brook, NY 11794, USA
[192]Center for Computational Astrophysics, Flatiron Institute, New York, NY 10010, USA
[193]Montclair State University, Montclair, NJ 07043, USA
[194]HUN-REN Institute for Nuclear Research, H-4026 Debrecen, Hungary
[195]Indian Institute of Technology Bombay, Powai, Mumbai 400 076, India
[196]Centro de Física das Universidades do Minho e do Porto, Universidade do Minho, PT-4710-057 Braga, Portugal
[197]Aix Marseille Univ, CNRS/IN2P3, CPPM, Marseille, France
[198]CNR-SPIN, I-84084 Fisciano, Salerno, Italy
[199]Scuola di Ingegneria, Università della Basilicata, I-85100 Potenza, Italy
[200]Western Washington University, Bellingham, WA 98225, USA
[201]SUPA, University of the West of Scotland, Paisley PA1 2BE, United Kingdom
[202]Barry University, Miami Shores, FL 33168, USA
[203]Eötvös University, Budapest 1117, Hungary
[204]Institute for Cosmic Ray Research, KAGRA Observatory, The University of Tokyo, 5-1-5 Kashiwa-no-Ha, Kashiwa City, Chiba 277-8582, Japan
[205]Department of Physics, Graduate School of Science, Osaka Metropolitan University, 3-3-138 Sugimoto-cho, Sumiyoshi-ku, Osaka City, Osaka 558-8585, Japan
[206]University of Sannio at Benevento, I-82100 Benevento, Italy and INFN, Sezione di Napoli, I-80100 Napoli, Italy
[207]University of California, Berkeley, CA 94720, USA
[208]Instituto de Fisica Teorica UAM-CSIC, Universidad Autonoma de Madrid, 28049 Madrid, Spain
[209]Laboratoire d'Acoustique de l'Université du Mans, UMR CNRS 6613, F-72085 Le Mans, France
[210]University of Southampton, Southampton SO17 1BJ, United Kingdom
[211]University of California, Riverside, Riverside, CA 92521, USA
[212]Dipartimento di Ingegneria Industriale, Elettronica e Meccanica, Università degli Studi Roma Tre, I-00146 Roma, Italy
[213]University of Nevada, Las Vegas, Las Vegas, NV 89154, USA
[214]University of Nottingham NG7 2RD, UK
[215]Ariel University, Ramat HaGolan St 65, Ari'el, Israel
[216]The University of Mississippi, University, MS 38677, USA
[217]Graduate School of Science, Institute of Science Tokyo, 2-12-1 Ookayama, Meguro-ku, Tokyo 152-8551, Japan
[218]Institute of Physics, Academia Sinica, 128 Sec. 2, Academia Rd., Nankang, Taipei 11529, Taiwan
[219]The Chinese University of Hong Kong, Shatin, NT, Hong Kong
[220]American University, Washington, DC 20016, USA
[221]Dipartimento di Fisica, Università degli studi di Milano, Via Celoria 16, I-20133, Milano, Italy
[222]INFN, sezione di Milano, Via Celoria 16, I-20133, Milano, Italy
[223]Department of Applied Physics, Fukuoka University, 8-19-1 Nanakuma, Jonan, Fukuoka City, Fukuoka 814-0180, Japan
[224]University of Cambridge, Cambridge CB2 1TN, United Kingdom
[225]University of Lancaster, Lancaster LA1 4YW, United Kingdom
[226]College of Industrial Technology, Nihon University, 1-2-1 Izumi, Narashino City, Chiba 275-8575, Japan
[227]Faculty of Engineering, Niigata University, 8050 Ikarashi-2-no-cho, Nishi-ku, Niigata City, Niigata 950-2181, Japan
[228]Department of Physics, Tamkang University, No. 151, Yingzhuan Rd., Danshui Dist., New Taipei City 25137, Taiwan
[229]Rutherford Appleton Laboratory, Didcot OX11 0DE, United Kingdom
[230]Department of Physical Sciences, Aoyama Gakuin University, 5-10-1 Fuchinobe, Sagamihara City, Kanagawa 252-5258, Japan
[231]Helmut Schmidt University, D-22043 Hamburg, Germany
[232]Nambu Yoichiro Institute of Theoretical and Experimental Physics (NITEP), Osaka Metropolitan University, 3-3-138 Sugimoto-cho, Sumiyoshi-ku, Osaka City, Osaka 558-8585, Japan
[233]Directorate of Construction, Services & Estate Management, Mumbai 400094, India
[234]Observatoire Astronomique de Strasbourg, 11 Rue de l'Université, 67000 Strasbourg, France
[235]Faculty of Physics, University of Białystok, 15-245 Białystok, Poland
[236]National Astronomical Observatories, Chinese Academic of Sciences, 20A Datun Road, Chaoyang District, Beijing, China
[237]School of Astronomy and Space Science, University of Chinese Academy of Sciences, 20A Datun Road, Chaoyang District, Beijing, China
[238]Sungkyunkwan University, Seoul 03063, Republic of Korea

[239]*Department of Physics, Ulsan National Institute of Science and Technology (UNIST), 50 UNIST-gil, Ulju-gun, Ulsan 44919, Republic of Korea*
[240]*Institute for Cosmic Ray Research, The University of Tokyo, 5-1-5 Kashiwa-no-Ha, Kashiwa City, Chiba 277-8582, Japan*
[241]*Chung-Ang University, Seoul 06974, Republic of Korea*
[242]*University of Washington Bothell, Bothell, WA 98011, USA*
[243]*Laboratoire de Physique et de Chimie de l'Environnement, Université Joseph KI-ZERBO, 9GH2+3V5, Ouagadougou, Burkina Faso*
[244]*Ewha Womans University, Seoul 03760, Republic of Korea*
[245]*National Institute for Mathematical Sciences, Daejeon 34047, Republic of Korea*
[246]*Korea Astronomy and Space Science Institute, Daejeon 34055, Republic of Korea*
[247]*Department of Astronomy and Space Science, Chungnam National University, 9 Daehak-ro, Yuseong-gu, Daejeon 34134, Republic of Korea*
[248]*Institute of Particle and Nuclear Studies (IPNS), High Energy Accelerator Research Organization (KEK), 1-1 Oho, Tsukuba City, Ibaraki 305-0801, Japan*
[249]*Division of Science, National Astronomical Observatory of Japan, 2-21-1 Osawa, Mitaka City, Tokyo 181-8588, Japan*
[250]*Nagoya University, Nagoya, 464-8601, Japan*
[251]*Department of Physics, Aristotle University of Thessaloniki, 54124 Thessaloniki, Greece*
[252]*Bard College, Annandale-On-Hudson, NY 12504, USA*
[253]*Technical University of Braunschweig, D-38106 Braunschweig, Germany*
[254]*Institute of Mathematics, Polish Academy of Sciences, 00656 Warsaw, Poland*
[255]*Astronomical Observatory, Jagiellonian University, 31-007 Cracow, Poland*
[256]*Department of Physics and Astronomy, University of Padova, Via Marzolo, 8-35151 Padova, Italy*
[257]*Sezione di Padova, Istituto Nazionale di Fisica Nucleare (INFN), Via Marzolo, 8-35131 Padova, Italy*
[258]*Department of Physics, Nagoya University, ES building, Furocho, Chikusa-ku, Nagoya, Aichi 464-8602, Japan*
[259]*Université de Montréal/Polytechnique, Montreal, Quebec H3T 1J4, Canada*
[260]*Indian Institute of Science Education and Research, Kolkata, Mohanpur, West Bengal 741252, India*
[261]*Seoul National University, Seoul 08826, Republic of Korea*
[262]*Department of Computer Simulation, Inje University, 197 Inje-ro, Gimhae, Gyeongsangnam-do 50834, Republic of Korea*
[263]*NAVIER, École des Ponts, Univ Gustave Eiffel, CNRS, Marne-la-Vallée, France*
[264]*Gravitational Wave Science Project, National Astronomical Observatory of Japan (NAOJ), Mitaka City, Tokyo 181-8588, Japan*
[265]*Department of Physics, National Cheng Kung University, No.1, University Road, Tainan City 701, Taiwan*
[266]*St. Thomas University, Miami Gardens, FL 33054, USA*
[267]*Scuola Normale Superiore, I-56126 Pisa, Italy*
[268]*Institució Catalana de Recerca i Estudis Avançats, E-08010 Barcelona, Spain*
[269]*Institut de Física d'Altes Energies, E-08193 Barcelona, Spain*
[270]*Institut fuer Theoretische Astrophysik, Zentrum fuer Astronomie Heidelberg, Universitaet Heidelberg, Albert Ueberle Str. 2, 69120 Heidelberg, Germany*
[271]*Institucio Catalana de Recerca i Estudis Avançats (ICREA), Passeig de Lluís Companys, 23, 08010 Barcelona, Spain*
[272]*Research Center for Space Science, Advanced Research Laboratories, Tokyo City University, 3-3-1 Ushikubo-Nishi, Tsuzuki-Ku, Yokohama, Kanagawa 224-8551, Japan*
[273]*Tsinghua University, Beijing 100084, China*
[274]*Institut des Hautes Etudes Scientifiques, F-91440 Bures-sur-Yvette, France*
[275]*Faculty of Law, Ryukoku University, 67 Fukakusa Tsukamoto-cho, Fushimi-ku, Kyoto City, Kyoto 612-8577, Japan*
[276]*Phenikaa Institute for Advanced Study (PIAS), Phenikaa University, Yen Nghia, Ha Dong, Hanoi, Vietnam*
[277]*University of Stavanger, 4021 Stavanger, Norway*
[278]*Physics Program, Graduate School of Advanced Science and Engineering, Hiroshima University, 1-3-1 Kagamiyama, Higashihiroshima City, Hiroshima 739-8526, Japan*
[279]*GRAPPA, Anton Pannekoek Institute for Astronomy and Institute for High-Energy Physics, University of Amsterdam, 1098 XH Amsterdam, Netherlands*
[280]*University College London, London WC1E 6BT, United Kingdom*
[281]*Observatoire de Paris, 75014 Paris, France*
[282]*Laboratoire Univers et Théories, Observatoire de Paris, 92190 Meudon, France*
[283]*Graduate School of Science and Technology, Niigata University, 8050 Ikarashi-2-no-cho, Nishi-ku, Niigata City, Niigata 950-2181, Japan*
[284]*University of Maryland, Baltimore County, Baltimore, MD 21250, USA*
[285]*CSIR-Central Glass and Ceramic Research Institute, Kolkata, West Bengal 700032, India*
[286]*Consiglio Nazionale delle Ricerche - Istituto dei Sistemi Complessi, I-00185 Roma, Italy*
[287]*Department of Astronomy, Yonsei University, 50 Yonsei-Ro, Seodaemun-Gu, Seoul 03722, Republic of Korea*
[288]*Department of Physics, University of Guadalajara, Av. Revolucion 1500, Colonia Olimpica C.P. 44430, Guadalajara, Jalisco, Mexico*
[289]*Hobart and William Smith Colleges, Geneva, NY 14456, USA*
[290]*INAF, Osservatorio Astronomico di Padova, I-35122 Padova, Italy*
[291]*Dipartimento di Ingegneria, Università del Sannio, I-82100 Benevento, Italy*
[292]*Museo Storico della Fisica e Centro Studi e Ricerche "Enrico Fermi", I-00184 Roma, Italy*
[293]*Kennesaw State University, Kennesaw, GA 30144, USA*

[294] *Subatech, CNRS/IN2P3 - IMT Atlantique - Nantes Université, 4 rue Alfred Kastler BP 20722 44307 Nantes CÉDEX 03, France*
[295] *Universidad de Antioquia, Medellín, Colombia*
[296] *Departamento de Física - ETSIDI, Universidad Politécnica de Madrid, 28012 Madrid, Spain*
[297] *Department of Electronic Control Engineering, National Institute of Technology, Nagaoka College, 888 Nishikatakai, Nagaoka City, Niigata 940-8532, Japan*
[298] *Trinity College, Hartford, CT 06106, USA*
[299] *Dipartimento di Fisica e Scienze della Terra, Università Degli Studi di Ferrara, Via Saragat, 1, 44121 Ferrara FE, Italy*
[300] *Faculty of Science, Toho University, 2-2-1 Miyama, Funabashi City, Chiba 274-8510, Japan*
[301] *Indian Institute of Technology, Palaj, Gandhinagar, Gujarat 382355, India*
[302] *Kavli Institute for Astronomy and Astrophysics, Peking University, Yiheyuan Road 5, Haidian District, Beijing 100871, China*
[303] *Laboratoire MSME, Cité Descartes, 5 Boulevard Descartes, Champs-sur-Marne, 77454 Marne-la-Vallée Cedex 2, France*
[304] *Faculty of Information Science and Technology, Osaka Institute of Technology, 1-79-1 Kitayama, Hirakata City, Osaka 573-0196, Japan*
[305] *NASA Goddard Space Flight Center, Greenbelt, MD 20771, USA*
[306] *Faculty of Science and Technology, Kochi University, 2-5-1 Akebono-cho, Kochi-shi, Kochi 780-8520, Japan*
[307] *Laboratoire de Physique de l'École Normale Supérieure, ENS, (CNRS, Université PSL, Sorbonne Université, Université Paris Cité), F-75005 Paris, France*
[308] *Faculty of Physics, University of Warsaw, Ludwika Pasteura 5, 02-093 Warszawa, Poland*
[309] *Laser Interferometry and Gravitational Wave Astronomy, Max Planck Institute for Gravitational Physics, Callinstrasse 38, 30167 Hannover, Germany*
[310] *The Hakubi Center for Advanced Research, Kyoto University, Yoshida-honmachi, Sakyou-ku, Kyoto City, Kyoto 606-8501, Japan*
[311] *Department of Physics, Kyoto University, Kita-Shirakawa Oiwake-cho, Sakyou-ku, Kyoto City, Kyoto 606-8502, Japan*
[312] *Yukawa Institute for Theoretical Physics (YITP), Kyoto University, Kita-Shirakawa Oiwake-cho, Sakyou-ku, Kyoto City, Kyoto 606-8502, Japan*
[313] *University of Catania, Department of Physics and Astronomy, Via S. Sofia, 64, 95123 Catania CT, Italy*
[314] *National Institute of Technology, Fukui College, Geshi-cho, Sabae-shi, Fukui 916-8507, Japan*
[315] *Department of Communications Engineering, National Defense Academy of Japan, 1-10-20 Hashirimizu, Yokosuka City, Kanagawa 239-8686, Japan*
[316] *Eindhoven University of Technology, 5600 MB Eindhoven, Netherlands*
[317] *Kavli Institute for the Physics and Mathematics of the Universe (Kavli IPMU), WPI, The University of Tokyo, 5-1-5 Kashiwa-no-Ha, Kashiwa City, Chiba 277-8583, Japan*
[318] *Department of Astronomy, Beijing Normal University, Xinjiekouwai Street 19, Haidian District, Beijing 100875, China*
[319] *School of Physics and Technology, Wuhan University, Bayi Road 299, Wuchang District, Wuhan, Hubei, 430072, China*